UNIVERSITA' DEGLI STUDI DI NAPOLI "FEDERICO II"

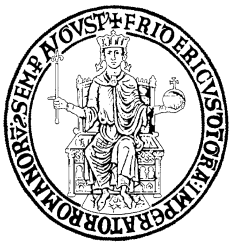

FACOLTA' DI FARMACIA

DOTTORATO IN SCIENZE DEL FARMACO: XXVIII CICLO

Structure-Based Design and Optimization of AIF/CypA peptide inhibitors with neuroprotective activity

Coordinatore

Prof.ssa Maria Valeria D'Auria

Dottoranda

Dott.ssa Fabiola Mascanzoni

Relatore

Prof. Ettore Novellino

Tutor

Dott. Menotti Ruvo
Dott.ssa Nunzianna Doti

"Lo scienziato nel suo laboratorio non è solo un tecnico, è anche un bambino davanti a fenomeni della Natura che lo affascinano come un racconto di fate."

(Marie Curie)

INDEX

Chapter II

ABBREVIATIONS

AD	Alzheimer's Disease
AIF	Apoptosis Inducing Factor
ALS	Amyotrophic Lateral Sclerosis
Apaf-1	Apoptotic Protease Activating Factor-1
APOE	Apolipoptrotein E
APS	Ammonium Persulfate
ATP	Adenosine Triphosphate
BBB	Blood Brain Barrier
Bcl-2	B-Cell Lymphoma 2
BSA	Bovine serum albumin
CARA	Computer Aided Resonance Assignment
CD	Circular Dichroism
Cdk1	Cyclin-dependent kinase-1
CNS	Central Nervous System
COSY	Correlated Spectroscopy
CsA	Ciclosporin A
CSP	Chemical Shift Perturbation
CTD	C-terminal Domain
CypA	Cyclophilins
DABCYL	4-(dimethylaminoazo)benzene-4-carboxylic acid
DIC	Diisopropylcarbodiimide
DIPEA	*N*,*N*-Diisopropylethylamine
DMF	*N*,*N*-Dimethylformamide
DMSO	Dimethyl sulfoxide
dNTP	Deoxy Nucleotide Tri-Phosphate
DR	Death Receptor
DTT	Dithiothreitol
Endo G	Endonuclease G
ESI	Electron Spray Ionization Source
ETC	Electrons Transport Chain
FAD	Flavin Adenine Dinucleotide
FasR	Fas Receptor
FPLC	Fast Protein Liquid Chromatography
FRET	Fluorescence resonance energy transfer
GSH	Reduced Glutathione
GST	Glutathione S-Transferase
HATU	1-[Bis(dimethylamino)methylene]-1H-1,2,3-triazolo[4,5-b]pyridinium 3-oxid hexafluorophosphate
HI	Hypoxia/Ischemia
HOBt	1-hydroxybenzotriazole
HPLC	High Performance Liquid Chromatography
Hq	Harlequin
HSP70	Heat Shock Protein 70
HSQC	Heteronuclear Single Quantum Coherence
HTS	High throughput screening
Kd	Dissociation Constant
KDa	KiloDalton

HCV	Hepatitis C Virus
HIV	Human Immunodeficiency Virus
IAPs	Inhibitor of Apoptosis Proteins
IC_{50}	Concentration Inhibition
IMM	Inner Mitochondrial Membrane
IMS	Intermembrane Space
IPTG	Isopropyl-Beta-D-Thiogalactopyranoside
ITC	Isothermal Titration Calorimetry
JNK	c-Jun N-terminal Kinases
LB	Luria-Bertani Broth
LC-MS	Liquid Chromatography Mass Spectrometry
LOPAC	Library of Pharmacologically Active Compounds
MEF	Mouse embryonic fibroblast
MOMP	Mitochondrial Outer Membrane Permeabilization
MWCO	Molecular Weight Cut Off
NADH	Nicotinamide Adenine Dinucleotide Hydrogen
NF-AT	Nuclear Factor of Activated T-cells
Ni-NTA	Nickel-NitriloTriacetic Acid
NMDA	*N*-Methyl-D-Aspartic Acid
NMR	Nuclear Magnetic Resonance
NOESY	Nuclear Overhauser Effect Spectroscopy
NTD	N-Terminal Domain
PARP	Poli ADP-ribose polymerase
PBS	Phosphate Buffer Saline
PCD	Programmed Cell Death
PCR	Polymerase Chain Reaction
PD	Parkinson's Disease
PDB	Protein Data Bank
PMSF	Phenylmethanesulfonyl fluoride
p-Na	N-succinylated tetrapeptide-4-nitroanilides
PPIase	Peptidyl Prolyl cis-trans Isomerase
PVDF	PolyVinyliDene Fluoride
ROESY	Rotating frame Overhause Effect Spectroscopy
ROS	Reactive Oxygen Species
SARS	Severe Acute Respiratory Syndrome
SD	Standard deviation
SOD	Superoxide Dismutase
STD	Saturation Transfer Difference
TNF	Tumor Necrosis Factor
TRAIL	Tumor necrosis factor-related apoptosis- inducing ligand
WHO	World Health Organization
TFA	Trifluoroacetic acid
TFE	Trifluoroethanol
TOCSY	Total Correlated Spectroscopy
TNF	Tumor Necrosis Factor

SUMMARY

In this research work, we described the importance of peptides as a therapeutic approach for the resolution of many diseases.

In particular, we focused our attention on the lethal role of complex protein AIF/CypA, involved in neuronal cell death.

The aim of this project was the structure-based design and optimization of AIF/CypA peptide inhibitors, using NMR studies and combinatorial chemistry.

The peptides were designed from AIF(370-394) peptide, mimetic of amino acidic region 370-394 of AIF protein, able to block in vitro the proteins interaction, through its bond to CypA and able to induce neuroprotection.

The identified peptides will be used to for the treatment of neurodegenerative disorders.

Moreover a second project was focused on development of a simple and homogenous fluorescent HTS assays for the discovery of CypA *cis-trans* isomerase activity inhibitors, using a new FRET-based substrate probe useful for Chymotrypsin-coupled isomerase assays.

For this purpose, we have designed a new fluorescent peptide substrate, useful to the use of in order to have a high proportion of *cis* conformers and to work by following fluorescence intensity increase or decrease, depending on enzyme activation or inhibition.

The assay is helpful to screening set of large compound libraries.

Chapter I

ABSTRACT

The AIF/CypA complex plays a key role in the mechanisms of cell death independent from the activation of caspases. Upon apoptotic stimuli, such as oxidative stress and hypoxia-ischemia, AIF moves from mitochondria to nuclei, where it induces large scale DNA fragmentation and cell death. In some neuronal cell lines and in mouse models of ischemic or hypoxic brain damage, the lethal activity of AIF depends on its interaction with Cyclophilin A (CypA). Starting from a predicted molecular model of the AIF/CypA complex, a peptide mimetic of the protein region of AIF involved in the interaction with CypA has been selected and investigated. A synthetic peptide reproducing this region and corresponding to residues 370-394, is capable of inhibiting the interaction between the two proteins in vitro, through its binding with CypA. The peptide encompasses a protein region containing a β- hairpin motif which likely plays a pivotal role in CypA recognition.

The transfection of this peptide in neuronal cells significantly blocks the glutamate-mediated mechanism of cell death, an effect caused by the failure of lethal complex translocation from mitochondria to the nucleus. These data not only confirmed the key role of the two proteins in inducing the neuronal death mechanism, but also indicate that molecules able to block in vivo the formation of this complex may represent "first-in-class" drugs for the treatment of cerebral ischemia and several neurological disorders.

Given the peptide size, its poor stability in biological media and its inability to cross biological membranes, it cannot be readily used for therapeutic purposes.

Thus, in the present study, using the peptide AIF(370-394) as starting template, a structure-based approach and a combinatorial studies have been applied for the design and optimization of new selective inhibitors of the AIF-CypA complex. In particular, by means of ^{1}H STD-NMR experiments, the AIF(370-394) residues crucial for the association with CypA have been identified and have been used to generate a shorter and more compact peptide having also an increased affinity for the target protein. Following peptide cyclization via a disulfide bridge and an Ala-scanning approach, a new peptide covering the region 381-389 (hereafter AIF(381-389)ox) has been identified and submitted to further investigation.

AIF(381-389)ox adopts a β- hairpin-like structure and shows a dose-dependent binding to CypA with a K_D value in the μM range as AIF(370-394). CSP-NMR studies, combined with STD-NMR studies have been used to generate a docking model of the CypA-AIF(381-389)ox complex, where residues from AIF(381-389)ox peptide have been included in the surface recognition region of AIF(370-394)/CypA.

To further improve the affinity of the new peptide and its propensity to adopt the β- hairpin conformation such as in the AIF protein, a combinatorial approach has been undertaken.

By this approach a set of simplified peptide libraries incorporating random residues on peptide positions not apparently involved in the recognition with the target protein have been prepared and screened in a positional scanning format.

The screening of libraries was performed using SPR-based Corning Epic label-free technology, and was lead to the identification of a single cyclic peptide that retained the β-hairpin conformation and bound CypA in the nanomolar range.

Altogether, the data suggest that the new selected peptide is a very good structural template for further refining structure and activity of AIF/CypA inhibitors and the deep knowledge of the binding hot-spots can be exploited to design small molecules with improved pharmacokinetic and pharmacodynamics features.

1. INTRODUCTION

1.1 Neurological disorders: the economic impact

"Ageing is a privilege and an objective of the company. It is also a challenge, which has an impact on all aspects of society in the twenty-first century."

The “World Health Organization” (WHO) proposes this message on public health, which indicates the importance of the phenomenon of aging: although the extension of life expectancy is a great achievement of modern medicine, the other side of the coin represented by an increase in the load of non-communicable diseases, such as cardiovascular disease, diabetes, cancer, Alzheimer's disease and other neurodegenerative diseases [1].

In particular, the report “*Neurological disorders: Public health challenges”* published in 2006 from the World Health Organization showed that neurological disorders, ranging from epilepsy to Alzheimer disease, from stroke to headache, affect up to one billion people worldwide. Statistical data report that neurological disorders are an important cause of mortality and constitute 12% of total deaths globally, bound to increase over the years. Within these, cerebrovascular diseases are responsible for 85% of the deaths due to neurological disorders (Figure 1.1).

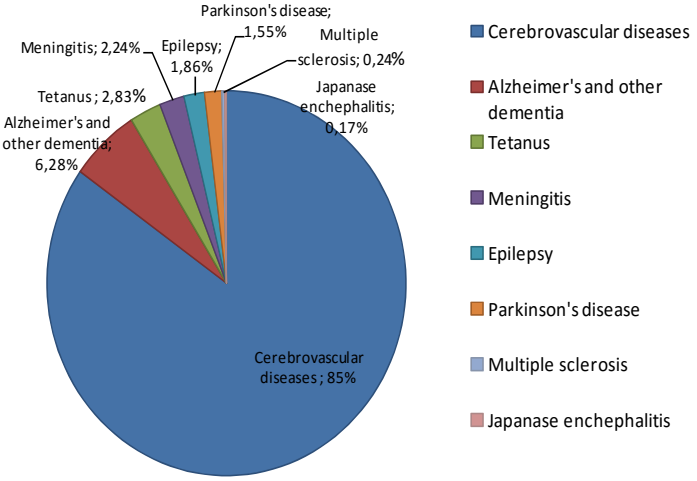

Figure 1.1: Deaths from selected neurological disorders as percentage of total neurological disorders

The social impact of these diseases, such as Alzheimer's, is devastating, with an average term of 10 years, during which the patient's autonomy decreases requiring commitment and rising costs from the family. These patients are rarely hospitalized and more than 75% of treatment and careis provided by families, living the daily drama of an emergency health still unresolved.

Given the impact of the disease in terms of health, social and political involvement, there are considerable investment in research on the pathogenesis, in outlining the causal risk factors, and in identifying preclinical markers in order to allowan early diagnosis, establish a prognosis and prepare effective treatments [1].

1.2 Neuronal Cell Death mechanisms

Neurological disorders are diseases affecting the brain and the central and autonomic nervous systems. They can affect an entire neurological pathway or a single neuron. Even a small disturbance to a neuron's structural pathway can result in dysfunctions.

The regulation of balance between neuronal life and death is a very delicate process, regulated by a constellation of trophic or proapoptotic factors [1, 2].

These last are responsible, by binding to specific receptors, of the activation of cell survival programs, growth and neuronal differentiation or conversely activation of programs that lead to cell self-destruction, represented by programed cell death pathways (PCD) [2].

The above processes are required for the normal development of the central nervous system, as well as for the removal of dysfunctional cells in pathological conditions, but excessive loss of neurons is also involved in many human neurological disorders, including acute brain injury, neurodegenerative diseases (PD), and amyotrophic lateral sclerosis (ALS) [3].

A better understanding of the molecular underpinnings of neuronal death is leading directly to novel preventative and therapeutic approaches to neurodegenerative disorders.

The mechanisms of cell death in several neurodegenerative diseases are often unclear; there are three major types of morphologically distinct cell death: necrosis, apoptosis and programmed cell death [4, 5, 6].

Necrosis

Necrosis is an acute and passive form of cell death associated with the loss of ATP.

Indeed, in hypoxic conditions, or even in ischemia, the reduction of oxidative phosphorylation results in a depletion of ATP and consequent malfunctioning of the ATP-dependent sodium-potassium -pump-(Na^+-K^+-ATP-ase pump) [7].

These events initially lead to reversible modifications such as cell swelling with formation of small vesicles.

If the process continues, there is a point of no return, characterized by dilation of mitochondria and the formation of large vesicles.

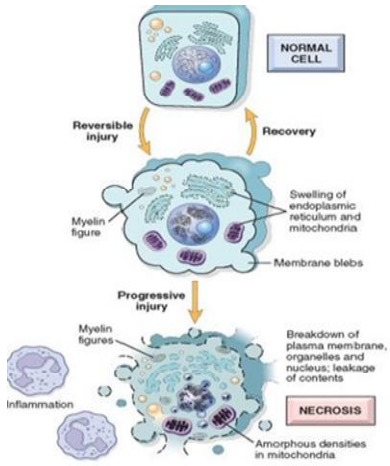

Figure 1.2: Phases of necrotic processes

This is followed by the lysis of cellular organelles and of the nucleus, due to the loss of the integrity of the membranes them selves (Figure 1.2).

Finally, when the cell is broken, there is the release of the cytoplasmic material in the extracellular milieu and the activation of inflammatory response elements [7, 8].

Apoptosis

Apoptosis describes a process of neuronal death, where the diying cells condense and fall off, with the support structures, in tissue on which they are growing [9].

In the initial phase, the cell undergoes a reduction in cytosolic volume and then a narrowing (shrinkage), due to the destruction of the cytoskeleton.

Later, there is a condensation of chromatin (pyknosis), paralleled by the nuclear disintegration and chromatin fragmentation [10].

Finally, the granules of degraded chromatin move to the periphery of the core reaching the plasma membrane, where they are surrounded by the evaginations membrane, giving to cells a bubble aspect (blebbing) (Figure 1.3).

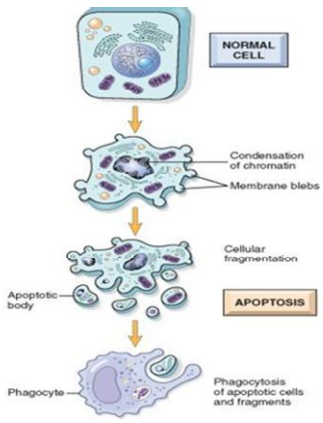

Figure 1.3: Phases of apoptotic processes

These bubbles are detached from the cell body constituting the so-called apoptotic bodies, that are engulfed by macrophages or neighboring cells [11]. Without this event there is an inflammatory reaction [11].

Apoptosis absolves an important physiological function in the replacement of senescent and excessive cells. In contrast to this role, pathological pathways of apoptosis have been associated with the progressive neuronal loss during several neuronal diseases, as well as with delayed cell death after acute brain damage caused by cerebral ischemia or traumatic brain injury [12, 13].

Programmed Cell Death (PCD)

Programmed Cell Death (PCD) was first described in a developmental context, even before apoptosis, as the cell death that occurs because of a genetic clock at a predetermined time [14].

PCD occurs in a regulated process, which usually confers advantage during an organism's life-cycle. Moreover, since the PCD is a predetermined process, it is potentially open to therapeutic intervention.

Apoptosis and autophagy are both forms of programmed cell death, where as necrosisis is considered a non-physiological process that occurs as a result of infection or injury [15].

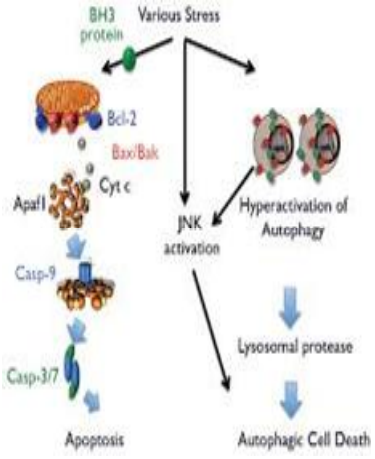

Figure 1.4: Molecular mechanisms of Programmed Cell Death

The cell death mechanisms that mediate the specific PCD processes include caspases and pro-apoptotic members of Bcl-2 family (apoptosis), JNK and ATG orthologs (autophagy), ERK2 (paraptosis, a cell death associated with trophotoxicity), PARP/AIF (PARP/AIF-dependent death), calpains/cathepsins (calcium-dependent death) and JNK (oncosis), among many others (Figure 1.4) [16, 17].

1.3 Molecular pathways involved in neuronal cell death

Pathways involved in neuronal cell death mechanism are manifold and generally are divided in: caspase-dependent and caspase independent mechanisms [18].

Caspase-dependent pathway

Caspases are cysteinyl aspartic acid-proteases activated by proteolytic cleavage.

The mechanisms that produce apoptosis require caspase-mediated cleavage of specific substrates.

In particular, caspase activation can happens through the extrinsic and intrinsic pathways [19].

The extrinsic signaling pathways involve transmembrane receptor-mediated interactions. These receptor families, as an example FasR, TNFR1, DR3, and DR4/DR5 bind to extrinsic ligands, including FasL, Trail, TNF-alpha, Apo3L and Apo2L respectively, to transduce intracellular signals that ultimately result in the destruction of the cell (Figure 1.5) [20, 21].

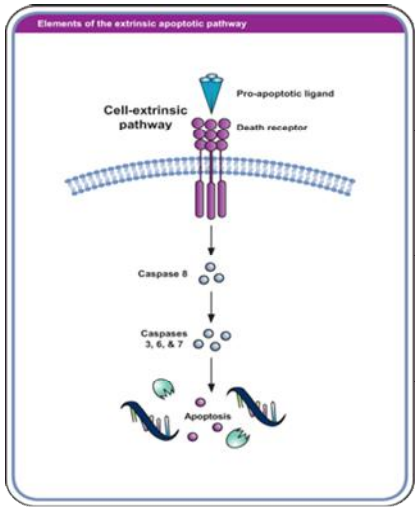

Figure 1.5: Elements of the extrinsic apoptotic pathway http://www.biooncology.com

In the intrinsic pathways, instead, a crucial role is played by the mitochondrial outer membrane premeabilization process (MOMP), which provides the release of cytochrome c in the cytosol where it induces activation of caspases [19].

The cytochrome c forms an ATP-dependent complex with the apoptotic protease activating factor-1 (Apaf-1), to make a multiprotein complex called apoptosome, that induces caspase activation, through the cleavage of an effector caspase, responsible for cell death (Figure 1.6) [22].

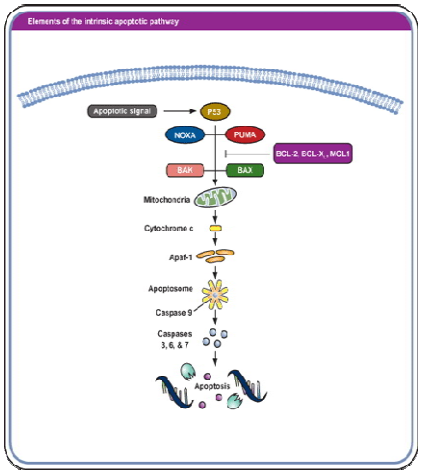

Figure 1.6: Elements of the intrinsic apoptotic pathway http://www.biooncology.com

Caspase-independent pathway

In caspase independent mechanisms, during oxidative stress, intracellular deregulation of Ca^{2+} concentration and DNA damage cause changes in the inner mitochondrial membrane (IMM) that results in an opening of the mitochondrial permeability transition (MPT) pore, loss of the mitochondrial transmembrane potential and release of proteins, including endonuclease G (Endo G), Smac/DIABLO, Omi/HtrA2 and AIF, from the mitochondrial intermembrane space to the cytosol and nucleous where they induce cell death [23].

Endo G traslocates to the nucleus where it is involved in DNA degradation, upon MOMP induction. It allows apoptosis to proceed even in the absence of caspase activation when the mitochondria are damaged [24].

The human protein Smac (and its murine orthologue DIABLO), once released, bind to different members of the inhibitor of apoptosis protein (IAP) family.

The inhibitory effects of IAP against caspases are neutralized by the protein Smac, which by interacting with the BIR2 domain, forms a stable complex with the IAP, and through steric encumbrance, destabilizes the interaction between caspase and IAP favoring the release of the active caspases and proteasome degradation of IAP [25].

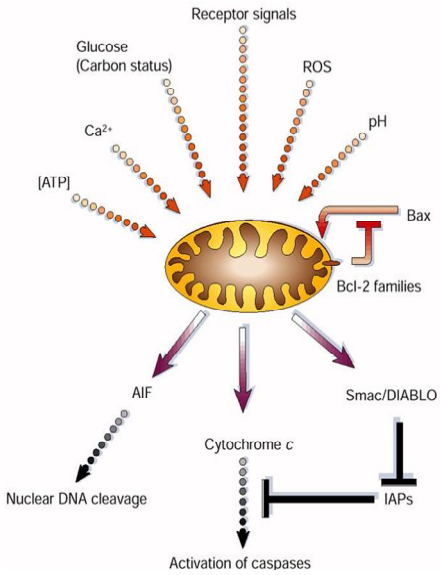

Figure 1.7: The death signal pathway through the mitochondrion

Omi is a molecule belonging to the family of serine proteases. Once released into the cytosol, it is capable to significantly improve the activity of caspases through direct proteolytic cleavage of IAPs. In addition, HtrA2/Omi can also induce apoptosis by its protease activity, acting independently of caspases [26, 27].

The Apoptosis Inducing Factor (AIF) is able to initiate the apoptotic process, inducing chromatin condensation and DNA fragmentation by a mechanism completely independent from the activation of caspases. (Figure 1.7) [28].

1.4 Apoptosis Inducing Factor (AIF): structure, functions and cellular localization

Apoptosis inducing factor (AIF) is a phylogenetically old flavoprotein with NADH oxidase activity normally contained in the mitochondrial intermembrane space (IMM). It is implicated in several vital and lethal cellular processes [29].

AIF is encoded in the nucleus and synthesized in the cytoplasm as a ~67 kDa precursor protein. It is imported to mitochondria by two mitochondrial localization sequences (MLS), that are placed within the N-terminal pro-domain of the protein.

Upon mitochondria import, the precursor is processed to a mature form of 62 kDa by proteolytic cleavage of MLS sequence removed by a mitochondrial endopeptidase.

On this configuration, AIF is an inner membrane-anchored protein whose N-terminus part is exposed to the mitochondrial matrix and whose C-terminal portion is exposed to the mitochondrial intermembrane space [30].

In this form, AIF plays a vital function related to the respiratory chain stability and/or to maintenance of the mitochondrial structure.

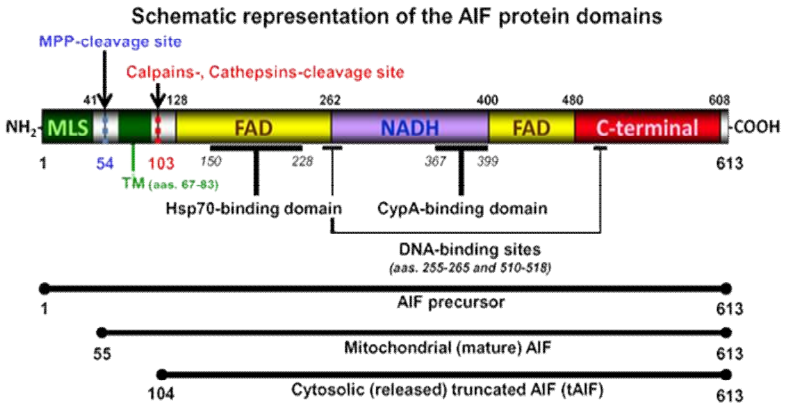

Figure 1.8: Primary structure of AIF, FAD-bipartite domain (FAD; yellow), NADH-binding domain (NADH; purple) and the C-terminal domain (red)

The mature human form of AIF comprises three structural domains: an N-terminal mitochondrial localization sequence (MLS) of 100 aminoacids (aa), a spacer sequence (aa 101-121), a FAD-binding domain (aa 122-262 and 400-477), a NADH-binding domain (aa 263-399) with two nuclear leading sequences (NLS) and a C-terminal region which consist of 136 aminoacids (Figure 1.8) [31]. The sites for the non covalent binding of FAD and relatively weak binding for NADH have been precisely mapped, and the mutants E313A and K176A have been shown to reduce FAD binding [32].

Moreover the C-terminal domain has become the most attractive part of AIF after recent data have confirmed the pro-apoptotic function of the this region [33].

The crystal structure of AIF reveals an oxidoreductase-like folding (Figure 1.9) [32].

Cloning of the full-length cDNAs of mouse AIF (mAIF), 612 aminoacids (aa) and human AIF (hAIF), 613 aa, showed that AIF is strongly conserved between these two mammalian species (92% aa identity in the whole protein) and bears a highly significant homology with oxidoreductases from all eukaryotic and prokaryotic kingdoms in its C-terminal portion (95% aa identity between aa 128-612 in mAIF and hAIF) [34].

Figure 1.9: Crystallographic structure of the human Apoptosis Inducing Factor (N- terminus= blu, C-terminus=red)

In vitro, AIF has been shown to have a redox activity accepting electrons from NADH to form superoxide anion [35].

Vital functions have been associated with the protein and have been confirmed by studies in the harlequin (Hq) AIF-mutant mouse, which has an 80% reduction in AIF expression.

Such studies have suggested that this protein acts as a free radical scavenger [36].

Indeed ,Hq mice develop blindness, ataxia, progressive retinal and cerebellar degeneration due to the age-associated, progressive loss of terminally differentiated cerebellar and retinal neurons [37].

Moreover, it has been observed that hypoxia/ischemia is particularly toxic to the hearts of Hq mice, compared to the control hearts, and that the administration of the synthetic superoxide dismutase and catalase mimetic EUK8 could reduce cardiac oxidative stress and ameliorate the survival of Hq mice subjected to experimental constriction of the aorta [38].

Similarly, in a model of neuronal cell death, the intensity of oxidative stress, measured by lipid peroxidation and protein nitrosylation, in the injured area of the Hq brains, increased compared to wild-type littermates [29].

Toghether with its vital functions, AIF is able to mediate nuclear and cytoplasmic effects of programmed cell death in response to several stimuli. While in healthy cells AIF is anchored to IMM by an amino-terminal

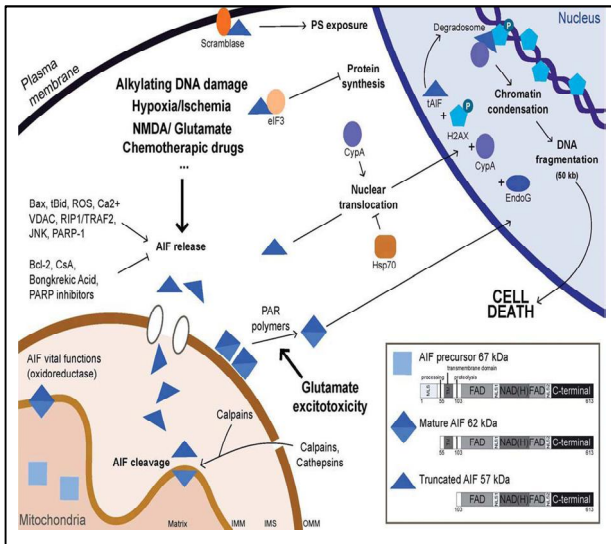

Figure 1.10: Schematic representation of AIF-mediated caspase-independent PCD

transmembrane segment, upon several cell death stimuli and MOMP, the 62 kDa AIF-mitochondrial form is cleaved by activated calpains and/or cathepsins to yield a soluble proapoptotic protein with an apparent molecular weight of 57 kDa, denoted as truncated AIF (tAIF) (Figure 1.10).

Once released from mitochondria to the cytosol, tAIF translocates to the nucleus and mediates chromatin condensation and degradation of DNA into ~50-kb fragments [39].

Several studies have demonstred that the pro-apoptotic function of AIF is independent from its vital functions [40].

Indeed, the chemical inactivation of the FAD moiety required for AIF redox activity does not block its apoptogenic function in cell free systems. In a similar way, mutations that destroy the FAD binding site do not affect the lethal function of AIF in transfection assays [41]. The lethal function of AIF is particularly relevant in neuronal cells.

Many papers have described the role of AIF in neuronal cell death in a variety of different rodent models of acute brain injury induced by cerebral hypoxia/ ischemia (HI), by middle cerebral artery occlusion, by cardiac arrest-induced brain damage, by epileptic seizures or even by brain trauma [42].

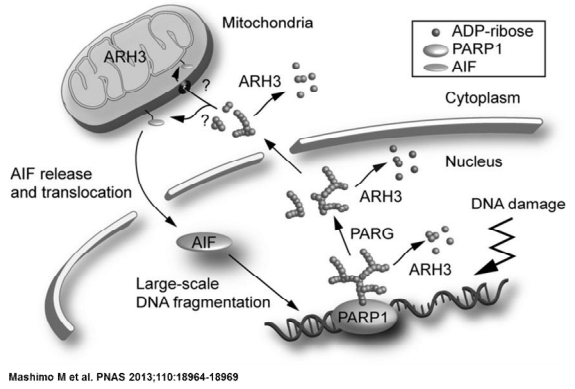

Figure 1.11: AIF-mediated cell death pathway. The excessive activation of poly ADP-ribose polymerase (PARP) sends the nuclear signal to the mitochondrion, triggering AIF release from the mitochondrion to the nucleus with chromatin condensation and DNA fragmentation

Experiments *in vivo,* performed on Hq mice, allowed confirmation of the neuro-lethal AIF activity, yet suspected from *in vitro* observations of AIF implication in poly (ADP-ribose) polymerase I (PARP1)-mediated neuronal death (Figure 1.11) [43].

The mechanism by which the PAR polymer causes AIF release is not known. However due to its highly charged nature, it could conceivably depolarize mitochondria leading to permeability transition and subsequent AIF release [44].

Moreover, *in vivo* excitotoxic studies using kainic acid-induced seizures revealed that the brains of Hq mice developed less hippocampal damage than wild-type animals. Accordingly, cortical neurons isolated from Hq mice are less susceptible to the exitotoxicity induced by glutamate, NMDA or kainic acid [33, 45]. In addition, compared with wild-type

animals, the brains of Hq mice are more resistant to ischemia-induced damage [29, 46].
A decrease in AIF levels protects primary neurons against glutamate, NMDA or hypoxia/hypoglycemia-induced death [46, 47, 48].

Another factor inducing neuroprotection is the inhibition of AIF translocation from the mitochondrion to the nucleus; indeed the prevention of the mitochondrial membrane permeability transition obstructs AIF translocation and cell death in a rat model of hypoglycemia-induced brain damage [49].
Furthermore, it has been demonstrated that also the overexpression of the chaperon HSP70, which binds to AIF and impedes its nuclear translocation [50], has a neuroprotective effect in a transgenic mouse model of hypoxia/ischemia [51].
Replacement of endogenous AIF by AIF mutants that cannot be either released from mitochondria or cannot translocate to the nucleus, improves the survival of AIF-deficient neurons that are treated with the otherwise lethal topoisomerase inhibitor camptothecin [52].
All evidences reported in the literature demonstrate the crucial role of AIF neuronal cell death mediated by a caspase-independent mechanism.

Recently, it has been demonstrated that in some neuronal models either in vitro and in vivo, the lethal action of AIF is directly dependent on the interaction with the cytosolic protein Cyclophilin A (CypA) [53, 54].

1.5 Cyclophilin A (CypA): structure, functions and cellular localization.

Cyclophilins (CyPs) are a family of ubiquitous proteins, evolutionarily present in all prokaryotes and eukaryotes, involved in a variety of functions related to cell metabolism and energy homeostasis [55]. Human CyPs family consists of 16 members, that are structurally distinct: 7 major cyclophilin isoforms in humans include CypA (also called hCyp-18a, where 18 denotes a molecular mass of 18 kDa), hCypB (also called hCyp-22, 22 kDa), hCypC, hCypD, hCypE, hCyp40 (40 kDa) and hCypNK (first identified from human natural killer cells) [56].

The existence of tissue and organelle specific isoforms, moreover, explains the diversity of pathways in which CyPs are involved.

The 18-kDa archetypal cyclophilin (CypA) is a cytosolic protein found in all tissues, and representing up to 0.1-0.6 % of the total cytosolic proteins.

CypA, also called Peptidyl-prolyl-Isomerase A, was originally characterized for its ability to catalyze the transition between *cis*- and *trans*- proline residues critical for proper folding of proteins. This protein is able to regulate protein folding and modify their molecular conformation [57].

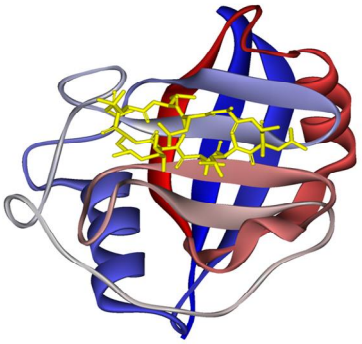

Figure 1.12: The structure of complex between the drug Cyclosporin A (CsA) and human Cyclophilin A (CypA)

The crystallographic structure of CypA [58, 59] reveals an eight-stranded antiparallel-barrel, with two helices enclosing the barrel from either side. Seven aromatic and other hydrophobic residues form a compact hydrophobic core within the barrel, usually in the area where Cyclosporin A (CsA) binds (Figure 1.12).

Indeed, CypA is known as the primary intracellular receptor of this immunosuppressive drug. Once formed, the complex between CsA and CypA, binds and inhibits calcineurin, a calcium-calmodulin-dependent phosphatase, resulting in different biological consequences depending on cell type. Firstly it provokes the block of the immune response against transplants. Indeed, when calcineurin is inhibited, it no longer dephosphorylates nuclear factor of activated T cells (NF-AT), which remains in its phosphorylated (inactive) form in the cytosol. The failed translocation of NF-AT to the nucleus prevents the activation of genes transcription encoding cytokines, such as interleukin-2, and thus of the immune response against transplants [60].

Moreover, besides its involvement in the processes of immune diseases, CypA can be secreted into the extracellular environment in various cell types due to inflammatory stimuli such as infection, hypoxia, and oxidative stress [61].

Several studies have demostrated the increased levels of soluble extracellular CyPA in patients with inflammatory responses such as in serum of patients with sepsis [62], in patients with asthma [63], and in plasma of patients with coronary artery disease [64].

In this regard, CypA is a critical molecular biomarker in the early pathogenesis of essential hypertension and in related cardiovascular disorders [64].

Therefore, CyPA is involved in diverse pathological processes of cancer development: it promotes cancer proliferation [65], regulates cell cycle progression [66], blocks apoptosis [67], and promotes cell migration/invasion [68].

Even more prominent appears to be the role of CypA in neurodegenerative diseases, indeed in brain tissue, its expression is particularly high. It is present mainly in the cytoplasm but can also be found in the nucleus [69].

The involvement of this protein in neurodegenerative diseases and in disorders caused by oxidative stress was identified a long time ago [55, 58, 70].

1.6 CypA and AIF in neurodegenerative diseases

In pathways of programmed cell death in neurons, the interaction of the cytosolic CypA and mitochondrial protein AIF, plays a key role, in vitro and in vivo [71].

However, the mechanism at the basis of the lethal action of the complex AIF/CypA is still not clear.

Two different models of action have been proposed: one proposes that the lethal translocation of AIF to the nucleus requires its interaction with CypA in the cytosol [72], while in the other it is proposed that AIF and CypA independently translocate to the nucleus, where they regulate chromatinolysis and programmed necrosis by generating an active DNA degrading complex involving the H2AX protein [73].

In support of the first hypothesis, it has been reported that the nuclear translocation of AIF is significantly reduced in a model of perinatal HI in $CypA^{-/-}$ mice compared with wild-type mice. Further, in AIF-deficient mice carrying the Hq mutation, CypA staining in the nucleus is reduced after injury and this correlates well with the protective effects in models of cerebral ischemia.[72].

In the second model, experimental data have shown the separate traslocation of the two proteins in the nucleus, underlying that the downregulation of CypA in MEF cells does not arrest nuclear translocation of AIF, but reduces DNA damage [73].

These controversial data suggest that the molecular events associated with caspase-independent cell death can depend on the cell type and the kind of apoptotic stimulus [71].

Recently, the group where I have performed the work of my PhD thesis, has demonstrated that the pharmacological inhibition of the AIF/CypA complex in neuronal cells is a very effective approach, not only to block neural loss, but at the same time to restore cell viability.

In particular, starting from the molecular model of the complex between AIF and CypA [72], we designed AIF peptides targeting the AIF-binding site on CypA. The peptide able to inhibit the interaction between AIF and CypA was identified by *in vitro* assays and the neuroprotective potential of such complex inhibitor was explored in living cells using a model of glutamate toxicity in immortalized mouse hippocampal HT-22 neurons [71].

This cell line lacks ionotropic glutamate receptors and glutamate-induced death is mediated by inhibition of the cellular cystine import, subsequent glutathione depletion and enhanced lipoxygenation, inducing a form of programmed cell death mostly due to AIF lethal nuclear translocation [74].

We provided evidences that the delivery of the peptide, that encompassed the region 370-394 of protein AIF, called AIF(370-394) peptide, induces neuroprotection by inhibiting the AIF-CypA axis.

These findings are supported by several evidences: (i) first, similar to the down-regulation of CypA the delivery of the peptide AIF(370-394) drastically reduces the sensitivity of glutamate-mediated oxidative stress in neuronal cell lines; (ii) AIF(370-394) blocks the nuclear translocation of AIF and CypA, the key event in the caspase-independent cell death mechanisms; (iii) the active peptide provides protection against glutamate-mediated mitochondrial dysfunctions and reduces the sustained rise in intracellular Ca^{2+} [71].

The oxidative stress is an important factor contributing to delayed neuronal death after acute brain injury by cerebral ischemia or brain trauma, and in neurodegenerative diseases, such as Parkinson's disease and Alzheimer's disease. As mentioned, the pathogenesis of neurodegenerative disorders is induced by multiple factors, such as Ca^{2+} overload, ROS production and mitochondrial dysfunction [75, 76].

Therefore, multitarget strategies are necessary for inducing neuroprotection or for the treatment of neurodegenerative diseases.

We demonstrated that inhibitory compounds targeting CypA, and perspectively AIF, can work as multitargeted neuroprotectants without apparent toxicity effects, and can therefore display advantageous pharmacological profiles.

1.7 Peptides as theraupeutical drugs

Recently the growth in knowledge of the pathogenesis of neurodegenerative diseases has led to the discovery of new target molecules capable to reduce the symptoms, but hardly the causes. Among many others, therapies based on the use of peptides have been proposed to restore proper protein mechanisms, to counteract oxidative stress and to correct protein misfolding [77].

Useful strategies to identify potentially therapeutic peptides are based on the rational design and on combinatorial chemistry.

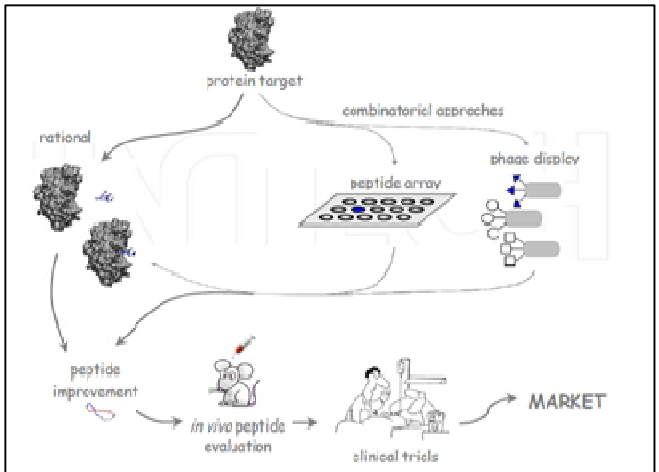

Figure 1.13: Development and Production of a peptide

The rational design of peptides is mostly based on the knowledges of structural information on a single protein or on protein-protein complexes involved in the development of pathological conditions.

More specifically, the rational design of a peptide inhibitor is based on an alternate process of design-synthesis and testing of molecules complementary in shape to the biomolecular target they will potentially bind [77].

Conversely, in absence of structural informations, combinatorial approaches can be used to generate and screen peptides binding target proteins (Figure 1.13).

Through combinatorial chemistry, a large number of structurally related peptides is synthesized and is then tested using a screening assay to identify the more active [78, 79].

Once a promising molecule (or lead coumpound) is identified, the affinity for the target can be matured affinity by progressive structural changes and testing.

When a sufficiently potent compound is identified, the peptide generally undergoes a process of “depeptidization” to enhance stability, uptake and delivery [80].

2. AIMS OF THE PROJECT

This research project is focused on the study of the molecular recognition between Cyclophilin A (CypA) and Apoptosis Inducing Factor (AIF), proteins involved in neuronal cell death mechanisms.

Previous studies have shown that the region of AIF spanning residues 370-394 mediates the interaction with CypA, and promotes neuronal death. The corresponding synthetic peptide does block the interaction between AIF and CypA and is able to inhibit cell death.

In the present study, using the peptide AIF(370-394) as starting template, we have undertaken a structure-based approach design new optimized and more selective inhibitors of the AIF-CypA complex.

A combined approach based on both rational drug design and combinatorial chemistry has been applied to obtain peptides with improved pharmacodynamic features.

^{1}H Saturation Transfer Difference NMR experiments have guided the *rationale* for restricting the template to a shorter peptide, while a screening of combinatorial libraries in a positional scanning format allowed the identification of residues essential for the interaction with CypA. Binding peptides have been identified by ITC and SPR-based Corning® Epic® label-free technology using an Enspire (Perkin Elmer) instrument.

Peptides with IC_{50}s in the micromolar range have been identified and characterized.

3. MATERIALS AND METHODS

3.1 Substrates and Chemicals

Oligonucleotide primers for PCR were purchased from Sigma-Aldrich (Milan); DNA extraction and purification kits were from Qiagen (Germany), Phusion polymerase (Finnzymes, Milan); expression vectors pET14b and pGEX4T3 were kindly provided by the Protein Expression and Purification Core Facility, EMBL (Heidelberg); the DNA molecular marker and the restriction enzymes were from New England Biolabs (Milan). GSTrap, HisTrapHP, Superdex 75 10/300 were from GE Healthcare (Milan). Bacterial expression strains were from Novagen, whilst the cloning strain TOP10F' was from Invitrogen (Milan). The prestained protein molecular marker was purchased from Bio-Rad (Milan). Protected amino acids, coupling agents (HATU) and Fmoc-Rink Amide AM Resin used for peptide synthesis were purchased from IRIS Biotech GmbH (Marktrewitz, DE). Solvents for peptide synthesis and purification, including acetonitrile (CH_3CN), dimethylformamide (DMF), trifluoroaceticacid (TFA) and methanol (CH_3OH) were purchased from ROMIL (Dublin, Ireland). Other products such as Sym-collidine, DIPEA, Piperidine, were from Sigma-Aldrich (Milan, Italy). Analytical HPLC analyses were performed on an Alliance HT WATERS 2795 system, equipped with a PDA WATERS detector 2996. Preparative purifications were carried out on a WATERS 2545 preparative system (Waters, Milan, Italy) fitted out with a WATERS 2489 UV/Visible detector. LC-MS analyses were performed using a ESI Ion Trap HCT ETD II Ultra PTM discovery mass spectrometer (Bruker) coupled with an HPLC System Alliance e2695 separation module fitted out with a 2998 PDA detector (Waters, Milan). An EnSpire Multimode Plate Reader (Perkin Elmer) was used to perform label-free direct binding assays.

3.2 Construction of recombinant plasmids

3.2.1 Human CypA cloning strategy in pET-14b

Human CypA (CypA) was cloned in pET-14b in order to obtain the protein with a tag of poly histidine at N-terminus. Firstly, the *cypA* gene was amplified by PCR from genomic DNA.

The amplification was performed by using the following couples of primers: *cypAFw* 5'-TATACTCGAGATTAGAGCTGTCCACAGTC-3' and *cypARev* 5'-TAGAAGACA TCATGGTCAACCCCACCGTG-3'. The forward primers contained the *XhoI* restriction

site, while the reverse primers were designed with the *Bbs*I restriction site and a stop codon. All amplification reactions were performed in a final volume of 50 µL, using 50 ng of template DNA. The reaction mixture contained the specific primers (0.25 µM each), dNTPs (0.25 mM each) and the *Phusion* polymerase (5U) with its buffer 1x. PCR was performed using a Bio-Rad apparatus, following the procedure indicated in Table 3.1.

Step	Procedure	Time and Temperature
1	Initial denaturation	3 min at 95°C
2	Denaturation	1 min at 95°C
3	Annealing	1 min at 56°C
4	Elongation for 25 cycle (from Step 2)	1 min at 72°C
5	Elongation	10 min at 72 °C

Table 3.1: PCR conditions

All amplification products were analyzed by 1% agarose (Euroclone) gel electrophoresis performed in TAE buffer (18.6 g/L EDTA, 242 g/L Tris base. Acetic acid added until pH 7.8). PCR products were purified by using the *QIAquick PCR Purification Kit* (Qiagen), and digested with *BbsI* (20 U/µL) and *XhoI* (20 U/µL) restriction enzymes. Each amplified fragment (1µg) was digested with 4 U of restriction enzymes for 3 h at 37ºC in a buffer containing 50 mM NaCl, 10 mM Tris-HCl, 10 mM $MgCl_2$, 1 mM DTT pH 7.9, supplemented with BSA 100 µg/mL.

Following digestion, each fragment was cloned into the corresponding sites of the pET-14b expression vector, downstream to the His-tag sequence. For this purpose, the expression vector was previously digested with the same restriction enzymes (4 U/µg), and treated with calf intestine phosphatase (CIP, 10 U) (NEB) for 30 min at 37ºC. The CIP enzyme (10 U/µL) was then inactivated at 75°C for 10 min at 1:3 molar ratio (vector/insert).

The T4 DNA Ligase was used for ligation reactions. The reactions were performed using 20 U/µg DNA of the T4 DNA Ligase (400 U/µL), in a final volume of 10 µL, for 3h at RT. *E. coli* TOPF'10 strain was used for cloning.

3.2.2 Human CypA cloning strategy in pGEX-4T3

Human CypA (CypA) was cloned in pGEX-4T-3 in order to produce CypA as GST-fusion protein. For this purpose, the *cypA* gene was amplified by PCR from genomic DNA.

The amplification was performed by using the following couples of primers: *cypAFw* 5'-GGATCCTCCAGCAAGTATATAGCATGGCC-3' and *cypARev* 5'-GAATTCGCA GATCGTCAGTCAGTCACGAT-3'. The forward primers contained the *BamHI* restriction site, while the reverse primers were designed with the *XhoI* restriction site and a stop codon. The cloning strategy was continued as previously reported.

3.3 Large-scale expression

The constructs pET14b-CypA and pGEX-4T3-CypA were transformed in *E.coli* to overexpress the corresponding recombinant proteins. Pilot expression trials were conducted to screen different strains in order to assess the best expression of soluble protein.

We investigated also different growing conditions, including different IPTG concentrations, times and temperatures of growth. Both constructs showed optimal expression levels in the BL21(DE3)strain. Optimal expression conditions obtained are reported in Table 3.2.

	His6tagged-CypA	**Gst-CypA**
OD_{600}nm	1	0.8
IPTG **(final concentration)**	1mM	0.1mM
Time	3h	16h
Temperature	37°C	22°C
Antibiotic	Ampicillin	Ampicillin

Table 3.2: Optimal expression conditions

Single clones of *E. coli* strain, previously transformed with each recombinant expression vector and grown at 37 ºC on LB agar containing the appropriate antibiotic, were inoculated into 10 mL of LB medium, containing the same antibiotic.

The overnight cultures were inoculated into 1L of pre-warmed LB medium.

Cultures were grown at 37°C under shaking until they reached the mid-log phase (OD_{600}= 0.7÷0.8nm); then, they were induced with the optimal IPTG concentration. After the cells were harvested by centrifugation (6000 rpm, 30 min, 4°C).

Cell pellets were resuspended in a lysis buffer containing 20 mM Tris/HCl pH 8.0, 150 mM NaCl, 0.1 mM DTT, 1mM PMSF, 0.1 mg/mL lysozyme and 0.1 mg/mL DNase and protease inhibitors.

The suspension was sonicated for 40 min by using a MisonixSonicator 3000 apparatus with

a micro tip probe and an impulse output of 1.5/2 (9/12 Watt).
Bacterial lysates were then centrifuged (17500 rpm, 30 min, 4°C) and the supernatant (soluble fraction) was collected and analyzed by SDS-PAGE to assess the presence of recombinant products of interest.

3.4 Purification of His6tagged-CypA

The lysates containing tagged recombinant protein was subjected to affinity chromatography onto His-Trap column (5ml) connected to an AKTA-FPLC system (GE Healthcare BioScience AB, Uppsala, Sweden).
Before loading the lysate, the resin was extensively washed with water and then equilibrated in buffer A (20 mM Tris/HCl pH 8.0, 150 mM NaCl, 0.1 mM DTT).
Flow-through containing all unbound proteins was collected and the resin was washed with buffer A. The bound proteins were eluted using an imidazole step gradient from 0 to 500 mM. Finally the His6tagged-CypA was eluted at 100 mM imidazole.
Relevant fractions (flow-through, washes and elutions) were analyzed on SDS–PAGE gel and stained with Coomassie Brilliant Blue G-250 (BioRad).
The protein migrated as a protein of ~20 KDa compatible with the theoretical MW of His6tagged-CypA. Pools of interest were dialyzed in buffer A (16h at 4°C) to remove imidazole by using membranes (Thermo) with the appropriate cut-off of 3500 Da.

3.5.Purification of GST-CypA

The column used to purify the bacterial lysates of pGEX-4T3-CypA was GSTrap affinity column (1 ml) connected to an AKTA-FPLC system.
The purification method is based on the high affinity of GST for glutathione. As above, flow-through containing all unbound proteins were collected and the resin was washed with buffer A. Finally the GST-tagged-CypA was eluted with a single step of 10 mM reduced glutathione. Indeed, the protein migrated as a protein of ~44 KDa compatible with the theoretical MW of GST-CypA.
Collected fractions were checked on SDS-PAGE and pools of interest were dialyzed in buffer A (16h at 4°C) to remove reduced glutathione by using membranes with a cut-off of 10000 Da (Thermo).

3.6 Size Exclusion Chromatography

Size exclusion chromatography was performed to purify all recombinant proteins, removing aggregates and contaminants. Purifications were carried-out at a flow rate of 0.5 ml/min onto a Superdex 75 10/300. The column was connected to AKTA Purifier system, using 20 mM Tris/HCl pH 8.0, 150 mM NaCl and 0.1mM DTT as running buffer.

Molecular weight standards from GE-Healthcare were used to calibrate the columns. Standards were: blue dextran (Mr 2,000,000), bovine serum albumin (Mr 66,399), ovalbumin (Mr 45,000), carbonic anhydrase (Mr 29,000), cytochrome c (Mr 12,000).

Pools of interest were concentrated on appropriate Amicon-Ultra membranes (Millipore).

3.7 Determination of protein and peptide concentrations

Protein concentration was determined according to the Bradford's method [81]. The Coomassie Brilliant (Bio-Rad) reagent was added to the samples and the absorbance at 595 nm was monitored. A solution of BSA was used as standard. Moreover, protein concentrations were determined by reading the absorbance at 280 nm in combination with the theoretical molar extinction coefficient (8730 $M^{-1}cm^{-1}$) by NanoDrop200c UV-Vis spectrophotometer (Thermo Scientific).

The peptides concentration, lacking tryptophan and tyrosine residues, was determined via the Scopes method [82], in which the absorbance of the peptide bond is monitored at 205 nm by NanoDrop200c UV-Vis spectrophotometer.

3.8 Electrophoretic analysis of proteins (SDS-PAGE)

Electrophoresis characterizations for CypA on 15% polyacrylamide gel in denaturing conditions were performed according to Laemmli's protocol [83].

Samples were denatured at 100°C for 5 min in Laemmli Sample Buffer (Bio-Rad) with 10% β-mercaptoethanol. Samples were then loaded on a polyacrylamide gel and the electrophoresis was performed in 0.025 M Tris/HCl, 0.2 M glycine pH 8.3 and 0.1% SDS, at 30 mA for ~1 h in Tris/Glycine/SDS Buffer for SDS application (Bio-Rad).

Proteins were then revealed by Coomassie Brilliant-Blue (Bio-Rad) staining; gels were submerged in the staining solution (0.1% Coomassie Brilliant-Blue G-250, 0.1% hydrochloric acid (J.T. Baker)) for 30 min under gentle agitation.

The gel was washed three times in deionized water, warmed in a microwave to remove the excess of Coomassie and then preserved in deionized water.

3.9 Mass spectrometryand trypsin digestion

LC-MS spectra was recorded to confirm the identity of CypA. Experiments were performed using a 10 cm EASY-Column, ID 100µm, 5µm particle size, C18-A1 (Thermo Scientific), equipped with a 2 cmpre-column having an ID of 100 µm, 5 µm particle size, 120 Å, ReproSil-Pur C18-AQ (Thermo Scientific). Data were collected on an Ion Trap mass spectrometer ETD II (Bruker Daltonics) equipped with a nanoESI ion source. Most runs were performed at 600 nL/min, applying a linear gradient of 0.1% formic acid (FA) in CH_3CN over 0.1% FA in H_2O from 0% to 60% in 45 min.

To characterize the protein primary structure, trypsin digestions were performed in 20 mM Tris-HCl, 150 mM NaCl pH 8.0.

Proteins were digested using a trypsin: protein molar ratio of 1:50 or 1:100. The reaction was allowed to proceed at 37°C and resulting peptides were analyzed at different time points (1, 2, 3, 4 h) by LC-MS, using an EASY-Column, 10 cm, ID75 µm, 3 µm, C18-A2 (Thermo Scientific).

3.10 Circular dichroism spectroscopy (CD)

Jasco J-715 spectropolarimeter, equipped with a PTC-423S/15 Peltier temperature controller, was used to register far-UV circular dichroism spectra of CypA, in a 0.1 cm quartz cells. The parameters used to acquire spectra were: far UV range 190-260 nm, band width of 1 nm, response of 8 sec, data pitch of 0.2 nm and scanning speed of 10 nm/min. Spectra were recorded at 20°C, on protein solutions at 15 µM in 20 mM phosphate buffer pH 7.4.

CD data were expressed as mean residue ellipticity (θ). Spectra processing was achieved by using the Spectra Manager software, while the analysis of the secondary structure content of the proteins was performed with the neural network program: CDNN [84].

Peptide CD spectra were registered in 20 mM phosphate buffer pH 7.4 at 25 °C in the far UV region from 190 to 260 nm in 0.1 cm path-length quartz cuvettes.

Each spectrum was obtained averaging three scans, subtracting the contribution from corresponding blanks and converting the signal to mean residue ellipticity in units of deg × cm^2 × $dmol^{-1}$ × res^{-1}.

The concentration of peptides was kept at 80 µM and spectra were acquired in different buffers (see “Results” for details).

3.11 Peptides synthesis and purification

The wild type peptide, called AIF(370-394), corresponding to the protein sequence 370-394 (QSVGVSSGKLLIKLKDGRKVETDHI) of the AIF protein was synthesized on solid phase, following the Fmoc (N-9-Fluorenylmethyloxycarbonyl) methodology [85].

Solid phase peptide syntheses were performed using a Rink amide resin (substitution 0.5 mmol/g) to afford a C-terminal amide sequence.

The coupling reactions were carried out with a four-fold excess of amino acid using a double coupling procedure: first coupling was carried out using Oxime Pure [86] and DIC (Diisopropylcarbodiimide), the second one was performed using 1-hydroxybenzotriazole (HOBt), 1-[Bis(dimethylamino)methylene]-1H-1,2,3-triazolo[4,5-b]pyridinium 3-oxid hexafluorophosphate (HATU) [87] and Collidine in DMF (*N*,*N*-dimethylformamide) as coupling reagents. Each coupling reaction was carried out for 30 minutes at room temperature.

However, the derivatives peptides from AIF(370-394), were synthesized by performing the coupling reactions with a four-fold excess of HATU, 4 equivalents of Fmoc-protected amino acids, HOBt and Collidine (relative to the synthesis scale), in DMF for a reaction time of 45 min under continuous mixing.

The deprotection step to remove the Fmoc group was performed firstly with 40% piperidine in DMF for 5 min, then with 20% piperidine in DMF for 10 min.

All peptides, except AIF(370-394) peptide, were acetylated at N-terminus by using a solution of acetic anhydride/DIEA 30%/5% in DMF. Crude materials were cleaved from the resin by treatment with trifluoroacetic acid (TFA)/H_2O/triisopropylsilane (TIS) (95:2.5:2.5: v/v/v) at room temperature for 3 h. The resin was finally filtered, and the peptide precipitated using cold diethyl ether.

Peptides were purified using an Onyx monolithic semi-PREP C18 column (100x10mm, Phenomenex, Castel Maggiore, Italy) operated at a flow rate of 15 mL/min; H_2O+0.1% TFA (solvent A) and CH_3CN+0.1% TFA (solvent B) were used as eluents, using a linear gradient of solvent B from 0 to 70% in 20 min. Purity and identity of peptides were assessed by analytical RP-HPLC and LC-MS (liquid chromatography mass spectrometry).

The peptides were cyclized dissolving the linear peptides with cysteines at N- and C-termini at a concentration of 10^{-3} to 10^{-4} M, in 0.015 M ammonium carbonate pH 8.0 for 24 h under agitation, at room temperature. Reactions were monitored by analytical HPLC and at the end, after acidification with trifluoroacetic acid (TFA), they were lyophilized and directly used for preparative HPLC purification.

3.12 Alanine-scanning strategy

Alanine scanning peptides [88] were prepared by the solid phase method on a 50 μmol scale, using standard Fmoc-derivatized amino acids [85]. Briefly, synthesis were performed on a fully automated multichannel peptide synthesizer Syro I (Multisynthech, Germany). RINK AMIDE resin (substitution 0.5 mmol/g) was used as solid support. The coupling reactions were carried out as previously reported.

The deprotection step to remove the Fmoc group was performed firstly with 40% piperidine in DMF for 5 min, then with 20% piperidine in DMF for 10 min.

Peptides were removed from the resin by treatment with a TFA:TIS:H2O (90:5:5, v/v/v) mixture, then they were precipitated in cold diethylether and lyophilized.

Peptides were cyclized and purified by preparative RP-HPLC using a linear gradient of solvent B from 10 to 45% in 8 min at a flow rate of 15 mL/min.

Purity and identity of the peptides were assessed by analytical RP-HPLC and LC-MS.

3.13 Positional scanning strategy

Positional scanning libraries [89] were prepared by the solid phase method, using RINK AMIDE resin as solid support. Syntheses were performed on a fully automated multichannel peptide synthesizer Syro I as described in the previous section.

Randomized positions were obtained by using equimolar mixtures of 7 building blocks employing a 100-fold excess of each amino acid.

After the test of binding carried out with Label-free Corning Epic technology [90], the best library was screened, synthesizing each peptide present in the 7-member peptide library.

Peptides were purified by preparative RP-HPLC using a linear gradient of solvent B from 10 to 45% in 8 min at a flow rate of 15 mL/min.

3.14 Isothermal Titration Calorimetry (ITC)

ITC experiments were performed at 25°C using a MicroCal ITC 200 (GE Healthcare Bio-Sciences AB, Sweden) following the standard procedure.

The protein and peptide samples were dialyzed in phosphate saline buffer (PBS) with 1 mM DTT, pH 7.4. In each titration, 20 injections of 2 μL each of AIF(370-394) at 0.7 mM peptide were added to a sample of 300 μL of CypA at 5 μM.

Since the signal from the first injection can usually not be used for data analysis only 0.4 μl were added in this step and the data point was omitted. Data were analyzed using the

"Origin" software (MicroCal). The association constant (Ka), molar binding stoichiometry (n) and the binding enthalpy (ΔH), entropy (ΔS) and Gibbs free energy (ΔG) were determined by fitting the binding isotherm to a one-site model with MicroCal Origin7 software. All ITC experiments were performed in triplicate.

3.15 Corning Epic label-free technology

Binding assays were performed using the Corning Epic label-free technology on the EnSpire Multimode Plate Reader (PerkinElmer, Rodgau, Germany) [91].

Label-free biochemical assays measure changes in refraction index following a binding event. This change is indicated by a shift in wavelength as shown in the following schematic Figure 3.1. The Enspire label-free system generates reproducible and high-quality information for protein-protein, and protein-small molecule interactions.

Label-free responses are measured as shifts in reflected wavelength and are expressed in picometers (pm).

Results were analyzed using the EnSpire label-free user interface software.

The difference between the last baseline measurements and the maximum signal was used to determine the K_D value. Graphs were generated using GraphPad PRISM® v5.01.

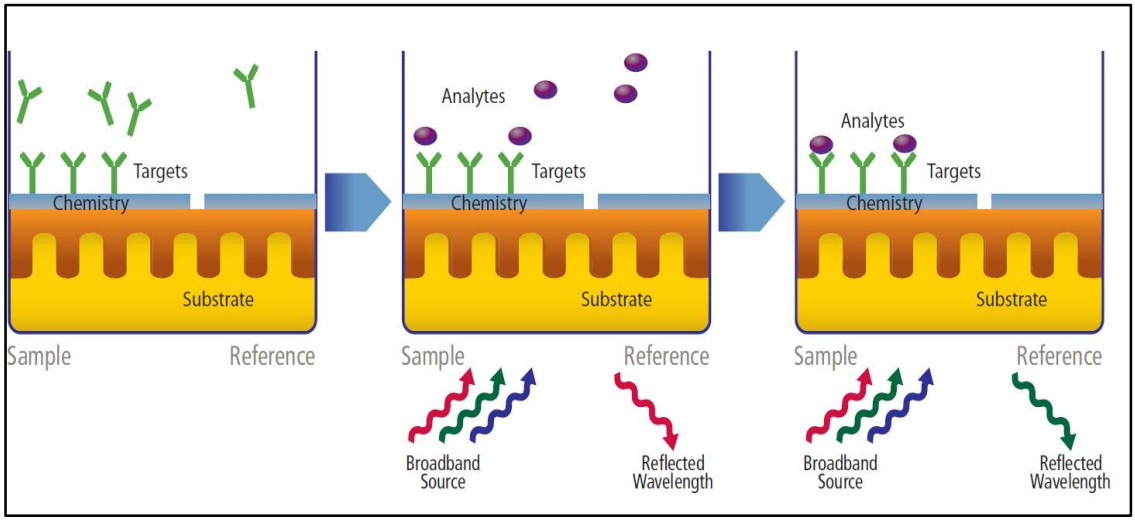

Figure 3.1: Schematic illustration of Corning Epic label-free technology

CypA immobilization on the optical biosensors was accomplished by adding 200 μg/mL protein in 20 mM sodium acetate, pH 5.5, using a 12-channel Thermo Scientific matrix multichannel equalizer pipette followed by overnight incubation at 4°C.

The microplate was subsequently washed three times with phosphate-buffered saline (PBS

1X; pH 7.4) buffer. After washing, the plate was equilibrated in the assay buffer (PBS) for 3 hours (30 μl). After incubation, a baseline reading was recorded. After another washing step, 15 μl of various peptides were dispensed in the plate wells.

Peptides used for the CypA assay were diluted with the assay buffer (PBS) at a working concentration of 300 μM (150 μM final concentration in the plate) and then further diluted in the assay buffer directly in a 384-well polypropylene plate for a total of twelve different concentrations. The final readings were taken over a period of 1 hour.

3.16 Cell Culture of HT-22 and transfection

HT-22 cells, derived from immortalized hippocampal neurons, were cultured at a density of 10 000 cells/well in a 96-well plate (Greiner Bio-One, Frickenhausen, Germany) at 37 °C and 5% CO_2 in Dulbecco's modified Eagle medium (Invitrogen, Karlsruhe, Germany) with 10% heat-inactivated calf serum and 100 U/ml penicillin, 100 μg/ml streptomycin and 2 mM glutamine. Peptide transient transfection was performed using the cationic lipid mixture Pro-Ject Protein Transfection Reagent kit according to the manufacturer's instructions (Pierce, Thermo Scientific, Munich, Germany, Prod no. 89850).

3.17 Induction of Apoptosis in HT-22 Cells

Neuronal cell death was induced for 24 hours after seeding of the cells. Induction of apoptosis was performed by glutamate-induced toxicity.

Glutamate-Induced Toxicity

For inducing glutamate toxicity [92], cell growth medium was removed and replaced by standard cell culture medium containing glutamate (3 mM) (Sigma-Aldrich, Munich, Germany). Cell viability was evaluated between 14 and 16 hours later.

3.18 Cell Viability Assay

Quantification of cell viability in HT-22 cells was performed either in standard 96-well plates or in standard 24-well plates by the method of 3-(4, 5-dimethylthiazol-2-yl)-2, 5-diphenyltetrazolium bromide MTT (Sigma-Aldrich) reduction. The reagent was used at 0.25 mg/ml for 1 hour. After terminating the reaction by removing the media and freezing the plate at −80°C for at least 1 hour, the MTT dye was dissolved in DMSO and absorbance was determined at 590 nm with the blank obtained at 630 nm (FluoStar OPTIMA; BMG

Labtech, Offenburg, Germany). Cell viability levels were determined by comparing absorption of treated cell samples with that of untreated control cells samples (100% cell viability). DMSO control was used as solvent control. For statistical analysis, experiments were repeated at least three times.

3.19 Expression of ^{15}N-labelled recombinant CypA for NMR studies

A single clone of CypA strain was cultured for 16 h at 37°C in 50 ml of LB medium with antibiotics. The harvested cells were centrifuged for 15 min at 5000 rpm and suspended in 10 ml of M9 medium (Table 3.3). Subsequently a spectrophotometric reading of cells was carried out to determine the start value of $OD_{600\ nm}$ (generally 0.15-0.18).

Cells were then inoculated in M9 medium, containing $^{15}NH_4Cl$ (Sigma Aldrich 1g/l) as the unique nitrogen source, and grown at 37°C. For the overexpression the cells were grown at 37°C till the mid log phase ($OD_{600\ nm}$ = 0.9 ± 0.5). At this point the expression was induced by addition of IPTG (1.0 mM). Cells were allowed to grow for further 15-16 hours at 25°C. After harvesting, the cells were lysed and ^{15}N-His6tagged-CypA was purified by affinity chromatography on a His-trap HP column.

NaCl	0.5g
KH_2PO_4	7.5g
K_2HPO_4	17.4g
$^{15}NH_4Cl$	1g
1 M MgSO4	1 ml
10 mM $CaCl_2$	10 ml
1M thiamine	1 ml
20% glucose	10 ml
ddH2O	877 ml
Antibiotic	1 ml
Total volume	1 l

Table 3.3: M9 medium composition

3.20 NMR spectroscopy

NMR experiments were carried out at 25°C using an Inova 600 MHz spectrometer (Varian Inc., Palo Alto, CA, USA), equipped with a cryogenic probe optimized for ^{1}H detection. NMR data were processed by the software VNMRJ 1.1.D (Varian Inc.). One-dimensional (1D) spectra were analyzed using ACD/NMR Processor 12.0 [ACD/NMR]; two and three-dimensional (2D and 3D) spectra were analyzed using tools available in CARA (Computer Aided Resonance Assignment) software (downloaded from cara.nmr.ch) [93].

The one-dimensional (1D) 1H STD-NMR spectra of AIF(370-394) and AIF(381-389)ox in presence of GST-CypA (100:1) were acquired with 1024 scans with on-resonance irradiation at -0.3 ppm for selective saturation of protein resonances and off-resonance irradiation at 30 ppm for reference spectra.

A train of 40 Gaussian shaped pulses of 50 ms with 1 ms delay between pulses were used, for a total saturation time of 2 s. 1D 1H STD spectra were obtained by internal subtraction of saturated spectrum from reference spectrum by phase cycling.

For AIF(381-389)red and AIF(381-389)ox chemical shift assignment and conformational analysis, 1D 1H spectra were acquired with a spectral width of 7191.66 Hz, relaxation delay 1.0 s, 7k data points for acquisition and 16k for transformation, bidimensional (2D) [1H, 1H] total correlation spectroscopy (TOCSY) [94], double quantum filtered correlated spectroscopy (DQF-COSY) [95] and nuclear Overhauser effect spectroscopy (NOESY) [96] were acquired with 32 or 64 scans per t1 increment, with a spectral width of 6712.0 Hz along both t1 and t2, 2048 and 256 data points in t2 and t1, respectively, and 1.0 srecycle delay. Water suppression was achieved by means of a double pulsed field gradient spin echo (DPFGSE) sequence [97].

The TOCSY experiment was recorded using a DIPSI-2 mixing scheme of 70 ms with 7.7 kHz spin-lock field strength. The NOESY spectrum was carried out with a mixing time of 250 ms. The data were typically apodized with a square cosine window function and zero filled to a matrix of size 4096 and 1024 before Fourier transformation and baseline correction. Chemical shift assignments (Tables 4.2 and 4.3) refer to residual water resonance (4.75 ppm).

To define the AIF(381-389)ox binding site on CypA by chemical shift perturbation (CSP) studies, the 2D ^{1}H- ^{15}N HSQC spectra were recorded on ^{15}N-CypA (80 μM) in the presence of increasing concentrations of AIF(381-389) peptide ranging from 0 to 800 μM in PBS buffer, pH 5.8.

The CSPs were quantified by the average combined chemical shift between the free form

and AIF(381-389) bound CypA protein using the following equation: $\Delta\delta HNav = [((\Delta\delta H^N)^2 + (\Delta\delta N/5)^2)/2]^{1/2}$ [98, 99, 100], where $\Delta\delta H^N$ and $\Delta\delta N$ are the chemical shift variations of the amide proton and nitrogen resonances, respectively.

3.21 Molecular Modeling

The HADDOCK web server [101] was used to generate a model of the CypA/AIF(381-389)ox complex. For CypA, the crystal structure available in the protein data bank was used for docking calculations (PDB ID:2CYH) [102].

For AIF(381-389), the 380-390 portion was extrapolated from the the crystal structure of AIF protein (PDB ID: 1M6I) [103], replacing the L^{380} and E^{390} with cysteine residues. CSP and STD data were used to introduce active and passive residues.

The four best cluster with negative Z-Scores were visually inspected, and solutions not compatible with NMR experimental data were rejected. On this basis, the best model of the first HADDOCK cluster was selected as representative of the CypA/AIF(381-389)ox complex.

4. RESULTS

4.1 Biochemical characterization of AIF(370-394)/CypA complex

In order to define the molecular basis of the recognition between AIF and CypA, I focused my attention on the biochemical and CD and NMR-based structural characterization of the complex between CypA and the AIF(370-394) peptide. For this purpose, my first aim has been the large scale synthesis of AIF(370-394) peptide and the production of soluble and highly pure CypA recombinant protein.

4.1.1 Cloning, overexpression and purification of His6tagged-CypA

Human *cypA* gene was cloned in pET-14b expression vector, enabling the expression of the protein as poly histidine tag (6His) product, containing a highly specific cleavage site for thrombin protease at N-terminus.

The host strain opted for improbe expression of the recombinant protein was the BL21(DE3) and the purification was achieved by one step of affinity chromatography using a His-Trap resin. The bound proteins were eluted using an imidazole step gradient from 0 to 500 mM (Figure 4.1 A) and the fractions obtained were analyzed by SDS-PAGE

The His6tagged-CypA was eluted at 100 mM imidazole, with a high purity degree.as shown in Figure 4.1 B.

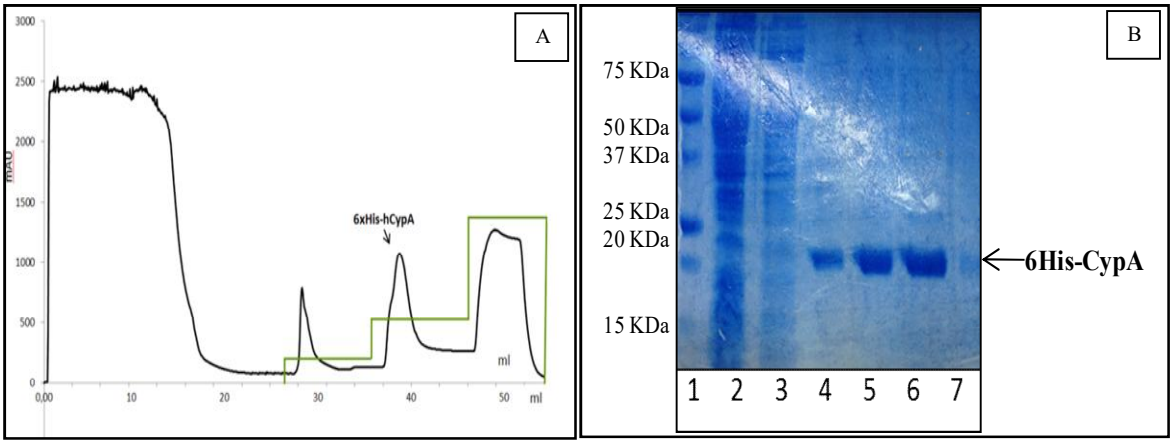

Figure 4.1: His6tagged-CypA purification profile. (**A**) Affinity chromatography profile of the His6-tagged CypA. (**B**) 15% SDS-page analysis after His-trap. Lane 1: Marker; Lane 2: flow through; Lane 3 pooled fraction of wash steps at 30 mM imidazole; Lanes from 4 to 6 samples eluted at 100 mM of imidazole; Lane 7 pooled fractions eluted at 500 mM of Imidazole.

The identity of the purified protein was confirmed using mass spectrometry. To this aim the protein of interest was digested with trypsin and fragments obtained were submitted to nano

flow liquid-chromatography coupled to mass spectrometry (LC-MS/MS).

Data deconvolution, using the MASCOT software [104], allowed the univocally identification the protein as CypA (Figure 4.2 A-D).

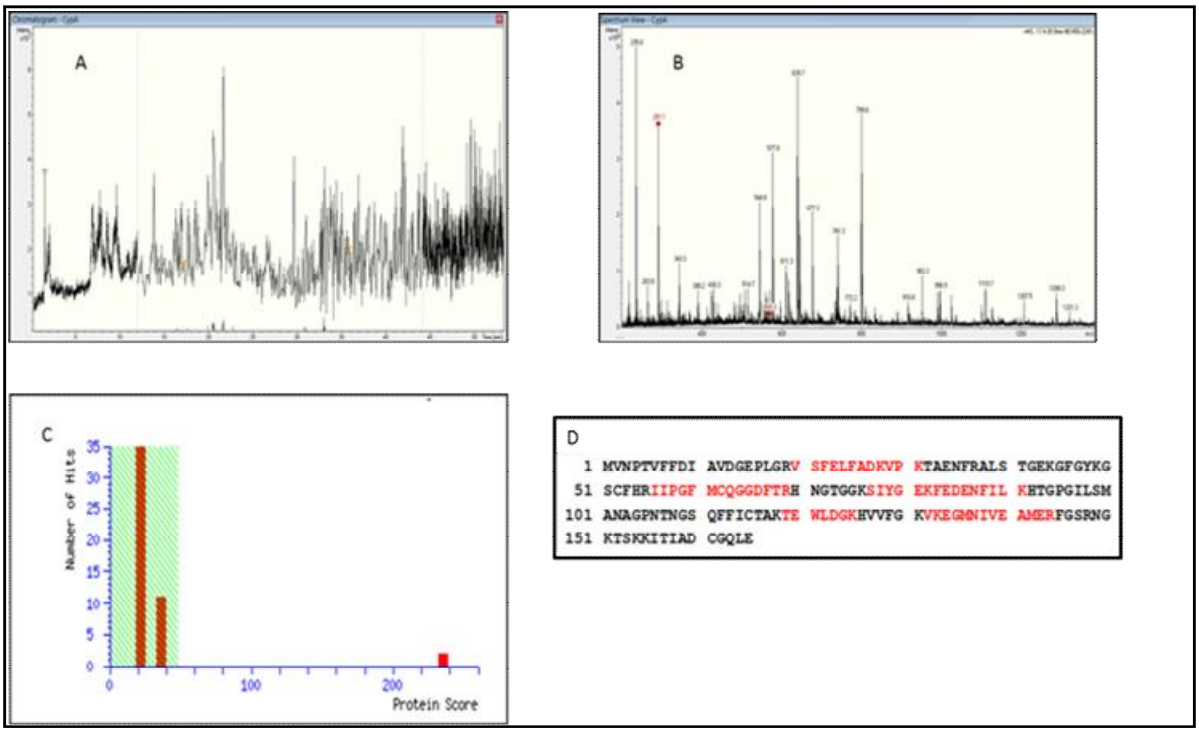

Figure 4.2: Peptide mass finger printing of CypA**.** (**A**) Chromatogram profile of CypA tryptic digestion. (**B**) Mass peaks assigned to peptides. (**C**) Mascot's match score. (**D**) CypA sequence; matched peptides are shown in red and correspond to a coverage sequence of 37.4%.

The folding status in solution of the recombinant His6-tagged CypA was assessed by far-UV CD spectroscopy.

As shown in Figure 4.3 A, the CD spectrum of the protein was dominated at 20°C and in 5 mM phosphate buffer at pH 7.4, by the presence of a maximum at 198 nm, a minimum at 208 nm and an absolute minimum at 222 nm [105] which are hallmarks of largely ordered structure, where β-strands are predominant in agreement with the crystallographic structure [102].

Thermal denaturation experiments determined a temperature of melting of 50°C (Figure 4.3 B). Moreover the spectra recorded at 20°C upon denaturation demonstrated the process is reversible indicating a high intrinsic stability of the protein (Figure 4.3 C).

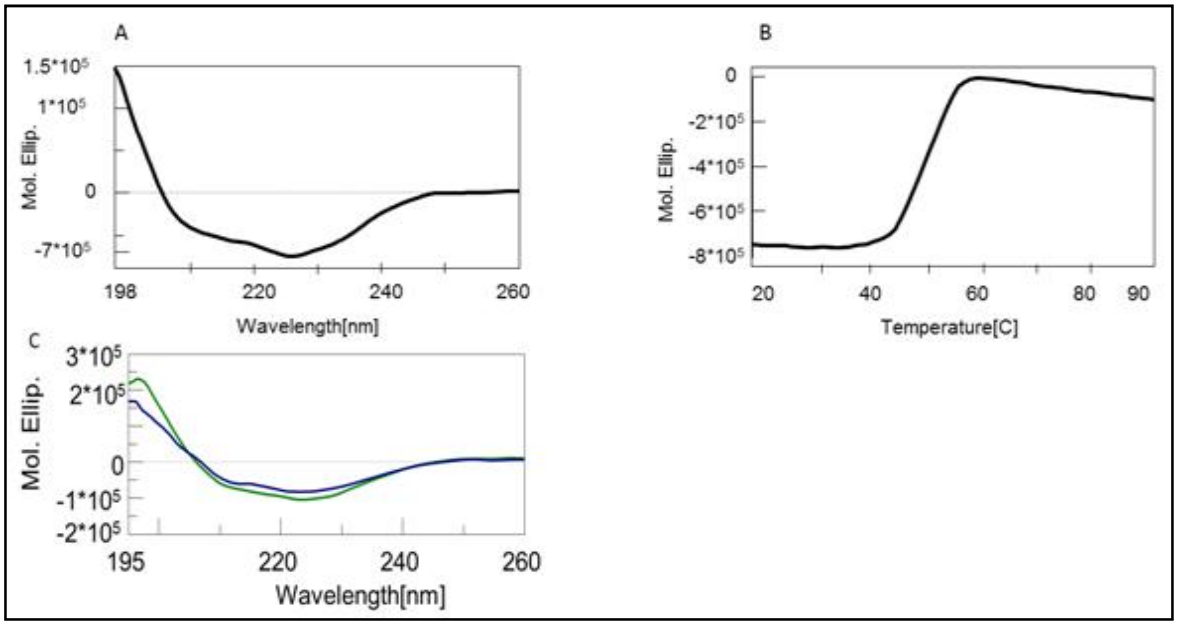

Figure 4.3: Characteristic far-UV CD spectra for CypA. (**B**) Thermal denaturation of CypA. CD signal was foll one at 222 nm in the temperature range 20-90°C. (**C**) Overlay of spectra at 20°C (green) and at 90°C (blue).

4.1.2 Cloning, overexpression and purification of GST-CypA

In order to perform NMR experiments, it was necessary to prepare the GST-CypA recombinant protein. In particular, *cypA* gene was cloned in the commercial expression vector pGEX-4T3. The purification of the chimeric protein was achieved by a step of affinity chromatography using a GSTrap column resin using 10 mM of reduced glutathione (GSH). The pulled fraction obtained by affinity chromatography was analyzed by SDS-PAGE (Figure 4.4 A, B).

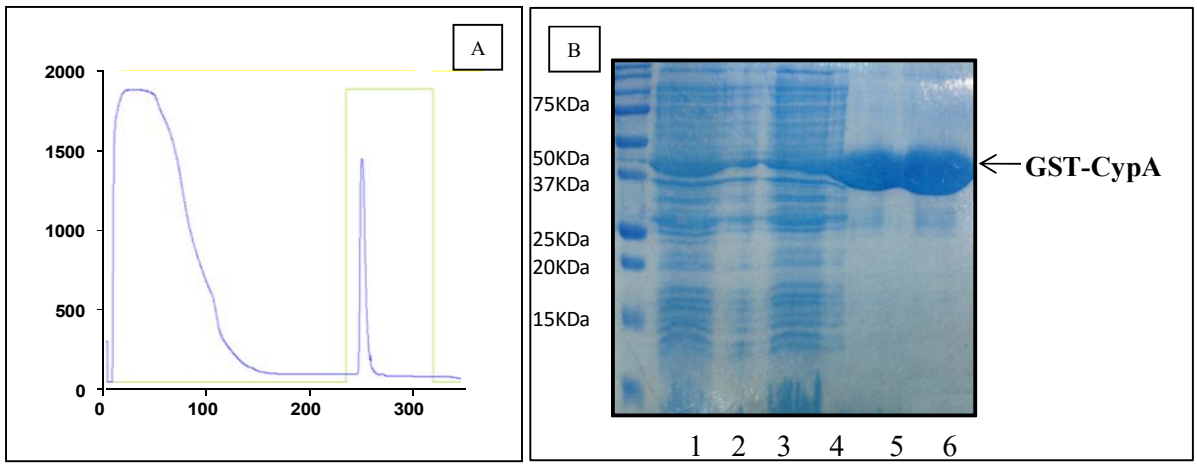

Figure 4.4 : Gst- CypA purification profile. (**A**) Affinity chromatography profile of the Gst-CypA (**B**) 15% SDS-page analysis after Gst-trap. Lane 1: Marker; Lane 2 to 4: flow through; Lanes 5 to 6 samples eluted at 10 mM of reduced glutathione.

A second step of purification by a Gel filtration on a Superdex 75 10/300 provided a highly pure protein (> 98%), as shown on SDS-PAGE (Figure 4.5).

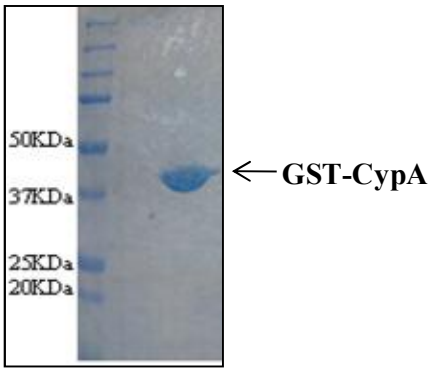

Figure 4.5: 15% SDS-page analysis after size exclusion chromatography of Gst-CypA: Lane 1: Marker; Lane 2: empty; Lane 3: Gst-CypA.

Indeed, the protein migrated as a protein of ~44 KDa compatible with the theoretical MW of GST-CypA.

4.1.3 AIF(370-394) preparation and structural characterization

The peptide AIF(370-394) (^{370}QSVGVSSGKLLIKLKDGRKVETDHI^{394}) was chemically synthesized using the Fmoc solid phase method [85] and purified by Reverse Phase (RP)-HPLC (Figure 4.6 A). Identity and purity of AIF(370-394) were assessed by LC-MS. (Figure 4.6 B).

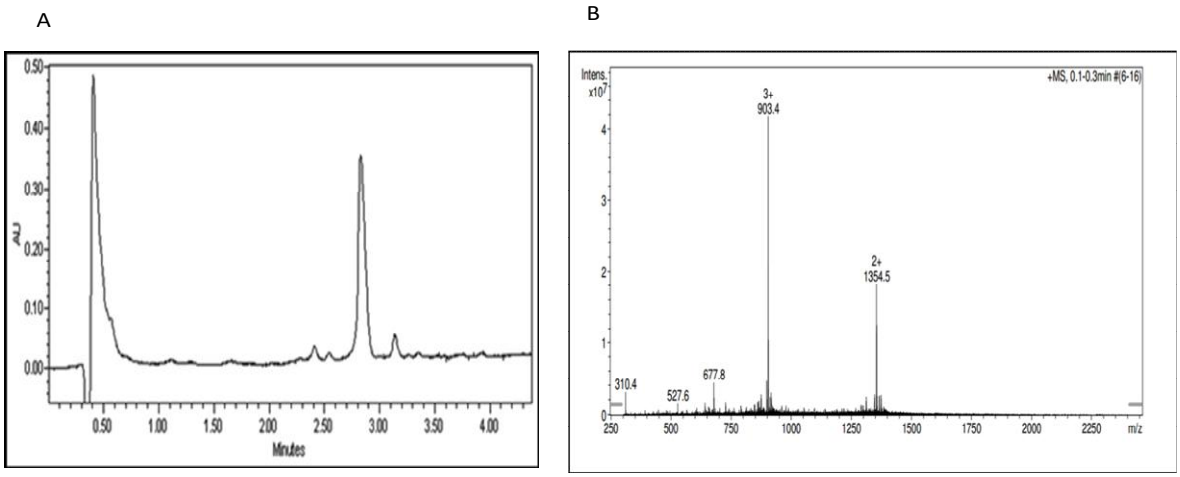

Figure 4.6:(**A**) Real time RP-HPLC chromatogram of AIF(370-394) peptide. Column: Onyx C18; eluent A: H2O with 0.1% TFA; eluent B: acetonitrile (ACN) with 0.1% TFA. Flow rate 0.6 mL/min. The gradient was from 5% to 70% eluent B in 5 minutes. (**B**) ESI mass spectrum of AIF(370-394) peptide.

The structural characterization of the isolated AIF(370-394) peptide was initially performed by CD. The CD spectrum of AIF(370-394) peptide in physiological conditions (5 mM

sodium phosphate buffer at pH=7.4), showed a minimum at 198 nm and a negative CD value at 190 nm, indicating the coexistence of several structures in which random coil conformations prevailed (Figure 4.7).

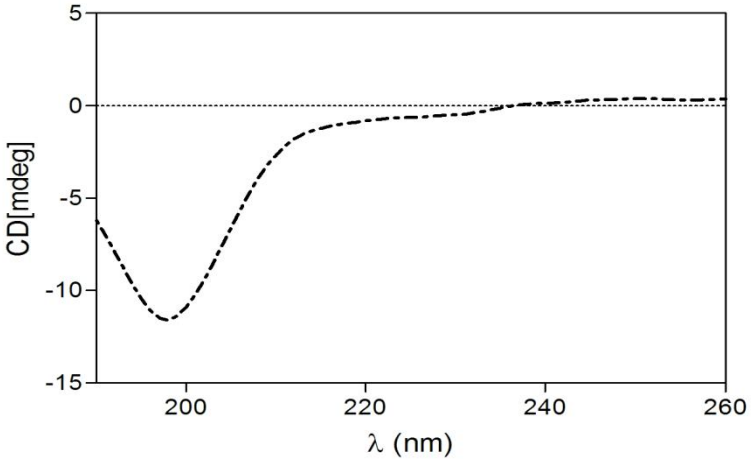

Figure 4.7: Representative CD spectrum of AIF(370-394) peptide in sodium phosphate buffer.

Moreover, to further investigate the propensity of these peptides to adopt ordered structures, we acquired CD spectra in the presence of different amounts of 2,2,2- trifluoroethanol (TFE), a solvent known for its ability to induce secondary structures [106].

As shown in Figure 4.8, CD spectra showed a limited increase of α-helical conformations in presence of TFE, as indicated by the gradual appearance of the canonical bands at 208 and 222 nm at high solvent concentration (up to 30%); this suggested only a partial increase of well-organized conformations of the peptide in solution.

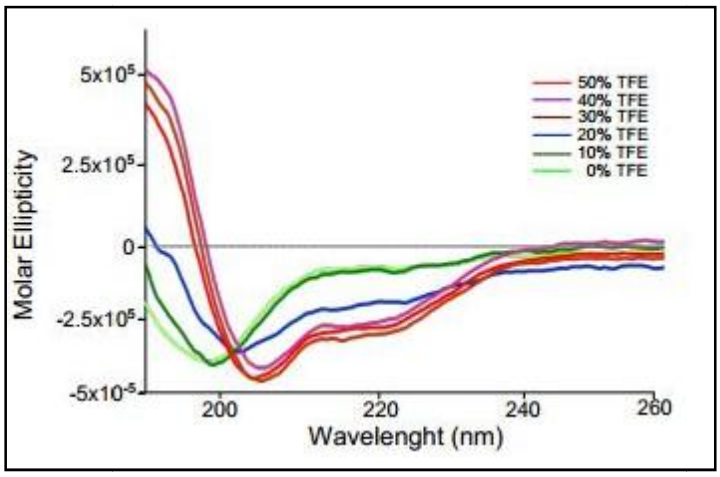

Figure 4.8: Overlay of far-UV CD spectra in 5 mM phosphate buffer, pH 7.4 of AIF(370-394) peptide at increasing concentrations of TFE.

The conformation of AIF(370-394) peptide in solution was also investigate by NMR studies developed in collaboration with the Dr.ssa Biancamaria Farina and the Professor Roberto

Fattorusso. Firstly, the resolution and dispersion of amide signals of the peptide was evaluated in different buffers, in order to choose the ideal condition.

In particular buffers tested were: 1) Tris-HCl 20 mM and 150 mM NaCl at pH = 7.5; 2) PBS 1X at pH = 7.4; 3) PBS 1X at pH = 5.8.

As possible to view, in Figure 4.9, the peptide showed sharper amide resonances in PBS buffer at pH 5.8 compared to the other conditions tested. For this reason, this buffer was chosen for the subsequent studies.

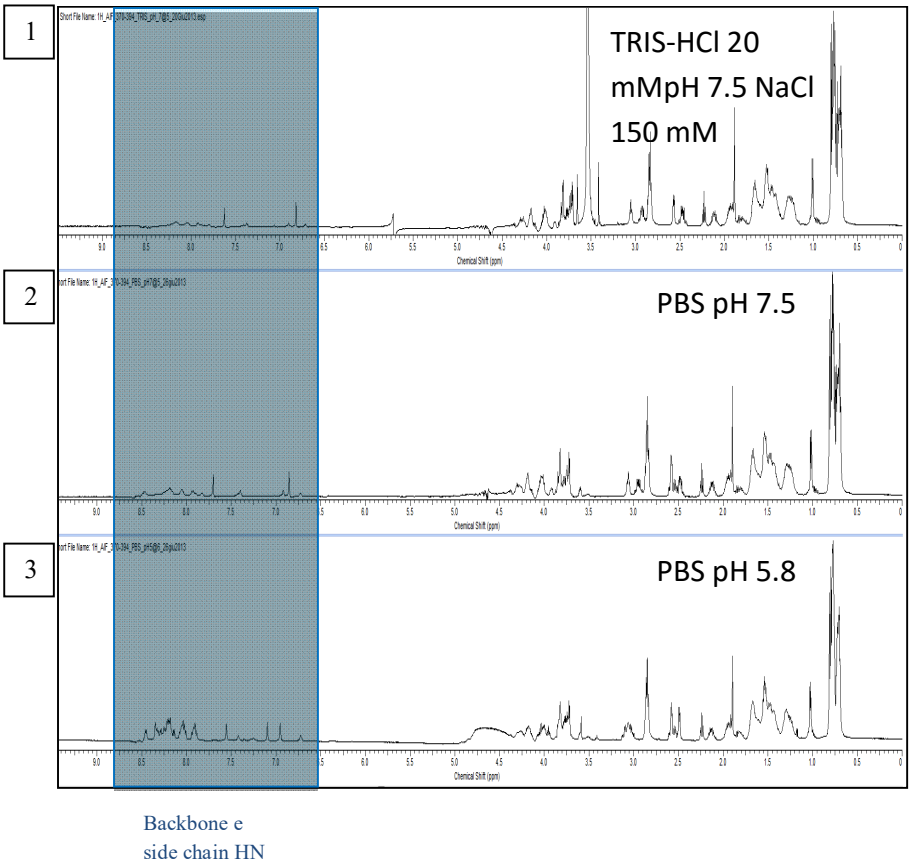

Figure 4.9: Buffer conditions tested to choose a better resolution for NMR studies.

An almost complete proton resonance assignment of AIF(370-394) was obtained using 2D [^{1}H, ^{1}H] TOCSY [94], NOESY [96] and COSY [95] spectra using the standard procedures [107].

The lack of a significant chemical shift dispersion, of long range NOEs indicated that AIF(370-394) was unstructured when alone in solution in agreement with CD data. However, several peculiarities are observed in the region 380-390.

Specifically, sequential H_N-H_N NOEs characteristic of α-helix- or turn-like conformation were observed between residues L^{380} and I^{381}, G^{386} and R^{387}, V^{389} and E^{390} (Figure 4.10 A).

Accordingly, the amide resonances of residues I^{381} and R^{387} exhibited large negative $\Delta\delta H_N$ and $\Delta\delta H_\alpha$ values consistent with a helix- or turn-like conformation (Figure 4.10 B). Nevertheless, large positive $\Delta\delta H_N$ and $\Delta\delta H_\alpha$ of E^{390}, together with strong sequential H_N-H_α NOEs between residues L^{380} and I^{381}, V^{389} and E^{390}, suggested that the peptide adopts a conformational ensemble containing also extended or β-strand-like conformations in these regions (Figure 4.10 B).

In addition, the $\Delta\delta H_N$ and $\Delta\delta H_\alpha$ protons of residues K^{382} and K^{388} showed also large positive shifts (Figure 4.10 B).

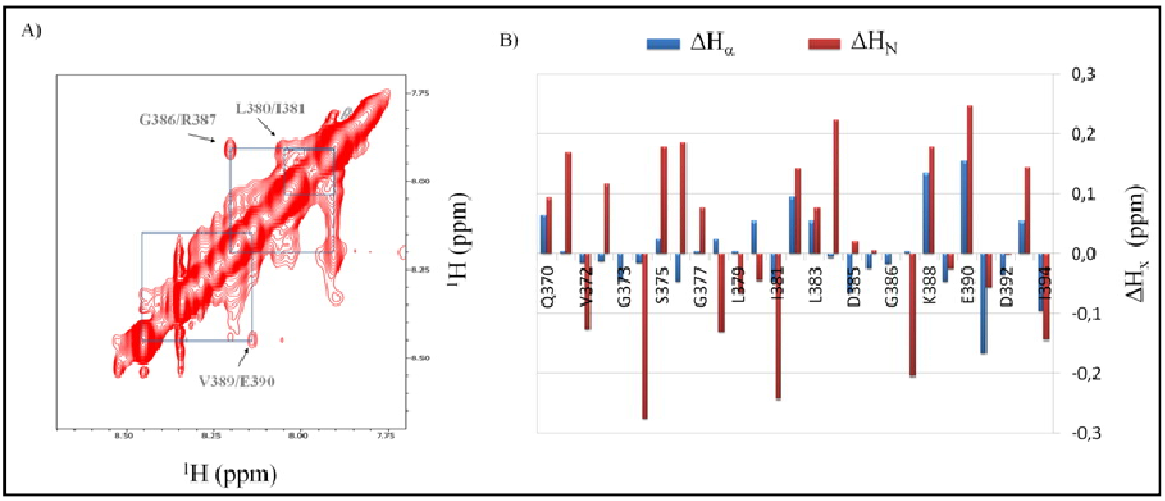

Figure 4.10 (A-B): NMR analysis of AIF(370-394) in PBS at pH 5.8 and H^N-H^N regionof 2D [^{1}H, ^{1}H] NOESY spectra **(A)**. Chemical shift deviation from random coil values of Hα and H^N backbone atoms plotted as a function of residue number (**B**). Secondary structure elements as observed in the AIF crystal structure (PDB ID: 1M6I) and as derived from the NMR conformational analysis in TFE 30%.

Overall, NMR data confirmed the elevated flexibility of AIF(370-394) peptide and the prevalence of disorder in aqueous solution, but highlighted a propensity of the peptide to adopt local secondary structure elements in the region 380-390.

To further asses the propensity of the peptide to assume partial secondary structure elements, we carried out a NMR conformational analysis in presence of TFE (30%) solvent. Accordingly to previous CD data, the 2D [^{1}H, ^{1}H] NOESY spectrum in presence of 30% TFE contains only a slightly higher number of signals with respect to those observed in PBS buffer, indicating only a limited increasing of ordered conformations (Figure 4.10 C).

This fact precluded a high-resolution structure determination. However, information on the conformational preferences can be obtained by $\Delta\delta H_N$ and $\Delta\delta H_\alpha$ and NOE pattern analysis. $\Delta\delta H_N$ and $\Delta\delta H_\alpha$ showed a stretch of strong negative values in the central region of the AIF(370-394) peptide, from K^{378} to L^{383}, indicative of a helical conformation (Figure 4.10

D), unlikely from the AIF protein in which they adopt a β-strand conformation.

According to $\Delta\delta H_N$ and $\Delta\delta H_\alpha$ values, new strong sequential H_N-H_N NOEs were observed in this region between residues I^{381}-K^{382}, L^{383}-K^{384}, D^{385}-G^{386} (Figure 4.10 C).

It is to note that possible H_N-H_N NOEs between K^{382}-L^{383}, K^{384}-D^{385} could not detected due to a partial or total overlap of the H_Ns. However, Hα-Hβ (i, i+3) were observed from S^{376} until to D^{385}, consistent with a α-helix conformation.

Negative ΔδHs were observed for the H_N, but not for the H_α, of the segment D^{385}-G^{386}-R^{387}, that in the AIF protein assumes a turn conformation (Figure 4.10 E).

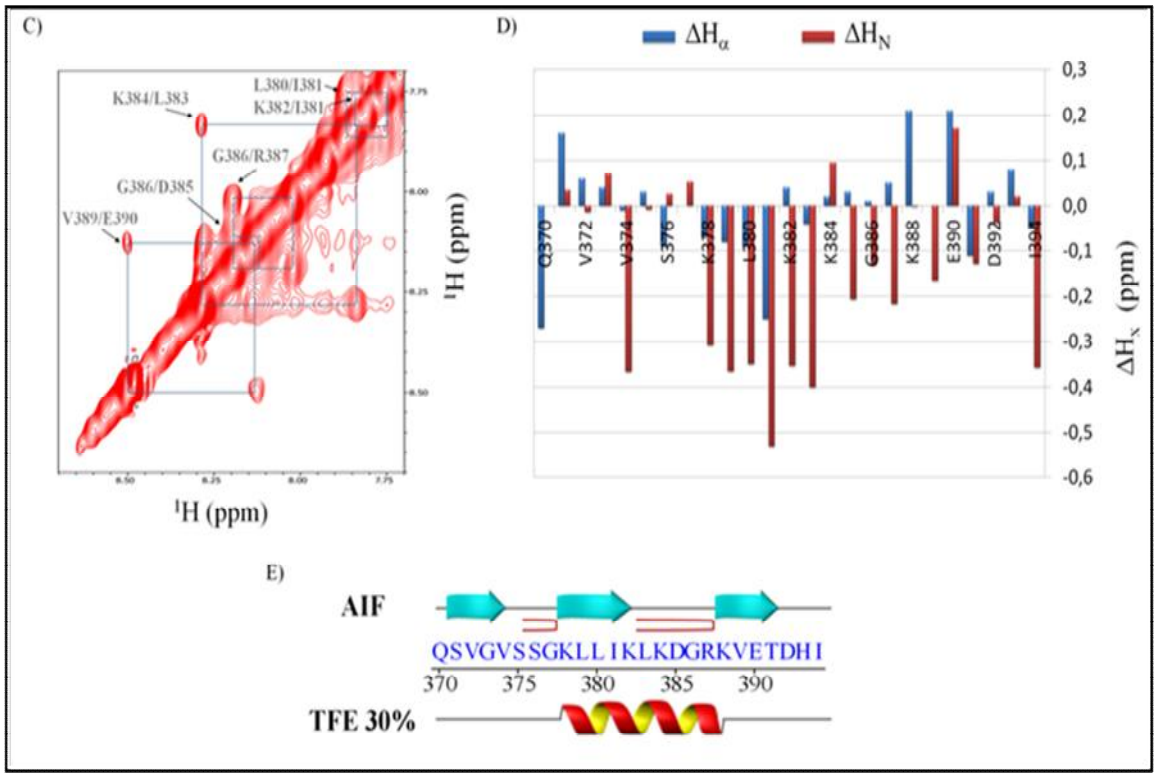

Figure 4.10 (C-E): NMR analysis of AIF(370-394) in PBS at pH 5.8 in presence of TFE 30%.H^N-H^N region of 2D [^{1}H, ^{1}H] NOESY spectra (**C**). Chemical shift deviation from random coil values of H_α and H^N backbone atoms plotted as a function of residue number (**D**). Secondary structure elements as observed in the AIF crystal structure (PDB ID: 1M6I) and as derived from the NMR conformational analysis in TFE 30% (**E**). Arrow and helix indicate β-strand and helical regions, respectively.

On the other hand, strong positive ΔδHs were observed for the H_α of K^{388} and H_N and H_α of E^{390}, indicative of a propensity of these residues to adopt an extended or β-strand conformation as in the AIF protein.

4.2 Conformational characterization of AIF(370-394) bound to CypA

The results obtained by NMR and CD analysis on the conformation of free AIF(370-394) peptide in solution are not surprising, since often small peptides in water are disordered and can assume a more organized structure only in presence of their binding partners [108]. To investigate whether the interaction of CypA with AIF(370-394) induced conformational changes on the peptide secondary structure, we next collected CD spectra on the complex using a solution containing 40 μM AIF(370-394) and 20 μM CypA.

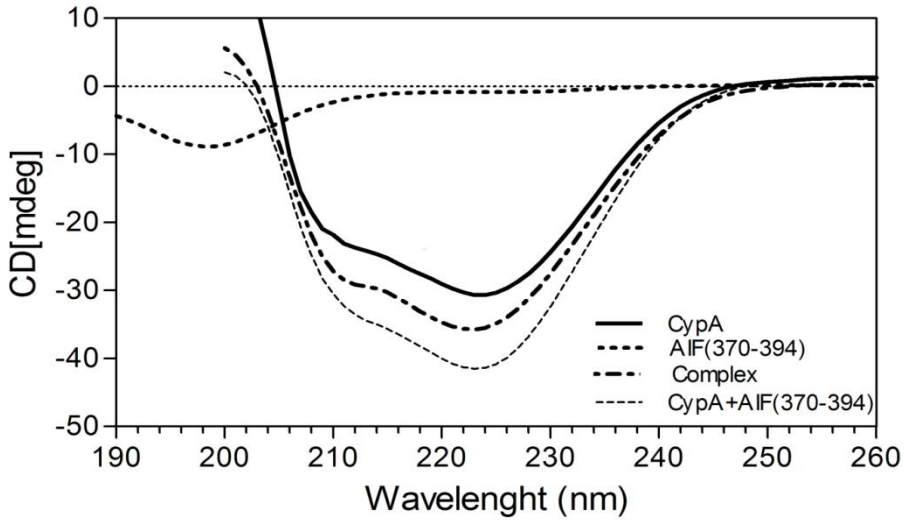

Figure 4.11: CD spectra of the sum of single spectra of AIF(370-394) peptide and CypA, compared to CypA/AIF(370-394) complex spectra.

As shown in Figure 4.11, the CD spectrum of the recombinant free CypA protein was characteristic of aroughly equal combination of β strands and α-helical protein with minima at 210 and 225 nm. Deconvolution of the secondary structure predicted a helical and beta/turn content of 45% and 37%, in agreement with previous data.

Therefore, the CD spectrum of CypA in complex with AIF(370-394) peptide, at molar ratio 1:2, revealed an increase of α-helical content (a helical and beta/turn content of 55% and 30%, respectively).

Indeed the sum of the individual spectra from CypA and AIF(370-394) peptide did not match the α-helical signal obtained with the complex, suggesting that CypA and/or AIF(370-394) increase their secondary structure content when they interact.

Because CypA is totally structured, we hypothesize that the gain in α-helical content occurs predominantly in AIF(370-394), indicating a disorder-to-order mode of interaction with CypA. To assess whether interaction with CypA influenced the peptide structure, we performed several attempts to observe trNOEs in NOESY spectra of AIF(370–394) in the

presence of substoichiometric amounts of CypA and/or GST-CypA. Unfortunately, the conformation of the peptide bound to CypA could not be determined because of the lack of a sufficient number of trNOEs, probably because of a slow off-rate of the peptide from the CypA. However, we could observe several differences in the NOESY of the peptide in the presence of GST-CypA (1:150 ratio) than that in the absence of the protein, for residues: K^{378}, K^{382}, L^{383}, K^{384}, R^{387}, K^{388}, E^{390}, T^{391}. Minor trNOE effects were also observed for residues: S^{371}, V^{374}, S^{375} and L^{380}.

4.3 CypA/AIF(370-394) binding studies

The interaction between recombinant His6tagged CypA protein and the AIF(370-394) synthetic peptide was monitored by means of Isothermal Titration Calorimetry (ITC) [109] and the label free techniques [91].

In Figure 4.12, a representative raw titration data and results of the data after integration and fitting with an appropriate model is shown.

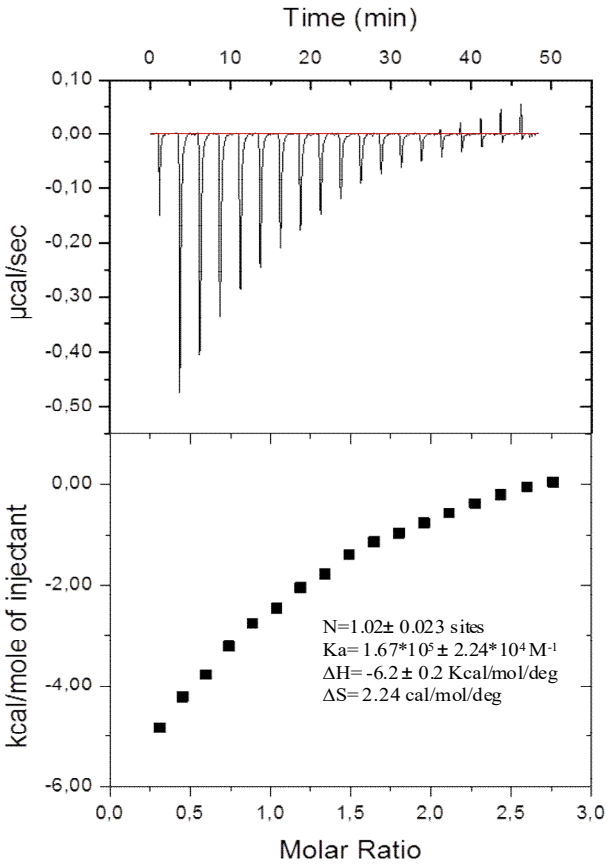

Figure 4.12. (**A**) Raw data for the titration of CypA with AIF(370-394) peptide. Each peak represents the differential power decrease as the sample cell temperature increases with each peptide addition, characteristic of an exothermic binding interaction. (**B**) Data is fit with a one set of single binding sites model to give the thermodynamic parameters shown in the inset.

ITC profiles showed that the binding of the AIF(370-394) to CypA was exothermic, resulting in negative peaks in the plots of power versus time (Figure 4.12 A, upper panel). Signals well fitted with a single site binding model to determine the KD, enthalpy (ΔH) and entropy (ΔS) changes of the binding reaction (Figure 4.12 B, lower panel).

Results obtained confirmed that AIF(370-394) binds CypA with a KD of about 6 μM through a favorable contribute of entropy and enthalpy, suggesting that the AIF(370-394)/CypA complex formation was not only driven by a large entropy gain (TΔS = 56 ± 1.5 cal/mol) presumably due to the high degree of freedom of the peptide but also by means of hydrogen bonding and/or van der Waals and Coulombic interactions (ΔH = -6.2 ± 0.2 kcal/mol).

Moreover, the binding constant underlying the interaction between AIF(370-394) and CypA was determined through a new label-free technique based on Corning Epic technology (See Methods section, for details) [91].

For this experiment, CypA was immobilized at a concentration of 200 μg/ml onto the amino-coupling surface of the EnSpire label-free biochemical microplate biosensor.

After washout of the unbound target and further equilibration of the biosensor, several concentrations of AIF(370-394) peptide were added to the immobilized CypA protein.

The background-corrected responses were well fitted by a one-site interaction model, yielding a K_D= 4.7 ± 0.2μM, comparable with the data previously reported (Figure 4.13) [71].

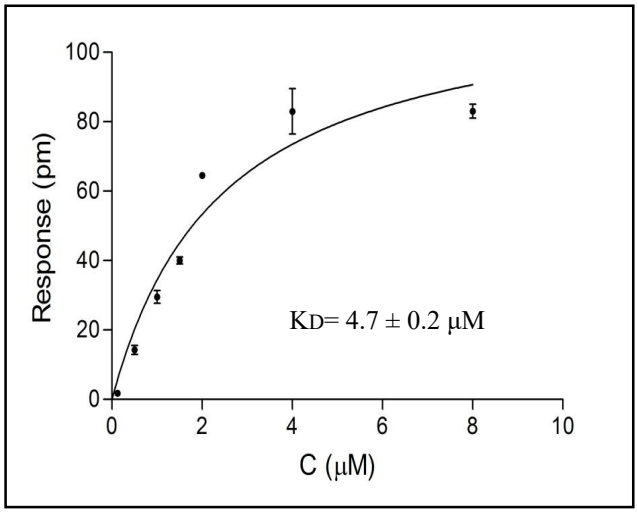

Figure 4.13 :Binding curve of AIF(370-394)peptide to CypA, through Label-free Corning® Epic® technology

4.4 STD Experiments of AIF(370-394)/CypA complex

To provide additional information regarding the peptide mode of binding, STD-NMR experiments were performed. The STD-NMR technique is a method which could give an epitope mapping by NMR spectroscopy.

Saturation Transfer Difference (STD)-NMR experiments have emerged as a powerful tool for detecting and characterizing binding of ligands to proteins and receptors [110, 111].

In these experiments, the protein resonances are selectively saturated, and the effect is transferred to the bound ligand by intermolecular spin diffusion.

Saturated resonances of the ligand in the free state are detected by subtracting the saturated spectrum from one without protein saturation.

The difference in intensity due to saturation transfer constitutes an indication of binding and allows to identify the residues of the ligand directly involved in the interaction with the protein.

Since the sensitivity of the STD experiments is dependent from the spin diffusion efficiency that increases with increasing molecular weight of the target protein, we decided to use GST-fused CypA [112].

A one-dimensional ^{1}H STD difference experiment is shown in Figure 4.14 for a sample, with a 150:1 excess of the peptide ligand over the GST-CypA, along with a reference ^{1}H spectrum.

As can be seen, some resonances both in the aliphatic and in the amide region receive saturation transfer from the protein, providing a further confirm of the AIF(370-394)/CypA complex formation and insight on the residues directly involved in the interaction with CypA.

Specifically, in the upfield region, the strongest STD signals were ascribed to the Hε, Hδ, Hγ and Hβ protons of K residues, the D^{385} Hβ protons and the T^{391} Hγ proton. Moreover, methyl protons of I^{381}, V^{389} or L^{380} residues showed saturation transfer from the protein, even if they could not identify unambiguously due to the spectral overlap.

In the downfield region, STD signals were observed for some H_N backbone atoms. However, except for the H_N of Leu^{383}, they could not be identified unambiguously.

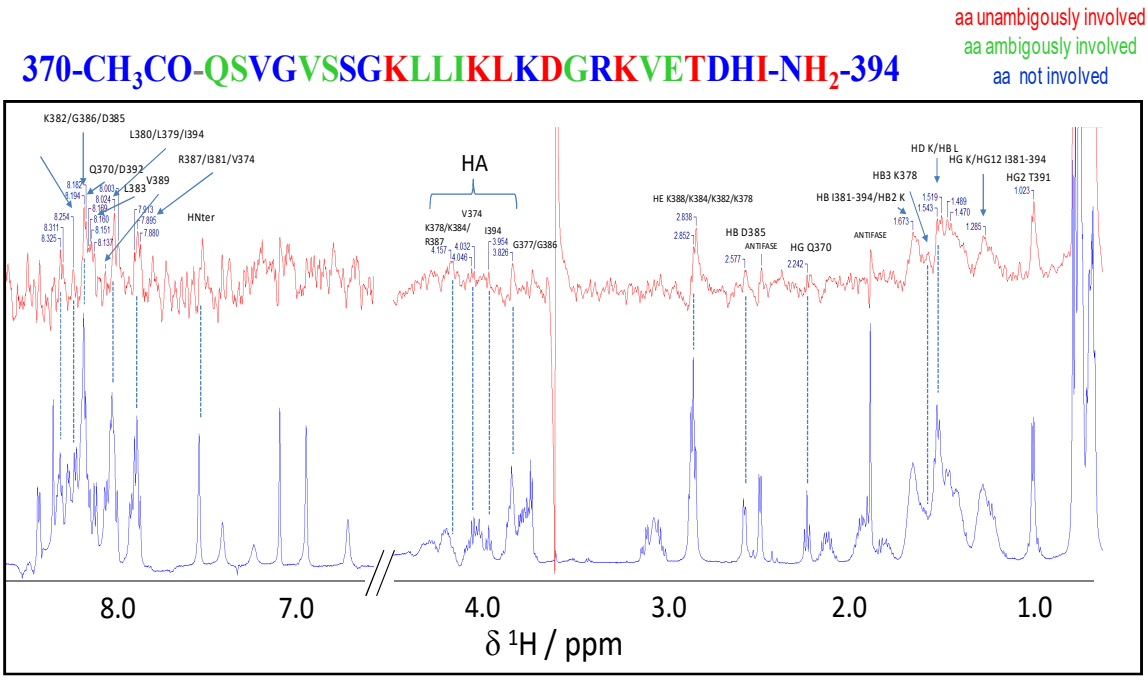

Figure 4.14: STD experiments of complex AIF(370-394)/CypA: in red residues more involved in the interaction with CypA; in green residues that could be involved in the interaction, but that could not be identified unambiguously; in blue residues not involved in the interaction.

Data obtained showed that several residues arranged along the sequence of the peptide seem to be involved in the interaction with CypA; however, in agreement with trNOESY experiments, most of them are included in the central region, encompassing residues 380-390 (Figure 4.14). Thus, based on these results was synthesized a new smaller peptide, that cover the region 380-390, hereafter AIF(380-390).

4 5 Design and characterization of a new bioactive AIF peptide

STD-NMR analysis provided crucial information about the amino acid residues of the peptide AIF(370-394) involved in the interaction with CypA.

Data indicated that many residues along the entire peptide sequence mediate the interaction with CypA. Most of them were arranged on the peptide central portion containing residues 380-390.

Notably, in the crystallographic structure of AIF this region is in a β-hairpin conformation [103] (Figure 4.15 A, B).

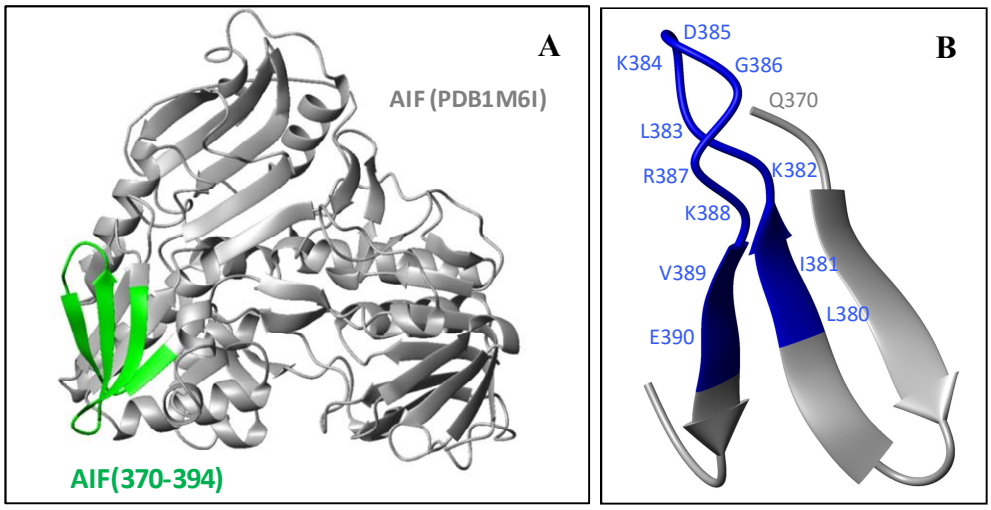

Figure 4.15: (**A**) Crystallographic structure of AIF protein (PDB ID: 1M6I); in green is reported the region AIF(370-394).(**B**) Zoom of the AIF(380-390) region which in the crystallographic structure shows a of β-hairpin conformation.

On the basis of these observations, we focused our attention on residues 380-390 and started to investigate the corresponding synthetic peptide.

The new peptide was synthesized with two cysteine residues (Cys) at the amino- and carboxy-termini to potentially stabilize a β-harpin structure through a disulfide bridge [113]. AIF(380-390) (C^{380}LIKLKDGRKVE^{390}C) was synthesized and characterized in its reduced (linear) and oxidized (cyclic) forms (see Methods section for details).

The structural analysis of the linear AIF(380-390)red and cyclic AIF(380-390)ox peptides was carried out by CD in 5 mM phosphate buffer at pH 7.4 (Figure 4.16).

CD spectra suggested the prevalence of unstructured conformations in solution for either peptides.

However, spectra demonstrated that the introduction of the disulfide bridge in the cyclic peptide, provided a limited but measurable increase of secondary structure, as indicated by the shift of the CD minimum from 198 nm to 202 nm, for AIF(380-390)ox compared to AIF(380-390)red.

AIF(380-390)ox had a minimum at 198 nm and a negative value at 190 nm, suggesting the coexistence of several structures in which random coil conformations prevailed, as previously shown also for AIF(370-394).

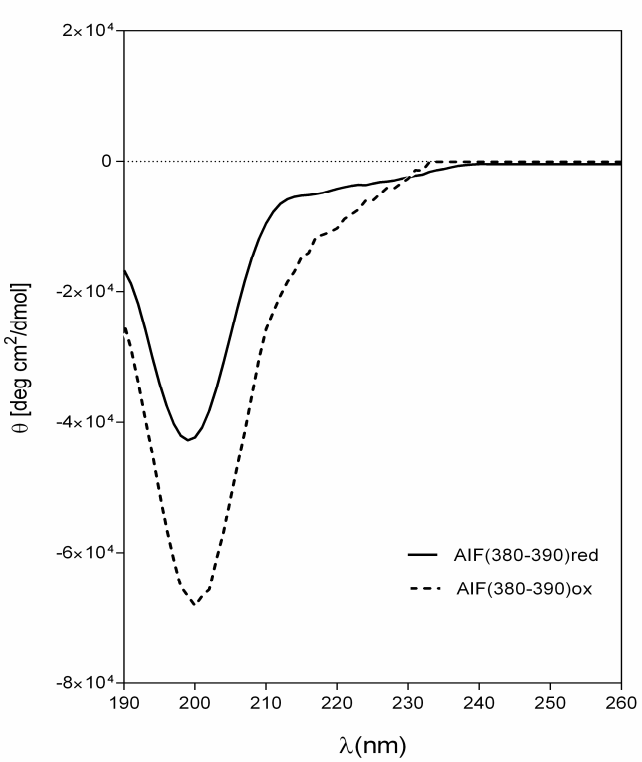

Figure 4.16: CD spectra of AIF(380-390)red and AIF(380-390)ox.

These data are also in agreement with a preliminary NMR analysis of AIF(380-390) in the oxide state, in which the presence of different, likely conformational, states for this peptide was observed.

Moreover, the complexity of the NMR spectra (data not shown) precluded a detailed NMR conformational analysis of this peptide.

4.6 CypA/AIF(380-390) binding studies

The affinity of both the linear and cyclic peptides for CypA was evaluated by direct-binding assays.

Synthetic peptides were then tested by the label-free Corning® Epic® technology (see Methods for details). As shown, in Figure 4.17 A and B, either variants bound CypA in a dose-dependent and saturable manner.

However, by fitting the binding curves with a non-linear regression algorithm, very different affinity values were extrapolated. Indeed AIF(380-390)red and AIF(380-390)ox bound CypA with K_Ds of 30 ± 2μM and 3.2 ± 0.2μM, respectively, suggesting an overall higher affinity of the cyclic peptide.

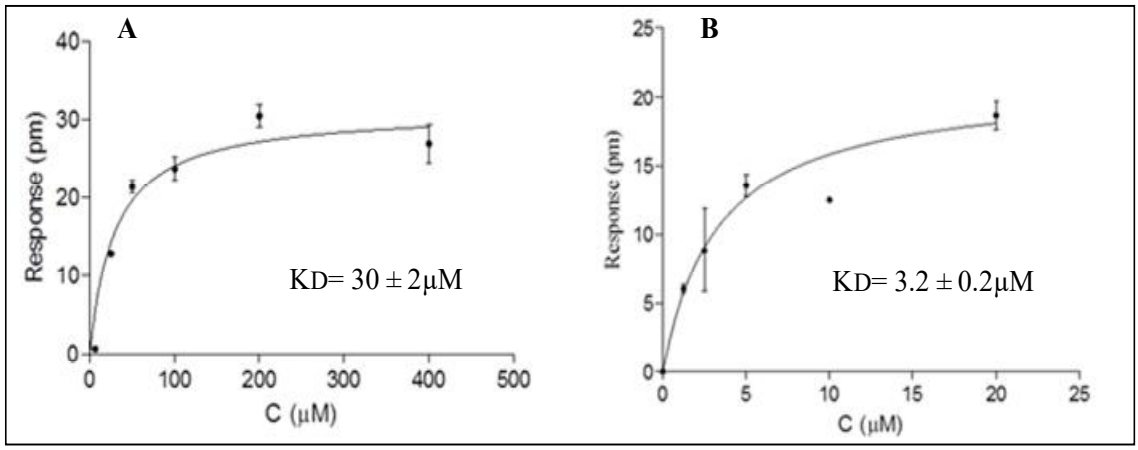

Figure 4.17: (**A**) Binding curve of AIF(380-390)ox peptide to CypA. (**B**) Binding curve of AIF(380-390)ox peptide to CypA using the Label-free Corning® Epic® technology.

All data demonstrated that reducing the size of AIF (370-394) to AIF(380-390) resulted in a significant loss of the peptide affinity toward CypA, however the introduction of the disulfide bridge restored the affinity to comparable levels, demonstrating a direct correlation between the structure and the function of the new peptide.

4.7 Identification of crucial residues of AIF(380-390)ox involved in CypA recognition: Alanine-scanning approach

In order to investigate crucial residues of AIF(380-390)ox involved in CypA recognition, we synthesized and analyzed Ala-scan peptides of this region [88].

By this approach,the wild-type residues are systematically changed to alanine.

The peptides were synthesized using the Fmoc solid phase method [85] and purified by Reverse Phase (RP)-HPLC (See Methods section for details).

Sequence, theoretical and experimental MW of the peptides are reported in Table 4.1, shown below.

Name	Sequence	Theoretical Mass (amu)	Experimental Mass (amu)
AIF(380-390)ox	CLIKLKDGRKVEC	1545.87	1545.65
ALA 1	C**A**IKLKDGRKVEC	1503.79	1503.49
ALA 2	CL**A**KLKDGRKVEC	1503.79	1503.38
ALA 3	CLI**A**LKDGRKVEC	1488.77	1488.15
ALA 4	CLIK**A**KDGRKVEC	1503.79	1503.22
ALA 5	CLIKL**A**DGRKVEC	1488.77	1488.35
ALA 6	CLIKLK**A**GRKVEC	1501.86	1501.16
ALA 7	CLIKLKD**A**RKVEC	1559.90	1560.22
ALA 8	CLIKLKDG**A**KVEC	1460.76	1460.28
ALA 9	CLIKLKDGR**A**VEC	1488.77	1488.32
ALA 10	CLIKLKDGRK**A**EC	1517.82	1517.52
ALA 11	CLIKLKDGRKV**A**C	1487.83	1487.32

Table 4.1: Sequences, theoretical and experimental mass of Ala-mutated peptides.

Their binding abilities of all peptides to CypA were evaluated through the label free techniques.

For this assay, CypA was immobilized at a concentration of 200 μg/ml onto the amino-coupling surface of the EnSpire label-free biochemical microplate biosensor and Ala peptides were initially tested at two different concentrations (10 and 20 μM) (Figure 4.18).

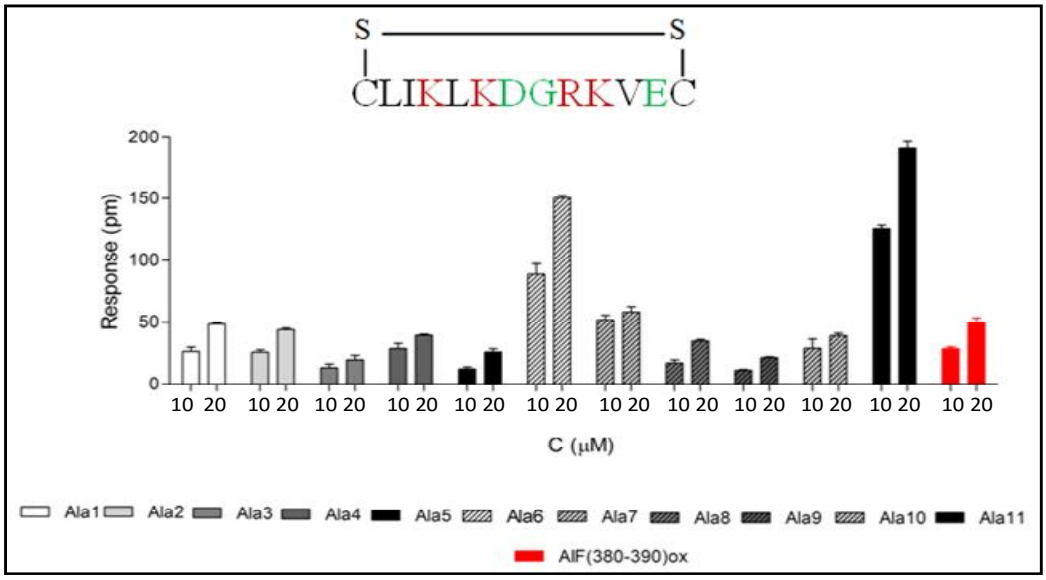

Figure 4.18: Enspire binding assay to immobilized CypAof Ala-peptides at two different concentrations (10 and 20 μM).

Data shown in Figure 4.18 suggested that peptides with alanines in place of K^{382}, K^{384}, R^{387} and K^{388} had lower affinity, while those having alanines replacing L^{380}, I^{381}, L^{383} and V^{389} had substantially unaltered binding affinities.

Remarkably, peptides where D^{385}, G^{386} and E^{390} were replaced with alanine had higher affinity for CypA.

Altogether data suggested that basic residues strongly influence the ability of AIF(380-390)ox to recognize CypA.

4.8 From AIF(380-390)ox to AIF(381-389)ox

Combining NMR and an Ala-scanning approach we ended up that residues Leu^{380} and E^{390} have a negligible effect on the binding with CypA.

For this reason, to further simplify the peptide structure, we designed and synthesized a new peptide spanning residues 381-389 still constrained by a disulfide bridge connecting two Cys at N- and C- termini.

The new peptide, hereafter AIF(381-389)ox, was studied by direct binding experiments to CypA and bound the target protein in a dose-dependent and saturable manner, showing a K_D of 2.3 ± 0.5μM.

The K_D was comparable to that of AIF(380-390)ox, indicating that deleting the two residues at N- and C- termini did not affect the interaction with CypA, as previously hypothesized (Figure 4.19).

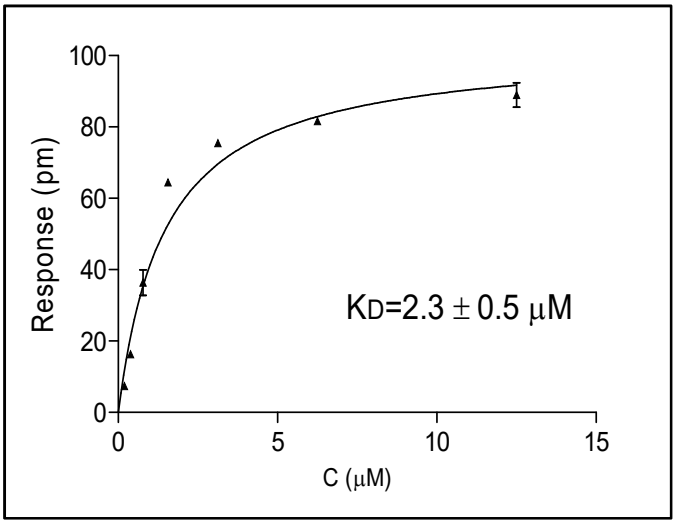

Figure 4.19: Binding curve of AIF(381-389)ox peptide to CypA.

4.9 Biological effects of peptides in HT-22 cells

Next, we investigated whether the peptide AIF(381-389)ox could antagonizes the detrimental effect of the AIF/CypA complex, in the model of glutamate toxicity.

The model of cell death chosen was the neuronal HT-22 cell line. In these cells treatment with high concentrations of glutamate (2-7mM) induces a cell death process exclusively mediated by the nuclear translocation of AIF [92].

Then, HT-22 cells were transfected with the synthetic peptides AIF(370-394), AIF(380-390)ox, AIF(380-390)red, AIF(381-389)ox at 50μM, using the Pro-Ject transfection kit (Thermo Scientific).

Following glutamate treatment at three different concentrations (5, 6 and 7 mM for 16h), cell viability was assessed by the MTT assays.

As shown in Figure 4.20, all peptides tested provided neuroprotection, however the cyclic peptides AIF(380-390)ox and AIF(381-389)ox provided a greater neuroprotective effect compared to AIF (370-394) and peptides in linear forms.

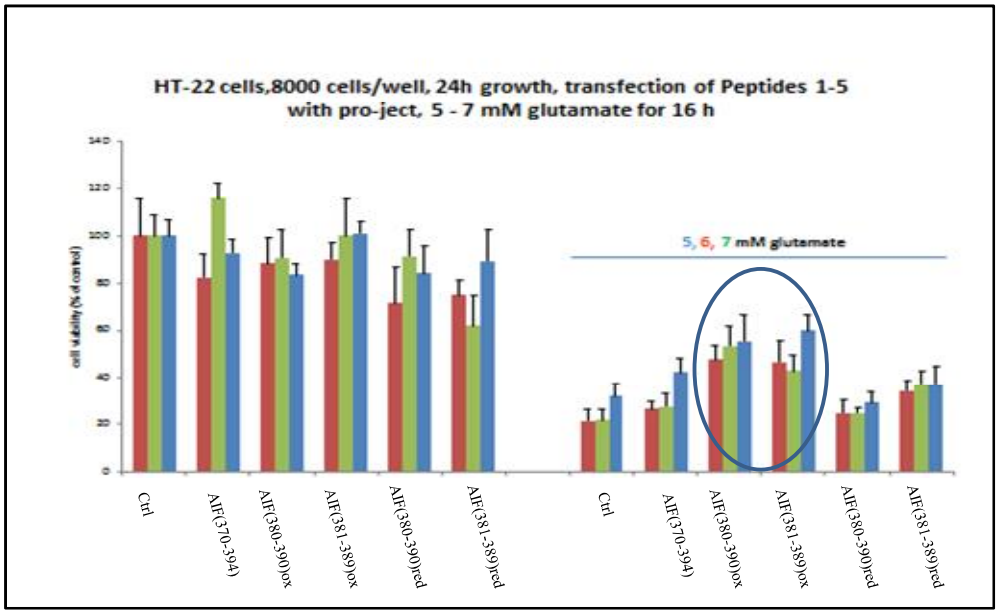

Figure 4.20: Neuroprotective effects of the different AIF peptides in the glutamate-induced HT-22 cellular model. Results obtained were showed as percentage of controls considered to be 100% and represent the mean ±S.D. of at least four independent experiments performed in quadruplicate.

4.10 NMR studies on AIF(381-389)ox and its interaction with CypA

Since the ability of the AIF(381-389)ox to bind CypA with a comparable affinity than the peptide AIF (370-394), together with its greater neuroprotective effect, we performed a detailed NMR analysis. In particular, a conformational analysis of AIF(381-389)ox was first carried out, then interaction studies based on the observation of both the peptide (STD experiments) and the CypA protein (Chemical shift perturbation analysis, CSP) were performed. Data NMR were used to developed a docking-model of the complex between CypA and AIF(381-389)ox.

4.10.1 NMR conformational analysis of AIF(381-389)ox

AIF(381-389) peptide NMR conformational analysis was performed in PBS at pH 5.8, as for AIF(370-394) peptide, both in the reduced and in the oxidized form. Under this condition, the peptide resulted well soluble with sharp resonances and, especially, showed a single signal set for each amino acid in both forms (Figure 4.21 and 4.22).

These results indicated that AIF(381-389) peptide exists in a homogeneous state differently from AIF(380-390), supporting the hypothesis that the heterogeneity observed for AIF(380-390) is due to different salt bridge that the negatively charged carboxyl group of E^{390} could establish with the positively charged ε-amino group of the different lysine along the sequence.

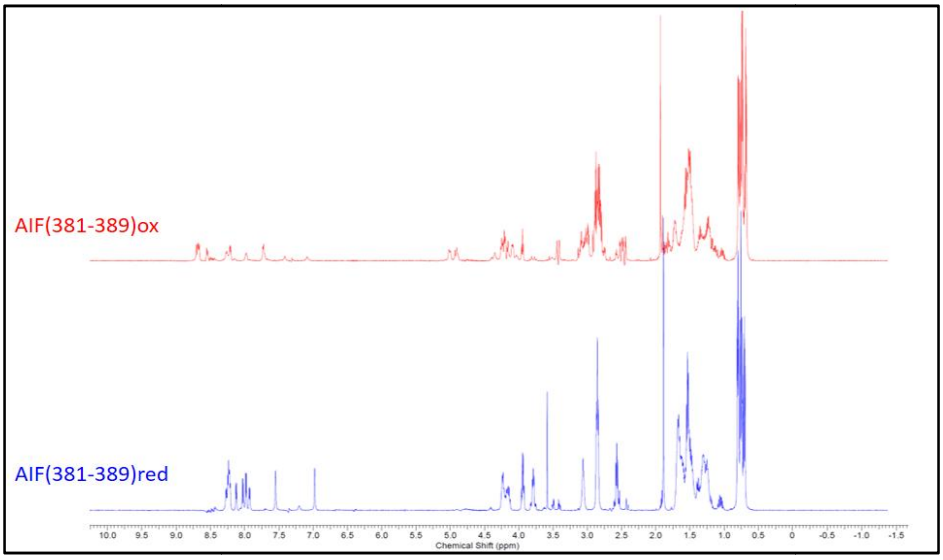

Figure 4.21: 1D^{1}H NMR spectra of AIF(381-389)red and AIF(381-389)ox in PBS at pH 5.8 ad 298K.

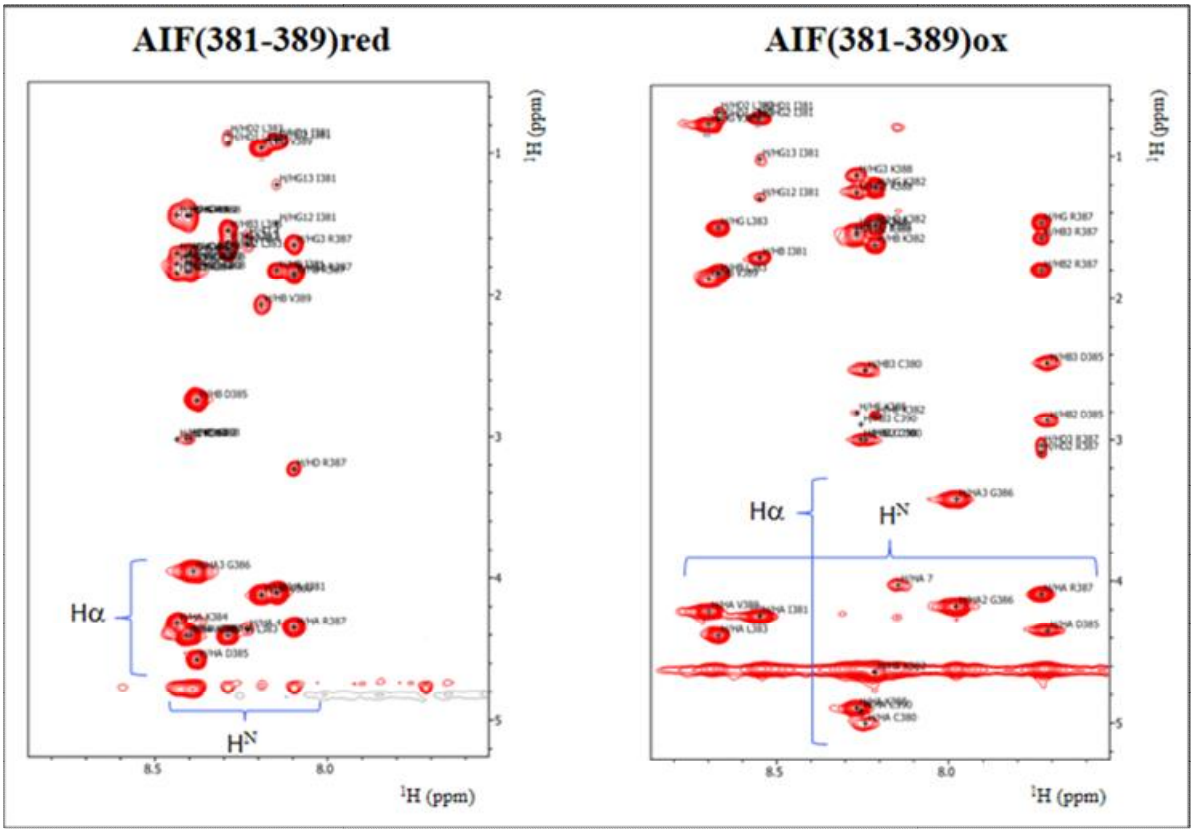

Figure 4.22: 2D [^{1}H, ^{1}H] TOCSY NMR spectra of AIF(381-389)red and AIF(381-389)ox in PBS at pH 5.8 ad 298K. The highest spread of H^N and Hα protons is clearly visible in the spectrum of AIF(381, 389)ox, indicative of its structuration.

Proton spin system identification and assignment of individual resonances of both AIF(381-389) were carried out by using a combination of TOCSY, [94] COSY, [95] and NOESY spectra, [96] according to the standard procedures [107].

Proton chemical shifts for all resonances are listed in Table 4.2 and 4.3.

Residue		Atom name	Chemical shift value	Residue		Atom name	Chemical shift value
381	ILE	H	8.15	384	LYS	HE3	3.02
381	ILE	HA	4.10	384	LYS	HZ	7.85
381	ILE	HB	1.83	385	ASP	H	8.38
381	ILE	HG12	1.50	385	ASP	HA	4.58
381	ILE	HG13	1.22	385	ASP	HB2	2.74
381	ILE	HG2	0.91	385	ASP	HB3	2.74
381	ILE	HD1	0.90	386	GLY	H	8.39
382	LYS	H	8.41	386	GLY	HA3	3.95
382	LYS	HA	4.41	387	ARG	H	8.10
382	LYS	HB2	1.83	387	ARG	HA	4.35
382	LYS	HB3	1.77	387	ARG	HB2	1.86
382	LYS	HG2	1.44	387	ARG	HB3	1.86
382	LYS	HG3	1.44	387	ARG	HG2	1.84
382	LYS	HD2	1.72	387	ARG	HG3	1.65
382	LYS	HD3	1.72	387	ARG	HD2	3.23
382	LYS	HE2	3.02	387	ARG	HD3	3.23
382	LYS	HE3	3.02	387	ARG	HE	7.37
382	LYS	HZ	7.71	388	LYS	H	8.40
383	LEU	H	8.29	388	LYS	HA	4.40
383	LEU	HA	4.41	388	LYS	HB2	1.83
383	LEU	HB2	1.68	388	LYS	HB3	1.77
383	LEU	HB3	1.55	388	LYS	HG2	1.44
383	LEU	HG	1.63	388	LYS	HG3	1.44
383	LEU	HD1	0.93	388	LYS	HD2	1.70
383	LEU	HD2	0.87	388	LYS	HD3	1.70
384	LYS	H	8.44	388	LYS	HE2	3.02
384	LYS	HA	4.32	388	LYS	HE3	3.02
384	LYS	HB2	1.84	388	LYS	HZ	7.71
384	LYS	HB3	1.78	389	VAL	H	8.19
384	LYS	HG2	1.44	389	VAL	HA	4.12
384	LYS	HG3	1.44	389	VAL	HB	2.07
384	LYS	HD2	1.70	389	VAL	HG1	0.96
384	LYS	HD3	1.70	389	VAL	HG2	0.96
384	LYS	HE2	3.02				

Table 4.2: ^{1}H Chemical shift assignment (ppm) of AIF(381-389)red in PBS buffer (pH 5.8) at 298 K.

Residue		Atom name	Chemical shift value	Residue		Atom name	Chemical shift value
380	CYS	H	8.37	385	ASP	H	7.84
380	CYS	HA	5.14	385	ASP	HA	4.48
380	CYS	HB2	3.13	385	ASP	HB2	2.99
380	CYS	HB3	2.64	385	ASP	HB3	2.59
381	ILE	H	8.68	386	GLY	H	8.11
381	ILE	HA	4.37	386	GLY	HA2	4.31
381	ILE	HB	1.84	386	GLY	HA3	3.55
381	ILE	HG12	1.42	387	ARG	H	7.86
381	ILE	HG13	1.15	387	ARG	HA	4.22
381	ILE	HG2	0.86	387	ARG	HB2	1.93
381	ILE	HD1	0.81	387	ARG	HB3	1.71
382	LYS	H	8.34	387	ARG	HG2	1.60
382	LYS	HA	4.77	387	ARG	HG3	1.60
382	LYS	HB2	1.75	387	ARG	HD2	3.22
382	LYS	HB3	1.75	387	ARG	HD3	3.17
382	LYS	HG2	1.35	388	LYS	H	8.40
382	LYS	HG3	1.35	388	LYS	HA	5.03
382	LYS	HD2	1.62	388	LYS	HB2	1.69
382	LYS	HD3	1.62	388	LYS	HB3	1.67
382	LYS	HE2	2.96	388	LYS	HG2	1.38
382	LYS	HE3	2.96	388	LYS	HG3	1.26
383	LEU	H	8.80	388	LYS	HD2	1.64
383	LEU	HA	4.51	388	LYS	HD3	1.64
383	LEU	HB2	1.95	388	LYS	HE2	2.94
383	LEU	HB3	1.95	388	LYS	HE3	2.94
383	LEU	HG	1.63	389	VAL	H	8.83
383	LEU	HD1	0.87	389	VAL	HA	4.34
383	LEU	HD2	0.81	389	VAL	HB	1.99
384	LYS	H	8.27	389	VAL	HG1	0.90
384	LYS	HA	4.08	389	VAL	HG2	0.90
384	LYS	HB2	1.85	390	CYS	H	8.38
384	LYS	HB3	1.85	390	CYS	HA	5.05
384	LYS	HG2	1.48	390	CYS	HB2	3.13
384	LYS	HG3	1.48	390	CYS	HB3	3.02
384	LYS	HD2	1.69				
384	LYS	HD3	1.69				
384	LYS	HE2	3.00				
384	LYS	HE3	3.00				

Table 4.3: ^{1}H Chemical shift assignment (ppm) of AIF(381-389)ox in PBS buffer (pH 5.8) at 298 K.

Analysis of Hα and H^N chemical shifts indicate that AIF(381-389)ox, differently from AIF(381-389)red, show significant deviations from random coil values (ΔδHα and $\Delta\delta H^N$) (Figure 4.23).

As shown in Figure 4.23, ΔδHα and $\Delta\delta H^N$of AIF(381-389)ox indicated the presence of two β-strands consisting of residues C^{380}-L^{383} and K^{388}-C^{390} separated by a turn constituted by residues K^{384}-R^{387}. This folded structure was confirmed by NOEs (Figure 4.24), indeed while AIF(381-389)red shows few and positive NOEs, typical of small and flexible molecules, AIF(381-389)ox exhibits a higher number and negative NOEs, characteristic of a more rigid structure.

However, the number of NOEs was not sufficient to obtain a high resolution structure of this peptide. Further NMR experiments also in different conditions could be addressed to increase the number of NOE to undertake the NMR structure calculation of AIF(381-389)ox.

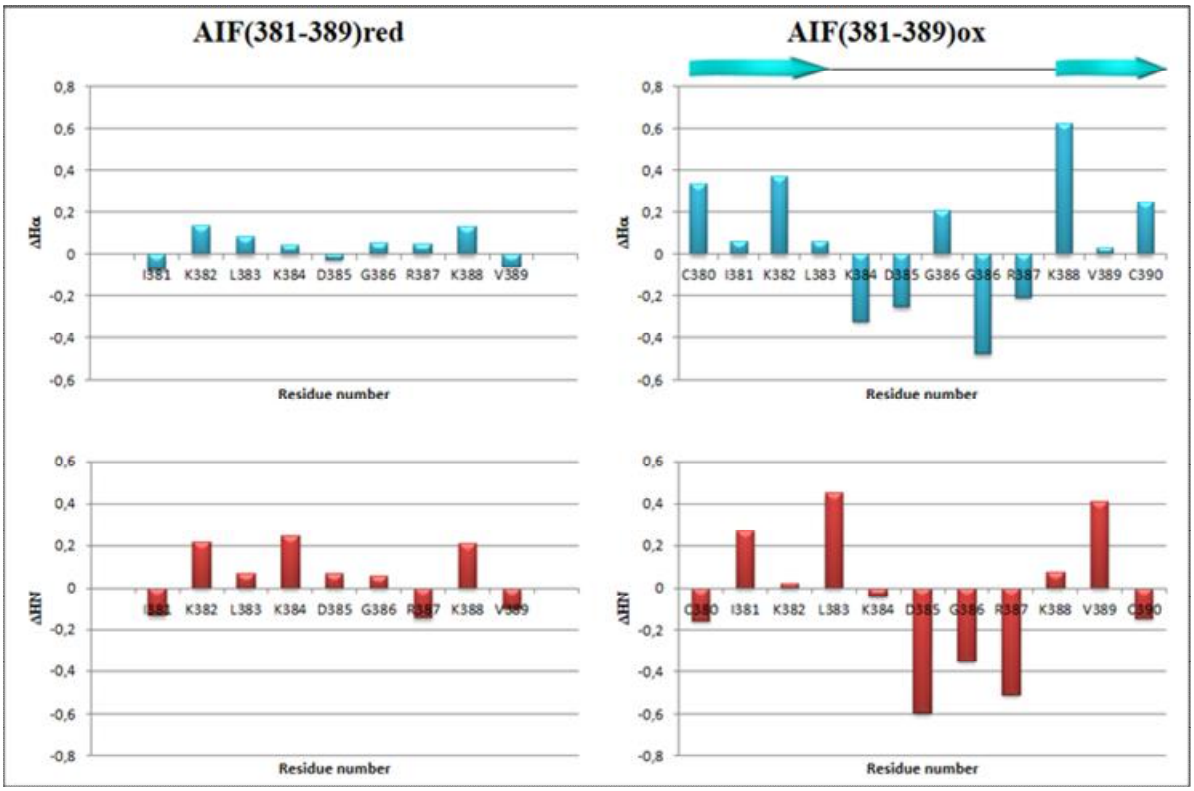

Figure 4.23: Chemical shift deviation from random coil values of H^N and Hα backbone atoms plotted as a function of residue number. Derived secondary structure elements for AIF(381-389)ox are indicated above the plots. Cyan arrows indicate β-strand regions.

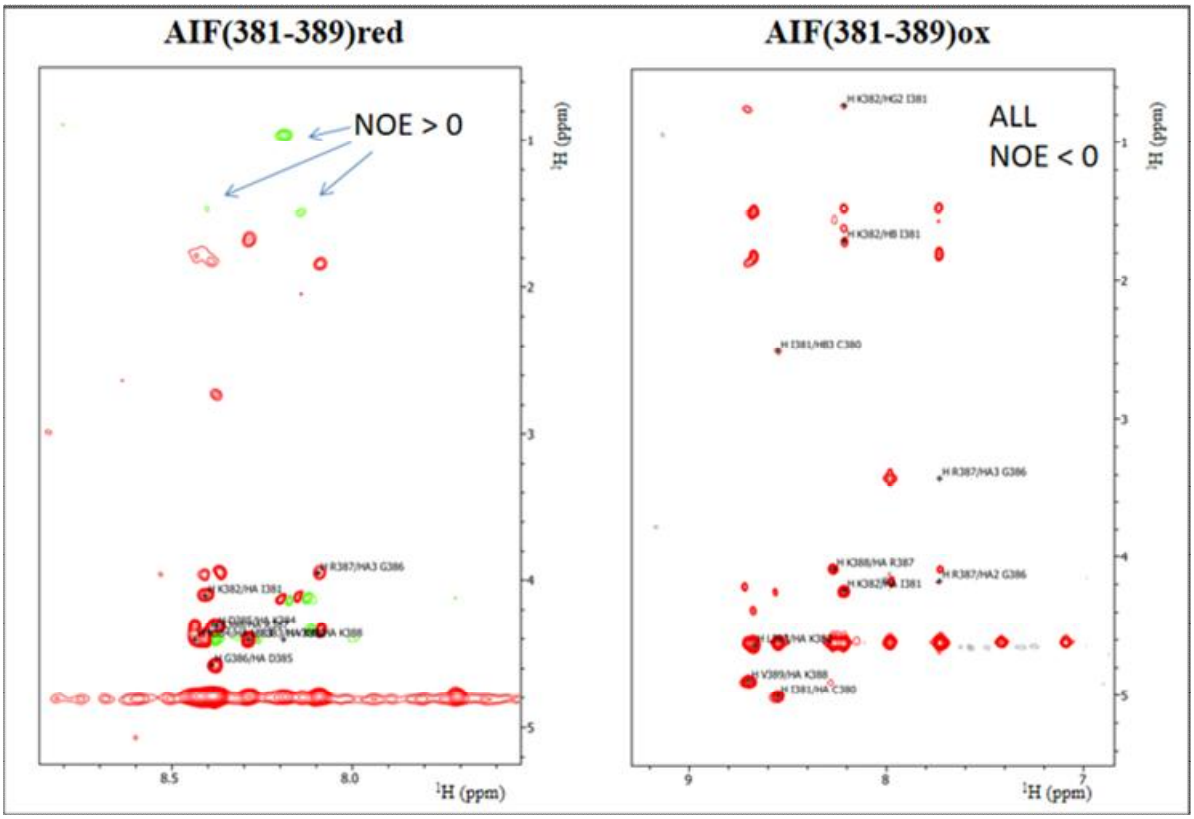

Figure 4.24: 2D [^{1}H, ^{1}H] NOESY NMR spectra of AIF(381-389)red and AIF(381-389)ox in PBS at pH 5.8 ad 298K. NOE > 0 are green cross-peaks, where NOE<0 are red cross-peaks.

4.10.2 STD experiments of AIF(381-389)ox/CypA complex

STD NMR experiments were performed on AIF(381-389)ox in the presence of GST-CypA, as for AIF(370-394). Similarly, the ^{1}H STD spectrum showed that AIF(381-389)ox receive saturation transfer in the presence of the protein (Figure 4.25 A), providing a further confirm of the AIF(381-389)ox/CypA complex formation and insight on the residues directly involved in the interaction with CypA.

In particular, the strongest STD signals were observed in the aliphatic region and were ascribed to the Hε and Hδ protons of K^{382}/K^{384}/K^{388}, the Hγ and Hβ of K^{384}, the Hβ of D^{385} and the overlapped methyl protons at about 0.8 ppm of I^{381}, L^{383} or V^{389} residues.

These data confirmed the importance of the lysine residues in the interaction of AIF(370-394) and AIF(370-394) derivatives according to NMR and Ala-scan experiments.

Moreover, they indicate that K^{382} and K^{388} could interact mainly with the terminal part of the side-chain (i.e ionic or polar interaction mediated by the ε-NH_2 group), while K^{384} could establish interaction also or only with the aliphatic side-chain.

4.10.3 CSP studies of AIF(381-389)ox/CypA complex

The formation of the CypA/AIF(381-389)ox complex was followed *via* chemical shift perturbations (CSP) of ^{15}N- His6tagged-CypA backbone signals (see Material and Methods for details) induced by AIF(380-390)ox in the 2D ^{1}H- ^{15}N HSQC spectra.

As shown in Figure 4.25 B, a number of resonances in the 2D ^{1}H- ^{15}N HSQC spectrum exhibited continuous and significant chemical shift variations upon the subsequent addition of the unlabeled AIF(381-389)ox peptide to ^{15}N-His6tagged-CypA until at a molar excess of 10–fold.

The largest perturbations on CypA (mapped in orange red on the docking model of the AIF(381-389)ox/CypA complex in figure 4.25 C) occurred on the loops β4-β5 (T^{68}), β5-β6 (A^{101}, N^{102}, A^{103}), and α2-β7 (V^{127}), and in the sheets β5 (S^{99}) and β7 (V^{128}).

Strong perturbations were also observed in the loops β4-β5 (R^{69}, G^{74}, K^{76}), β5-β6 (Q^{111}) and α2-β7 (H^{126}). The latter were mapped in gold on the docking model in Figure 4.25 C.

These data indicate that the binding surface of AIF(381-389)ox on CypA is consistent with that of AIF(370-394).

4.10.4 Docking model of AIF(381-389)ox/CypA complex

To gain insight into the binding mechanism of CypA by AIF(381-389)ox, we carried out molecular docking studies by HADDOCK webserver using as input CSP and STD data. In particular, T^{68}, R^{69}, G^{74}, K^{76}, A^{101}, N^{102}, A^{103}, Q^{111} and H^{126} of CypA and K^{382}, K^{384}, D^{385}, K^{388} of AIF(381-389)ox were considered as active residues.

S^{99}, V^{127} and V^{128} were set as passive residues for CypA, whereas they were set automatically for AIF(381-389)ox. Moreover, since the AIF(381-389)ox assumes a β-hairpin conformation, we used as input the structure of the 381-389 region as it is in the AIF crystal structure (PBD: 1M6I) [103].

The docking calculations generated four clusters characterized by negative Z-score and showing small but significant differences in the molecular recognition of CypA by AIF(381-389)ox.

Interestingly, the first cluster with the lowest Z-Score was also more in line with the NMR data (STD and CSP).

Therefore, we selected the first model inside this cluster having the lowest binding energy conformation as a representative model of the AIF(381-389)ox/CypA complex (Figure 4.25 C). In this model, the binding site of AIF(381-389)ox on CypA, adjacent to the catalytic site,

is constituted by the residues: T^{68}, R^{69}, G^{72}, T^{73}, G^{74}, G^{75}, K^{76}, E^{81}, K^{82}, A^{101}, N^{102}, A^{103}, T^{107}, Q^{111}.

Importantly, almost all them show CSP effects. On the other side, AIF(381-389)ox establishes an extensive number of interactions with CypA, mainly hydrogen bonds, by means of K^{382}, L^{383}, K^{384}, D^{385}. In particular, the K^{382} ε-amino group forms two hydrogen bond with the A^{101} backbone oxygen and the Q^{111} amide oxygen.

In addition, the K^{382} Cε aliphatic chain interacts with the T^{107} backbone oxygen with an unconventional hydrogen bond.

The L^{383} forms with its backbone oxygen two conventional and one unconventional hydrogen bonds with the hydroxyl of T^{68}, the backbone Cα of G^{74} and the backbone amide H^N of G^{75}.

However, the L^{383} side-chain points away from the binding site of AIF(381-389)ox on CypA. K^{384} also establishes interactions by means of its backbone oxygen with Hε of R^{69} and Cβ of T^{68}, according with STD data in which Hβ and Hγ resulted most saturated, differently from the other lysine residues.

The K^{384} side-chain points in a hydrophobic groove constituted by F^{46}, F^{67}, T^{68} and K^{76} side-chains. In addition, the backbone oxygen of D^{383} forms a hydrogen bond with a hydrogen of the R^{69} guanidinium group.

Hydrophobic interactions were observed between the N-terminal C^{380} and I^{381} side chains with the A^{103} and K^{82} side chains, respectively.

Finally, only weak hydrophobic interactions were observed between K^{388} and T^{63} side chains.

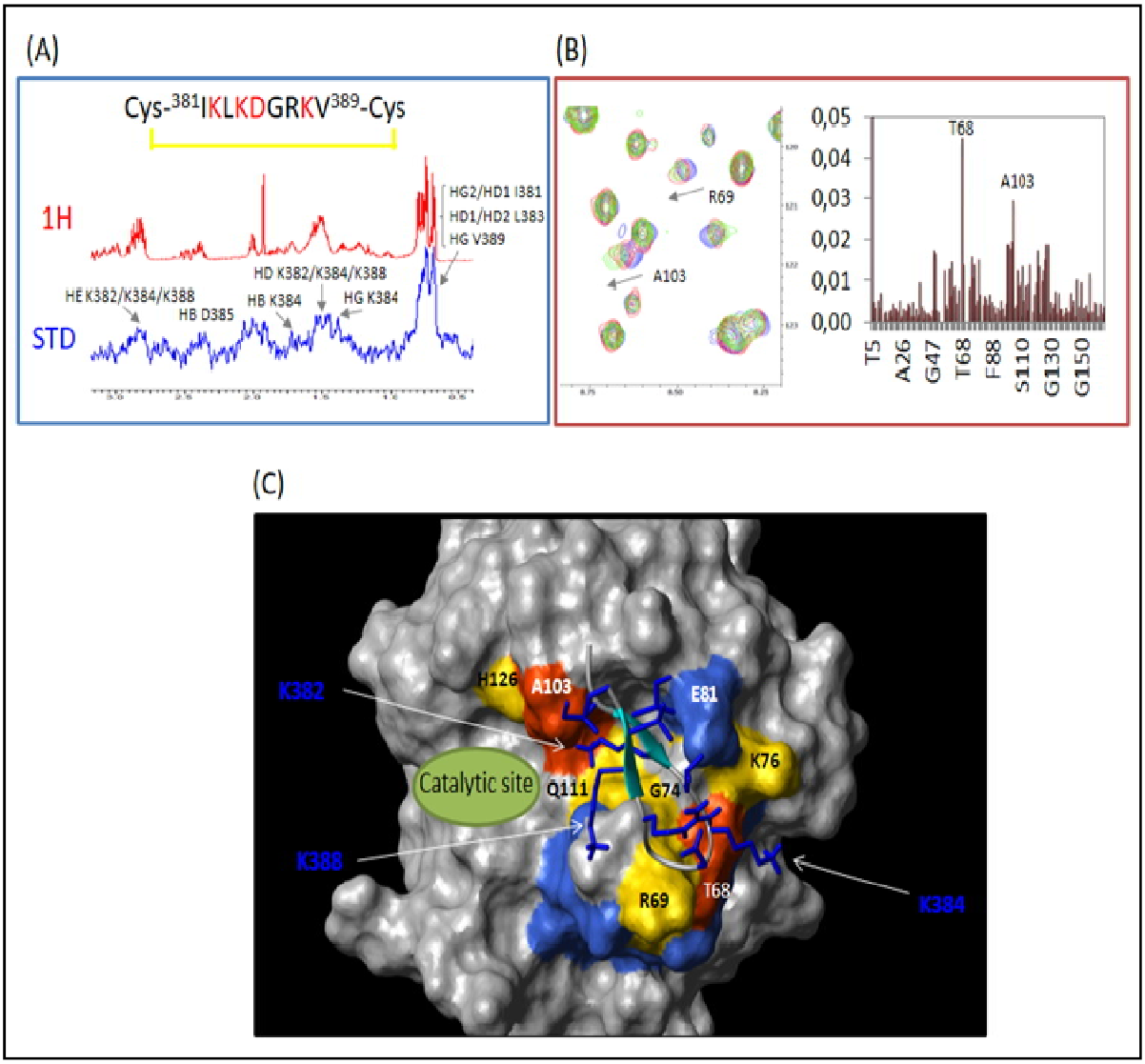

Figure 4.25: (A) Expansion of the aliphatic region of the reference 1H (red) and STD (blue) spectra of AIF(381-389)ox in the presence of GST-CypA (1:100). AIF(381-389)ox sequence is reported. Residues showing the strongest STD effects are highlighted in red. (**B**) Superposition of a 2D [^{1}H, ^{15}N] HSQC section of CypA in the absence (blue) and in the presence of AIF(381-389)ox 1:5 (red), 1:10 (green). Bar graphs of the average combined chemical shift differences (ΔHNav) as a function of residue number. Residueswith the strongest CSP are indicated. (**C**) AIF(381-389)ox binding mode on CypA surface as derived by docking studies. CypA residues most affected by peptide binding are colored, as obtained by CSP studies, in orange red (ΔHNav > mean+SD) and in gold (ΔHNav > mean) on the surface of CypA (PDB ID: 3K0N). AIF(381-389)ox is represented as ribbon drawing, with the side chains shown as a neon representation.

4.11 Generation of new AIF-mimetics through a focused simplified peptide library

In order to further optimized the peptide AIF(381-389)ox, we screened a focused simplified peptide library [89]. This library was designed on the basis of Ala-scanning and NMR results, replacing residues in positions 385-386 appearing as not directly responsible of the interaction with CypA. In our approach we employed a minimum number (7 instead of 20) of non redundant amino acids as building blocks (Figure 4.26), chosen on the basis of their ability to induce β-hairpin structures [114]. Positional scanning libraries were prepared by the solid phase method, using the "Pre-mix" [115] approach and the characterization of peptide mixtures was performed by pool amino acid analysis of sub-libraries, and by LC-ESI mass spectrometry. Their experimental compositions were in agreement with a theoretical distribution of pseudo-equimolar mixtures (data not shown).

The amino acids selected for the random insertion include: alanine, glycine, threonine, β-alanine, leucine, proline and aspartic acid [114, 116].

The library thereby consisted of seven sub-libraries, each containing a set of seven different peptides, in which the position 385 was fixed and the position 386 was randomized (See Methods for details).

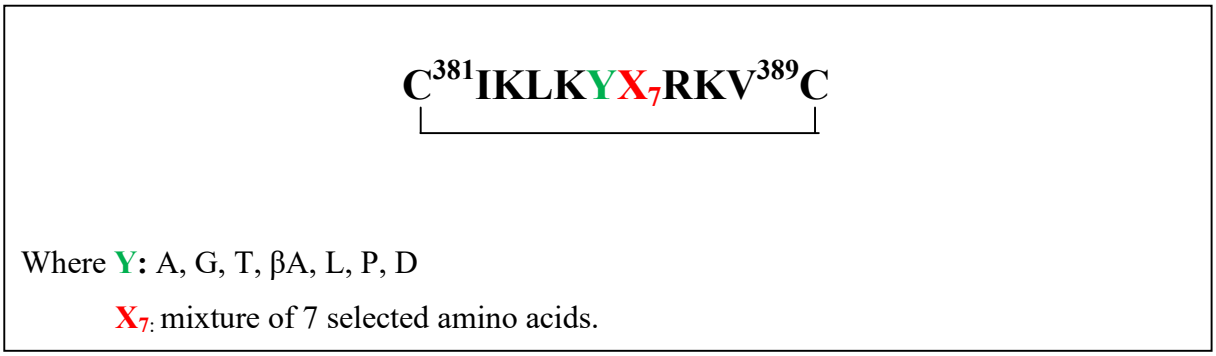

Figure 4.26.: Schematic illustration of synthetic positional scanning libraries

Libraries were screened in parallel on multiple plates, through Label-free Corning Epic technology at concentrations ranging between 0.07 µM and 150 µM (Figure 4.27).

By data analysis, none of the screened sub-libraries showed an improved affinity toward CypA peptides compared to AIF(381-389)ox and this can be ascribed to a concentration effect. Indeed each sequence in the mixtures is 7-fold less concentrated compared to the wild-type AIF(381-389) single peptides. The Figure 4.27 shows the IC_{50} values of each library reported.

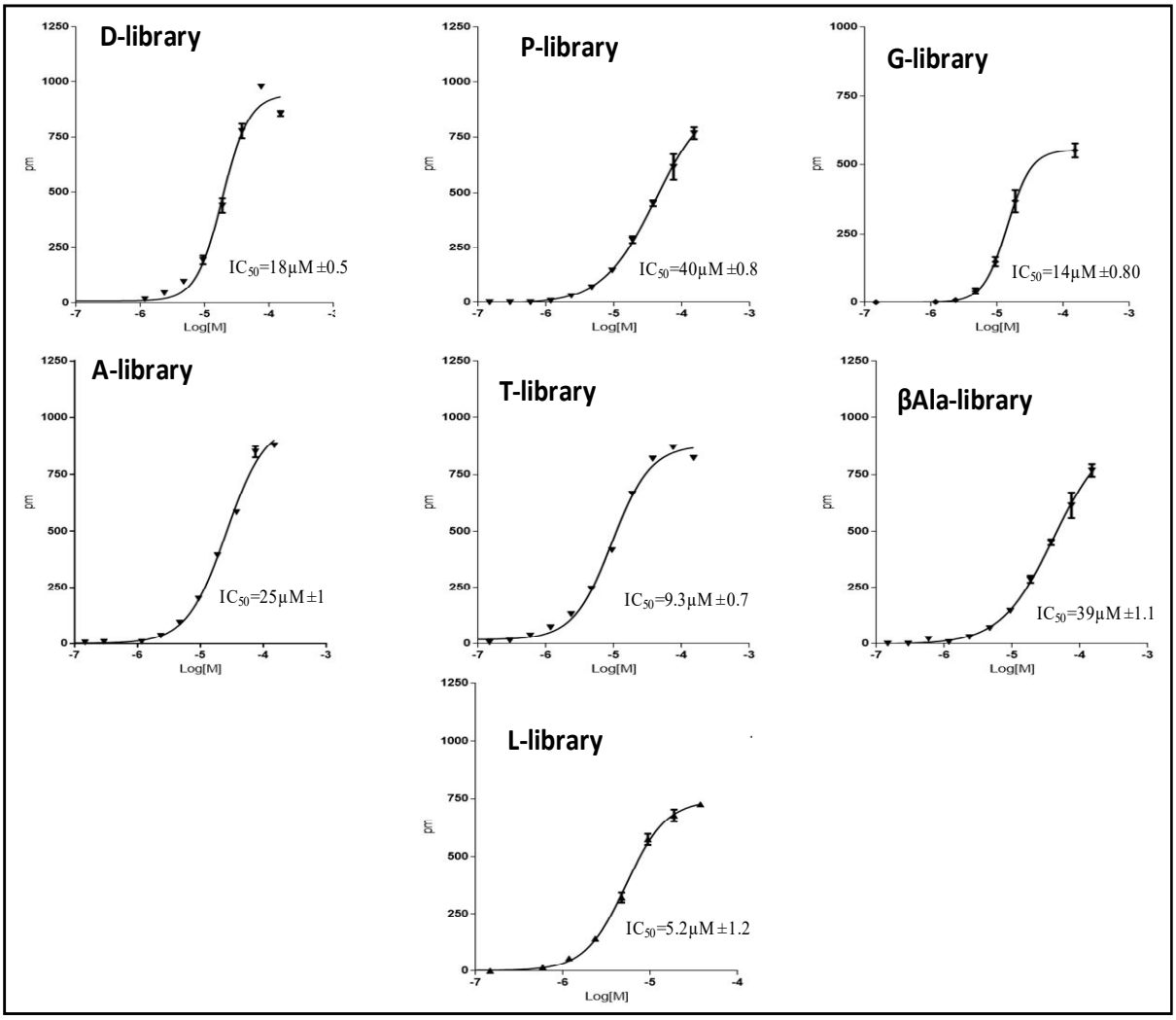

Library Name	IC_{50}
D-Library	18.0±0.5 μM
P-Library	40.0±0.5 μM
G-Library	14.0±0.5 μM
A-Library	25.0±0.5 μM
T-Library	9.30±0.5 μM
β-Ala-Library	39.0±1.1 μM
L-Library	5.20±1.1 μM

Figure 4.27: IC_{50} values for the sub-libraries tested. Values were calculated for each library from the dose-response curves using a single site equation model.

We therefore selected the L-library, showing the lowest IC_{50} (5.2 ± 1.2 µM) and prepared the single components. Peptides were synthesized and purified by RP-HPLC and identified by LC-MS (data not shown). Their binding abilities to CypA were again analyzed through label free techniques (Figure 4.28).

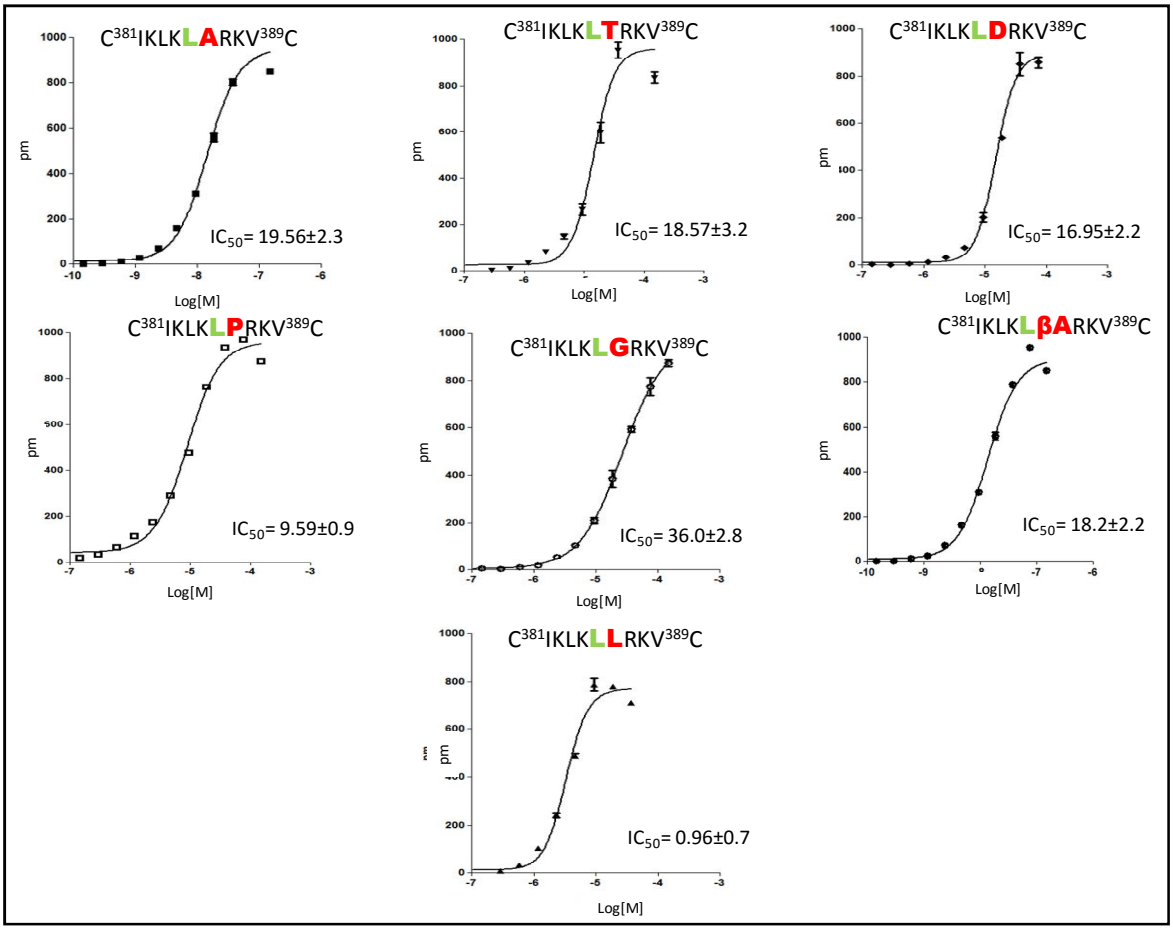

Peptide Sequence	IC_{50}
C^{381}IKLKLARKV^{389}C	19.0 ±2.3 µM
C^{381}IKLKLTRKV^{389}C	18.6±3.2 µM
C^{381}IKLKLDRKV^{389}C	16.9±2.2 µM
C^{381}IKLKLPRKV^{389}C	9.6±0.9 µM
C^{381}IKLKLGRKV^{389}C	36.0 ±2.8 µM
C^{381}IKLKLβARKV^{389}C	18.2±2.2 µM
C^{381}IKLKLLRKV^{389}C	0.96±0.7 µM

Figure 4.28: Concentration-dependent curves and IC_{50} values for the single peptides composing the L-library from the previous experiment. Values were calculated for each peptide from the dose-response curve using a single site equation model.

These experiments allowed to select a new peptide with an affinity toward CypA largely enhanced compared to AIF(381-389)ox. The peptide, resulting from the introduction of two leucine residues in position 385 and 386, called AIF(381-389)$mod_{LL,}$ shows the highest affinity to CypA, with an IC_{50} of 0.96 ± 0.7μM.

4.12 Characterization of a new peptide: AIF(381-389)mod_{LL} peptide

Structural studies on AIF(381-389)mod_{LL}, performed by CD, have shown that the presence of the two leucine, results in a significant increase of well organized structures compared to the parent AIF(381-389)ox peptide.

As shown in Figure 4.29, AIF(381-389)mod_{LL} has a positive maximum at 195 nm and a shift of the absolute minimum from 198 nm to 202 nm, indicative of a very well defined conformation.

The data suggested that the selected peptide represents the best template for the design and selection of new specific antagonists of the complex AIF/CypA.

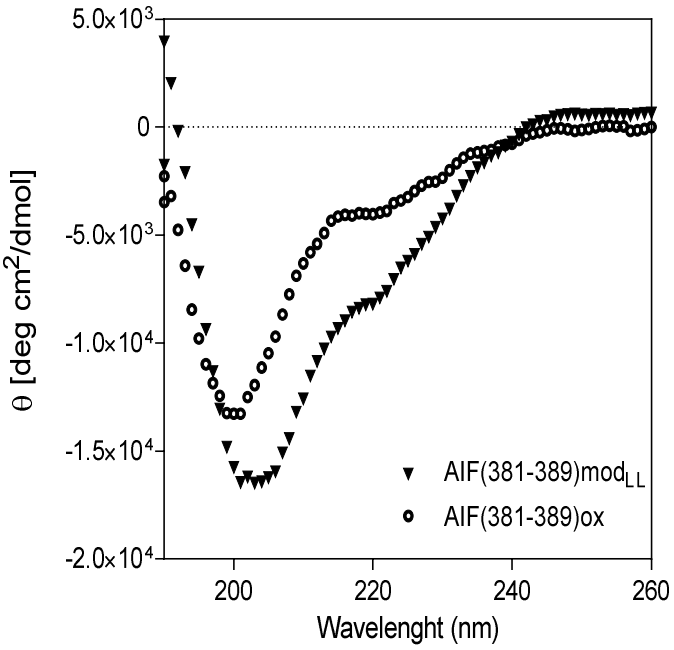

Figure 4.29: CD spectra of AIF(381-389)$mod_{LL}$and of AIF(381-389)ox.

Biological studies are underway to evaluate the effects of the new peptide on apoptosis mechanisms. Ligand-based structural studies are also in progress to design new molecules or peptidomimetic for further structural and functional improvements and for potential application in in vivo models of AIF-dependent neurological diseases.

5. DISCUSSION

Protein-protein interactions (PPIs) are known to play a critical role in the normal function of cellular structure, immune response, protein enzyme inhibitors, signal transduction, and apoptosis [117].

The ability of proteins to assemble into different protein complexes in cellular environments enables these macromolecules to perform different functional roles.

The molecular recognition between proteins and the identification of compounds that might inhibit such interactions and control chemical complex formation is a major challenge in the drug discovery field.

Several studies have demonstrated that PPIs can be addressed with small molecule drugs, however the large surfaces and the several contact points involved make this task difficult [118].

In the last years, research efforts have focused on inhibitors able to interact with the protein targets on multiple hot-spots thanks to their large size and intrinsic flexibility.

Peptides can fulfil this task and have the further advantage of simple preparation by the solid phase method and straight forward structural characterization by NMR [119]. For these reasons, peptides have drawn the attention for innovative drug development.

The availability of structural information on protein-protein complexes and the possibility to readily map protein segments that participate in protein-protein interactions [120] allowed the rational design of new bioactive peptides, that are becoming increasingly attractive as potential drug candidates.

A useful method to search for peptides that inhibit a protein-protein interaction is to mimic the segment of one of the interacting proteins with the corresponding synthetic peptides.

This general approach constitutes the essential cornerstone of this work that is focused on the identification of specific inhibitors of the AIF/CypA complex, whose formation is involved in relevant apoptotic processes.

Apoptosis-inducing factor (AIF) is a highly conserved, phylogenetically old mitochondrial flavoprotein implicated in embryonic development, cardiac cell survival, carcinogenesis and neurodegenerative disorders [34].

Several studies in vitro and in vivo have demonstrated that the pro-apoptotic action of AIF in neurological disorders is triggered by its release through mitochondrial membrane and its translocation to the nucleus, where induces chromatinolysis [30].

The translocation of AIF to the nucleus after cerebral hypoxia-ischemia, requires interaction with Cyclophilin A (CypA), suggesting a model in which the two proteins, that normally

reside in separate cytoplasmic compartments, acquire novel properties when moving together to the nucleus [54].

A model of docking between CypA and AIF suggested that CypA and AIF establish extensive molecular contacts [72].

Recent data demonstrated that the region 370-394 of AIF, predicted from this model, is involved in the interaction with CypA [71].

Indeed the peptide mimicking this region, AIF(370-394), bound CypA with an affinity in the low micromolar range (K_D= 4.7 ± 0.2 μM) and provided neuroprotective effects in HT-22 cells, a model of AIF-mediated neuronal cell death, by inhibiting the formation of the AIF-CypA lethal complex.

A major disadvantage of using this peptide in cellular experiments and in perspective in vivo, is associated with the difficulty to transduce it into cells and in neuronal tissues.

On this basis, the aim of this work was focused on the identification of new peptide inhibitors of the AIF/CypA complex designed on the peptide AIF(370-394) and possessing an improved pharmacokinetic profile.

To this end, we designed, synthesized and characterized by NMR and biochemical assays, a series of new peptides to reduce the size of the parent molecule and to identify the crucial hot spot residues involved in the interaction. These data will be useful for the design of peptidomimetics or molecules with a therapeutic potential.

In order to identify the AIF(370-394) residues more involved in the recognition with CypA, we performed Saturation Transfer Difference (STD) NMR experiments using the recombinant CypA protein in complex with the synthetic AIF(370-394) peptide.

^{1}H-STD NMR experiments demonstrated that several aminoacids arranged along the sequence of the peptide are involved in the interaction with CypA and that most of them are included in the region 380-390.

On the basis of these data, a new AIF peptide, spanning residues from 380 to 390, named AIF(380-390), was synthesized and characterized.

Remarkably, this region adopts a β-harpin conformation in the full length protein, as demonstrated by the crystallographic structure of AIF protein [32], we therefore introduced two cysteine residues at N and C terminus to promote the β-hairpin conformation by a disulfide-bridge.

The decrease of the molecular surface caused the expected reduction of affinity toward the target protein. Indeed, AIF(380-390)red showed a K_D value of 30 ± 2μM, about 6-fold higher than that of the parent AIF(370-394) (K_D= 4.7 ± 0.2 μM).

Notably, the cyclization of the peptide through the two cysteines restored the affinity to CypA (K_D= 3.2 ± 0.2 μM), indicating a direct correlation between the structure and activity of the peptide.

We next evaluated the role of each amino acid of the new cyclic peptide in the interaction with CypA, by an Ala scanning approach. Each single amino acid was systematically substituted with an alanine and the resulting peptides were tested in direct binding assay with CypA.

Data showed that the critical residues of AIF(380-390)ox peptide for the CypA recognition were K^{382}, K^{384},K^{387} and R^{388}, while residues L^{380}, E^{390}, D^{385} and G^{386} appeared poorly involved in the interaction with the target protein, in agreement with the STD-NMR data on AIF(370-394) in complex with CypA.

A preliminary NMR analysis of the cyclic AIF(380-390) peptide also showed the presence of different conformations, stabilized by salt bridges between the carboxyl group of E390 and the ε -amino group of the various lysine salong the sequence.

We thus designed and synthesized a smaller cyclic peptide encompassing the region 381-389, called AIF(381-389)ox.

Interestingly, this last peptide bound CypA with an affinity similar to that of AIF(380-390)ox, in agreement with the Ala-scanning and NMR data.

This peptide also resulted more structurally homogeneous around a β-hairpin conformation, as indicated by NMR studies.

Although the affinity of the new peptide was comparable to that of AIF(370-394), a significant difference was observed in cell-based assay. Indeed, both AIF (381-389)ox and AIF (380-390)ox provided a greater neuroprotection against glutamate treatment in HT-22 cells, compared to the precursor peptide.

NMR binding studies of AIF(381-389)ox with the protein were performed by both chemical shift perturbation (CSP) analysis, using ^{15}N-labelled CypA, and by STD experiments, using the peptide and the unlabelled protein. These NMR data were used to generate a docking model of the CypA-AIF(381-389)ox complex.

Data clearly showed that CypA residues mostly involved in the interaction with AIF(381-389)ox are located on a contiguous region very close to the catalytic site of CypA. Moreover, the interacting residues on AIF(381-389)ox were included in the recognition region of AIF(370-394)/CypA, as also shown by other studies (unpublished data).

Although structure-based design represents an important approach for the development of inhibitors of protein-protein interactions, another useful approach is based on the screening

of combinatorial collections. In this case, starting structural information on protein and peptide interacting regions, our purpose was the further enhancement of native conformation of the peptide, to obtain a more active compound.

To this end, starting from STD and Ala-scanning results, we prepared and screened a simplified short combinatorial library, obtained replacing the amino acids D^{385} and G^{386}, poorly involved in the interaction with CypA, with residues known as inducer of *turns,* such as alanine, glycine, threonine, β-alanine, leucine, proline and aspartic acid.

We designed and synthesized seven peptide pools, each containing a set of seven different peptides, in which the position 385 was fixed and the position 386 was randomized with a mixture of preselected amino acids.

Testing these libraries by direct-binding assays, demonstrated that all had K_D values in the micromolar range. The L-library, however, where in position 385 a leucine was present, displayed a stronger binding.

The seven single peptides composing the L-library, were synthesized and tested, selecting a new peptide, where both position 385 and 386 were occupied by a leucine.

This peptide (C^{381}IKLKLLRKV^{389}C), named AIF(381-389)$mod_{LL,}$ showed an affinity for CypA in the nanomolar range.

Structural studies performed on this peptide showed a higher content of secondary structures compared to AIF(381-389)ox, proving the contribution of leucine residue to the overall peptide stability.

In conclusion, by this work we have identified the minimal region of AIF involved in the interaction with CypA. This region corresponds to the cyclic nonapeptide AIF(381-389)ox, obtained by a systematic and structure-driven approach of size reduction of the original AIF(370-394) template, containing 25 residues.

A docking model of the CypA/AIF(381-389)ox complex has also been generated which will be used for structure-based drug design of new compounds inhibiting the AIF/CypAcomplex.

The amino acid sequence of this AIF peptide has been further optimized to obtain AIF(381-389)mod_{LL} by changing two key residues that induce the β-hairpin conformation adopted by this fragment in the native AIF protein.

Cellular experiments in HT-22 neurons with AIF(381-389)mod_{LL} are currently ongoing to assess its therapeutic potential.

6. REFERENCES

1. World Health Organization Department of Health Statistics and Informatics in the Information, Neurological disorders: public health challenges, (2006) Geneva: WHO,
2. Morrison, Richard S.; et al. Neuronal Survival and Cell Death Signaling Pathways. Landes Bioscience (2000-2013), Madame Curie Bioscience Database .
3. Amor S.; et al. Inflammation in neurodegenerative diseases. Immunology. (2010), 129, 154-169.
4. Loo DT; Copani A.; Pike CJ; et al. Apoptosis is induced by beta-amyloid in cultured central nervous system neurons. Proc. Natl. Acad. Sci. U.S.A. (1993), 90, 7951-55.
5. Mattson MP; et al. Molecular functionalization of carbon nanotubes use as substrates for neuronal growth, Journal of Molecular Neuroscience (2000), 14, 175-182.
6. Culmsee C.; et al. Molecular insights into mechanisms of the cell death program: role in the progression of neurodegenerative disorders. Curr Alzheimer Res (2006), 3, 269-83.
7. Zong W-X; et al. Alkylating DNA damage stimulates a regulated form of necrotic cell death, Genes & Development (2004), 18, 1272-1282.
8. Majno G.; Joris I.; .Apoptosis, oncosis, and necrosis. An overview of cell death. Am J Pathol. (1995), 146, 3-15.
9. Green; Douglas. Means to an End: Apoptosis and other Cell Death Mechanisms. Cold Spring Harbor, NY (2011).
10. Kerr JFR; et al. Apoptosis: a basic biological phenomenon with wide-ranging implications in tissue kinetics. British journal of cancer (1972), 26, 239-257.
11. Wickman *G. R.*; et al. Blebs produced by actin–myosin contraction during apoptosis release damage-associated molecular pattern proteins before secondary necrosis occurs. Cell Death & Differentiation (2013), 20: 1293-1305.
12. Mattson Mark P. Apoptosis in neurodegenerative disorders , Nature Reviews Molecular Cell Biology 1. (2000), 120-130.
13. Piao C.S.; et al. Combined inhibition of cell death induced by apoptosis inducing factor and caspases provides additive neuroprotection in experimental traumatic brain injury. Neurobiology of Disease. (2012), 745-758.
14. Lockshin RA; Williams CM. Programmed cell death. II. Endocrine potentiation of the breakdown of the intersegmental muscles of silkmoths. Histochem J. (1964), 10, 643-649.

15. Chaabane W.; et al. Autophagy, Apoptosis, Mitoptosis and Necrosis: Interdependence Between Those Pathways and Effects on Cancer, Arch. Immunol. Ther. Exp. (2013) 61, 43-58.
16. Bredesen DE. Key note lecture: toward a mechanistic taxonomy for cell death programs. Stroke. (2007), 38, 652-660.
17. Bredesen DE. Programmed cell death mechanisms in neurological disease. Curr. Mol. Med. (2008), 8, 173-186.
18. Ricci S. M. and Zong Wei-Xing. Chemotherapeutic Approaches for Targeting Cell Death Pathways. Oncologist. (2006), 11, 342-357.
19. Yakovlev AG; Faden AI. Caspase-dependent apoptotic pathways in CNS injury Mol NeuroBiol. (2001), 24, 131-144.
20. Sartorius U.; Schmitz I.; Krammer P. H. Molecular mechanisms of death receptor-mediated apoptosis. Chembiochem. (2001), 2, 20-29.
21. Ashkenazi A. Targeting death and decoy receptors of the tumour-necrosis factor superfamily. Nat. Rev. Cancer, (2002), 2, 420-430.
22. Zou H.; Henzel W. J.; et al. Apaf-1, A human protein homologous to C. elegans CED-4, participates in cytochrome c-dependent activation of caspase-3.Cell (1997), 90, 405-413.
23. Van Loo G; Saelens X.; et al. The role of mitochondrial factors inapoptosis: a Russian roulette with more than one bullet. Cell Death Differ. (2002), 9, 1031-1042.
24. Li L.Y.; Luo X.; and Wang X. Endonuclease G is an apoptotic DNase when released from mitochondria. Nature (2001), 412, 95-99.
25. Chai J.; Shiozaki E.; et al. Structural basis of caspase-7 inhibition by XIAP. Cell. (2001), 104, 769-780.
26. Suzuki Y; Imai Y.; et al. A serine protease, HtrA2 is released from the mitochondria and interacts with XIAP, inducing cell death. Mol. Cell. (2001), 8, 613-621.
27. Verhagen AM.; Silke J; et al. HtrA2 promotes cell death through its serine protease activity and its ability to antagonize inhibitor of apoptosis proteins. J. Biol. Chem. (2002), 277, 445-454.
28. Candè C.; Vashen N.; et al. Apoptosis-inducing factor (AIF): caspase- independent after all.Cell Death and Differentiation. (2004), 11, 591-595.
29. Zhu C.; Wang X.; et al. Apoptosis inducing Factor is a major contributor to neuronal loss induced by neonatal cerebral hypoxia-ischemia. Cell Death Diff. (2007), 14, 775-784.

30. Otera H.; et al. Export of mitochondrial AIF in response to proapoptotic stimuli depens on processing at the intermembrane space. Embo J.(2005), 24, 1375-1384.
31. Sevrioukova I.F. Redox-linked conformational dynamics in apoptosis-inducing factor. J. Mol. Biol. (2009), 390, 924-938.
32. Matè M. J.; et al. The crystal structure of the mouse apoptosis-inducing factor AIF. Nature Structural Biology. (2002), 9: 442-446.
33. Cheung EC.; et al. Apoptosis-inducing factor is a key factor in neuronal cell death propagated by BAX-dependent and BAX independent mechanisms. J. Neurosci. (2005), 25, 1324-1334.
34. Susin SA; Lorenzo HK; et al. Molecular characterization of mitochondrial apoptosis inducing factor. Nature. (1999), 397, 441-446.
35. Miramar MD; Costantini P.; et al. NADH oxidase activity of mitochondrial apoptosis-inducing factor. J Biol Chem. (2001), 276, 16391-16398.
36. Klein JA Longo-Guess CM.; et al. The harlequin mouse mutation down regulates apoptosis-inducing factor. Nature (2002), 419, 367-374.
37. Hangen E.; Blomgren K.; et al. Life with or without AIF. Trends Biochem Sci (2010), 35, 278-287.
38. Van Empel VP; Bertrand AT; et al. EUK-8, a superoxide dismutase and catalase mimetic, reduces cardiac oxidative stress and ameliorates pressure overload-induced heart failure in the harlequin mouse mutant. J Am Coll Cardiol. (2006), 48, 824-832.
39. Delavallée L.; et al. AIF-mediated caspase-independent necroptosis: A new chance for targeted therapeutics. IUBMB Life (2011), 63, 221-232.
40. Brown D, Yu BD, Joza N, et al., Loss of Aif function causes cell death in the mouse embryo, but the temporal progression of patterning is normal. Proc. Natl. Acad. Sci. U. S. A. (2006) 103, 9918–9923.
41. Kruse SE; Watt WC; Marcinek DJ; et al. Mice with mitochondrial complex I deficiency develop a fatal encephalomyopathy. Cell Metab. (2008) 7, 312-320.
42. Koene S. and Smeitink J. Mitochondrial medicine: entering the era of treatment. J. Intern. Med. (2009) 265, 193-209.
43. Yu S.W.; et al. Mediation of poly(ADP-ribose) polymerase-1-dependent cell death by apoptosis inducing factor. Science (2002), 297, 259-263.
44. Xiao CY; Chen M.; et al. Poly(ADP-Ribose) polymerase promotes cardiac remodeling, contractile failure, and translocation of apoptosis-inducing factor in a murine

experimental model of aortic banding and heart failure. J Pharmacol Exp Ther. (2004), 312, 891-898.

45. Landshamer S.; et al. Bid-induced release of AIF from mitochondria causes immediate neuronal cell death. Cell Death Differ (2008), 15, 1553-1563.
46. Culmsee C.; Zhu C.; et al. Apoptosis-inducing factor triggered by poly(ADPribose) polymerase and Bid mediates neuronal cell death after oxygen-glucose deprivation and focal cerebral ischemia. J. Neurosci. (2005), 25, 10262-10272.
47. Wang H.; Yu SW; et al.. Apoptosis-inducing factor substitutes for caspase executioners in NMDA-triggered excitotoxic neuronal death. J Neurosci. (2004), 24, 10963-10973.
48. Cao G.: Xing J.; Xiao X.; et al. Critical role of calpain I in mitochondrial release of apoptosis-inducing factor in ischemic neuronal injury. J. Neurosci. (2007), 27, 9278-9293.
49. Ferrand-Drake M.; et al. Cyclosporin A prevents calpain activation despite increased intracellular calcium concentrations, as well as translocation of apoptosis-inducing factor, cytochrome c and caspase-3 activation in neurons exposed to transient hypoglycemia. J. Neurochem. (2003), 85, 1431-1442.
50. Ravagnan L.; Gurbuxani S.; et al. Heat-shock protein 70 antagonizes apoptosis-inducing factor. Nat Cell Biol. (2001), 3, 839-843.
51. Matsumori Y.; et al. Hsp70 overexpression sequesters AIF and reduces neonatal hypoxic/ischemic brain injury. J. Cereb. Blood Flow Metab. (2005), 25, 899-910.
52. Cheung EC; Joza N.; et al. Dissociating the dual roles of apoptosis inducing factor in maintaining mitochondrial structure and apoptosis. EMBO J. 2006, 25, 4061-4073.
53. Slemmer JE; Zhu C.; Landshamer S.; et al. Causal role of apoptosis-inducing factor for neuronal cell death following traumatic brain injury. Am J Pathol. (2008), 173, 1795-1805.
54. Zhu C.; Wang X.; et al. Cyclophilin A participates in the nuclear translocation of apoptosis-inducing factor in neurons after cerebral hypoxia-ischemia. J. Exp. Med. (2007), 204, 1741-1748.
55. Nigro P.; Pompilio G.; Capogrossi MC. Cyclophilin A: a key player for human disease. Cell Death Dis. (2013), 31; 4:e888
56. Wang P.; Heitman J. The cyclophilins. Genome Biol (2005), 6, 226
57. Obchoei S.; Wongkhan S.; et al. Cyclophilin A: potential functions and therapeutic target for human cancer. Med Sci Monit. (2009), 5, 221-232.

58. Jin L.; Harrison SC. Crystal structure of human calcineurin complexed with cyclosporin A and human cyclophilin. Proc Natl Acad Sci USA. (2002), 99, 13522-13526.
59. Huai Q.; Kim HY; Liu Y.; et al. Crystal structure of calcineurin-cyclophilin cyclosporin shows common but distinct recognition of immunophilin drug complexes. Proc Natl Acad Sci USA. (2002), 99, 12037-13042.
60. Sieber M. and Baumgrass R. Novel inhibitors of the calcineurin/NFATc hub alternatives to CsA and FK506? Cell Communication and Signaling : CCS. (2009), 7, 25.
61. Satoh K; Shimokawa H.; Berk BC. Cyclophilin A: Promising New Target in Cardiovascular Therapy. Circulation Journal. (2010), 74, 2249-2256.
62. Tegeder A.; Schumacher S. J.; et al. Elevated serum cyclophilin levels in patients with severe sepsis, Journal of Clinical Immunology, (1997), 17, 380-386.
63. Stemmy E. J.; Benton A. S.; et al. Extracellular cyclophilin levels associate with parameters of asthma in phenotypic clusters, The Journal of Asthma, (2011), 48, 986-993.
64. Chang C.-S.; et al. Cyclophilin-A: a novel biomarker for untreated male essential hypertension," Biomarkers, (2013), 18, 716-720.
65. Li Z.; Zhao X.; Bai S.; et al. Proteomics identification of cyclophilin as a potential prognostic factor and therapeutic target in endometrial carcinoma. Mol Cell Proteomics (2008), 7, 1810-1823.
66. Semba S.; Huebner K.; Protein expression profiling identifies cyclophilin A as a molecular target in Fh it-mediated tumor suppression. Mol Cancer Res (2006), 4, 529-538.
67. Choi KJ; Piao YJ; et al. Overexpressed cyclophilin A in cancer cells renders resistance to hypoxia- and cisplatin-induced cell death. Cancer Res (2007), 67, 3654-3662.
68. Calhoun CC; Lu YC; Song J; Chiu R. Knockdown endogenous CypA with siRNA in U2OS cells results in disruption of F-actin structure and alters tumor phenotype. Mol Cell Biochem. (2009), 320, 35-43.
69. Goldner FM; Patrick JW. Neuronal localization of the cyclophilin A protein in the adult rat brain. J Comp Neurol (1996), 372, 283-293.
70. Satoh K.; Nigro P.; et al,. Cyclophilin A enhances vascular oxidative stress and the development of angiotensin II-induced aortic aneurysms. Nat Med (2009); 15: 649–656.
71. Doti N.; Reuther C.; Scognamiglio PL; et al. Inhibition of the AIF/CypA complex protects against intrinsic death pathways induced by oxidative stress. Cell Death Dis. (2014) 16;5:e993.

72. Candé C.; Vahsen N.; Kouranti I.; et al. AIF and cyclophilin A cooperate in apoptosis-associated chromatinolysis. Oncogene. (2004), 23, 1514-1521.
73. Artus C.; Boujrad H.; et al. AIF promotes chromatinolysis and caspase-independent programmed necrosis by interacting with histone H2AX. Embo J. (2010),29, 1585-1599.
74. Fukui M.; Song JH; et al. Mechanism of glutamate-induced neurotoxicity in HT22 mouse hippocampal cells. Eur J Pharmacol (2009), 617, 1-11.
75. Mariani E.; et al. Oxidative stress in brain aging, neurodegenerative and vascular diseases: An overview. Journal of Chromatography B . (2005), 827, 65-75.
76. Maraldi T. Natural Compounds as Modulators of NADPH Oxidases. Oxidative Medicine and Cellular Longevity. (2013).
77. Balakin K.V.; Kozintsev A.V.; et al. Rational design approaches to chemical libraries for hit identification. Curr Drug Discov Technol .(2006), 3, 49-65.
78. Ecker D.J. and Crooke S.T. Combinatorial drug discovery: which methods will produce the greatest value? Biotechnology (N Y) (1995), 13, 351-360.
79. Kennedy J.P.; et al. Application of combinatorial chemistry science on modern drug discovery. J Comb Chem. (2008), 10, 345-354.
80. Oliyai R. and Stella J.V. Prodrugs of peptides and proteins for improbe formulation and delivery, Annu. Rev. Pharmacol.Toxicol. (1993), 32, 521-544.
81. Bradford MM. A rapid and sensitive method for the quantitation of microgram quantities of protein utilizing the principle of protein-dye binding. Anal. Biochem. (1976), 72, 248-254.
82. Scopes RK. Measurement of protein by spectrophotometry at 205 nm. Anal. Biochem. (1974), 59, 277-282.
83. Laemmli U. K. Cleavage of structural proteins during the assembly of the head of bacteriophage T4. Nature. (1970), 227, 680-685.
84. Bohm G.; Muhr R. J. Quantitative analysis of protein far UV circular dichroism spectra by neural networks. Protein Eng (1992), 5, 191-195.
85. Fields G. B.; Noble R. L. Solid phase peptide synthesis utilizing 9-fluorenylmethoxycarbonyl amino acids. Int. J. Pept. Protein Res. (1990), 35, 161-214.
86. Funosas S. R. Oxyma: An Efficient Additive for Peptide Synthesis to Replace the Benzotriazole-Based HOBt and HOAt with a Lower Risk of Explosion. Chemistry: A European Journal. (2015), 20, 93-94.
87. Knorr R.; Trzeciak A.; Bannwarth. W. et al. New coupling reagents in peptide chemistry. Tetrahedron Lett. (1989), 30, 1927-1930.

88. Raguine L.; et al. Alanine scan of an immunosuppressive peptide (CP): analysis of structure-function relationships. Chem. Biol Drug Des. (2013), 81, 167-174.
89. Sandomenico A.; et al., Small peptide inhibitors of acetyl-peptide hydrolase having an uncommon mechanism of inhibition and a stable bent conformation. J Med Chem. (2012), 55, 2102-2121.
90. Oppermann S.; et al. Novel N-phenyl-substituted thiazolidinediones protect neural cells against glutamate- and tBid-induced toxicity. J. Pharmacol. Exp. Ther. (2014), 350, 273-289.
91. O'Malley S.M.; et al. Label-free high-throughput functional lytic assays. J Biomol Screen. (2007) 12, 117-121.
92. Fukui M.; Song JH; Choi J.; Choi HJ; Zhu BT. Mechanism of glutamate-induced neurotoxicity in HT22 mouse hippocampal cells. Eur J Pharmacol. (2009), 617, 1-11.
93. Keller R. The CARA/Lua Programmers Manual. Internal document NMR. 0.14 (2003).
94. Braunschweiler L.; Ernst R. R. Coherence transfer by isotropic mixing: application to proton correlation spectroscopy. J. Magn. Reson. (1969-1992) 1983, 53, 521.
95. Rance M.; Sørensen O.W.; Bodenhausen G.; et al. Improved spectral resolution in cosy ^{1}H NMR spectra of proteins via double quantum filtering. Biochem. Biophys. Res.Commun. (1983); 117, 479-485.
96. Kumar A.; Ernst R.R.; Wuthrich K. A two-dimensional nuclear Overhauser enhancement (2D NOE) experiment for the elucidation of complete proton–proton cross-relaxation networks in biological macromolecules. Biochem. Biophys. Res. Commun. (1980), 95, 1-6.
97. Nguyen BD; Meng X.; Donovan KJ; Shaka AJ. SOGGY: solvent-optimized double gradient spectroscopy for water suppression. A comparison with some existing techniques. J Magn Reson. (2007), 184, 263-274.
98. Foster M.P.; et al. Chemical shift as a probe of molecular interfaces: NMR studies of DNA binding by the three amino-terminal zinc finger domains from transcription factor IIIA. J. Biomol. NMR (1998), 12, 51-71.
99. Garrett D.S.; et al. Identification by NMR of the binding surface for the histidine-containing phosphocarrier protein HPr on the N-terminal domain of enzyme I of the Escherichia coli phosphotransferase system. Biochemistry (1997), 36, 4393-4398.
100. Grzesiek S.; et al. The solution structure of HIV-1 Nef reveals an unexpected fold and permits delineation of the binding surface for the SH3 domain of Hck tyrosine protein kinase. Nat. Struct. Biol. (1996), 3, 340-345.

101. Dominguez C.; Boelens R.; Bonvin A. HADDOCK: A protein-protein docking approach based on biochemical or biophysical information. Journal of the American Chemical Society . (2003), 125, 1731-1737.

102. Zhao Y.; Ke H. Mechanistic implication of crystal structures of the cyclophilin-dipeptide complexes. Biochemistry. (1996), 35, 7362-7368.

103. Ye H.; Cande C.; Stephanou N.C.; et al. DNA binding is required for the apoptogenic action of apoptosis inducing factor. Nat.Struct.Biol. (2002), 9, 680-684.

104. Hirosawa M.; Hoshida M.; et al. MASCOT: multiple alignment system for protein sequences based on three-way dynamic programming. Comput Appl Biosci. (1993), 2, 161-167.

105. Stephens P. J. et al., Circular dichroism and magnetic circular dichroism of nitrogenase proteins. Proc Natl. Acad. Sci U S A. (1979), 76, 2585-2589.

106. Buck M. Trifluoroethanol and colleagues: cosolvents come of age. Recent studies with peptides and proteins. Q Rev Biophys, (1998), 31: 297-355.

107. Wutrich K. Nmr studies of structure and function of biological macromolecules. Nobel Lecture,(2002).

108. Mucsi Z.; et al. Binding-induced folding transitions in calpastatin subdomains A and C. Protein Science (2003), 12, 2327-2336.

109. Liang Y. Applications of isothermal titration calorimetry in protein science. Acta Biochim Biophys Sin (Shanghai). (2008), 40, 565-576.

110. Mayer M.; Meyer B. Group Epitope Mapping by Saturation Transfer Difference NMR To Identify Segments of a Ligand in Direct Contact with a Protein Receptor. J .Am. Chem. Soc. (2001), 123, 6108-6117.

111. Mayer M.; Meyer B. Characterization of ligand binding by saturation transfer difference by NMR spectroscopy. Angew Chem Int Edn Engl. (1999), 38, 1784-1788.

112. Skinner AL, Laurence JS. High-field Solution NMR Spectroscopy as a Tool for Assessing Protein Interactions with Small Molecule Ligands. Journal of pharmaceutical sciences. (2008), 97, 4670-4695.

113. Tasiemski A.; Vandenbulcke F.; et al. Molecular characterization of two novel antibacterial peptides inducible upon bacterial challenge in an annelid, the leech Theromyzon tessulatum. J Biol Chem. (2004), 279, 30973-30982.

114. Andreetto E.; Malideli E.; et al. A Hot-Segment-Based Approach for the Design of Cross-Amyloid Interaction Surface Mimics as Inhibitors of Amyloid Self-Assembly. Angew Chem Int Ed Engl. (2015), 54, 13095-13100.

115. Marasco D.; Perretta G.; Sabatella M. and Ruvo M. Past and future perspectives of synthetic peptide libraries. Curr Protein Pept Sci. (2008), 9, 447-467.
116. Blanco F.; et al. Formation and stability of beta-hairpin structures in polypeptides. Curr Opin Struct Biol. (1998), 8, 107-111.
117. Chautard E.; Thierry-Mieg N.; Ricard-Blum S. Interaction networks: From protein functions to drug discovery. A review. Pathologie Biologie (2009), 57, 324-333.
118. Ideker T.; Sharan R. Protein networks in disease. Genome Res. (2008), 18, 644-652.
119. Fletcher P.W.; Blume A.J.; Schaffer L.; and Goldstein N.I. Peptides identify the critical hotspots involved in the biological activation of the insulin receptor. J Biol Chem (2002), 277, 22590-22594.
120. Nevola L. and Giralt E. Modulating protein-protein interactions: the potential of peptides. Chem Commun. (2015), 51, 3302-3315.

Chapter II

ABSTRACT

In this work, a sensitive and convenient protease-based fluorimetric HTS assay for determining prolyl-peptidyl *cis-trans* isomerase activity was developed.

The assay was based on a new intramolecularly quenched substrate, whose fluorescence and structural properties were examined together with kinetic constants and the effects of solvents on its isomerization process.

Pilot screens performed using the LOPAC library and Cyclophilin A, as isomerase model enzyme, indicated that the assay is robust for HTS, and that comparable results are obtained with CypA inhibitor tested both manually and automatically.

Moreover, a new compound that inhibits CypA activity with an IC_{50} in the low micromolar range has been identified.

Molecular docking studies revealed that the molecule shows a notable shape complementarity with the catalytic pocket confirming the experimental observations.

Due to its simplicity and precision in the determination of extent of inhibition and reaction rates required for kinetic analysis, this assay offers many advantages over other commonly used assays.

7. INTRODUCTION

7.1 Peptidyl-prolyl isomerases (PPIases) family

Peptidyl-prolyl *cis-trans* isomerases (PPIases) are ubiquitously expressed and highly conserved proteins found both in prokaryotic and in eukaryotic cells [1-5].

PPIases, on the basis of drug specificity and primary sequence homology, have been divided into three distinct families: i) the cyclosporin A (CsA)-binding proteins, cyclophilins, ii) the FK506 and rapamycin binding proteins, FKBPs, and iii) the parvulins, which do not bind immunosuppressant drugs [1-5].

The principal function of PPIases is to participate in protein folding by catalyzing the *cis-trans* isomerization of X-Pro peptide bonds in polypeptide chains (where X is any amino acid) [1-5]. Among all aminoacids, the proline is unique able to adopt completely distinct cis and trans conformations, which allow it to act as a backbone switch controlled by prolyl *cis-trans* isomerization (Figure 7.1).

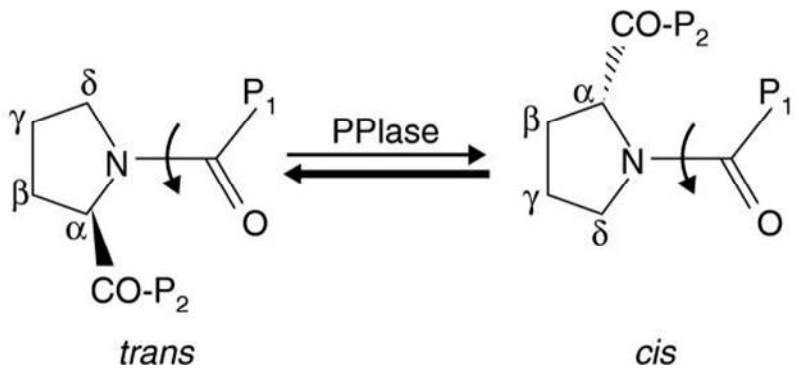

Figure 7.1: Schematic illustration of the reaction catalyzed by the cyclophilins

The Figure 7.1 shows the trans and cis isomers of the peptide bond between proline (on the left of each structure shown) and another amino acid (P_1, on the right).

The interconversion between the two forms is catalyzed by cyclophilins and other peptidyl-prolyl isomerases (PPIases). The carbon atoms of the proline are indicated by Greek letters; P_2 indicates a third amino acid on the other side of the proline. The peptide bond has some double-bond character and is planar.

The local environment of the proline can influence the relative free energies of the *cis* and *trans* isomeric states leading to wide variations in the ratio of *cis*/*trans* populations in different proteins and peptides. In the context of native protein folds, most structures require proline to adopt one or the other isomer.

When ΔG is small, both isomers are significantly populated at thermal equilibrium. However, due to the relatively large energy barrier (ε^{u}=14–24 kcal/mol), uncatalyzed isomerization is a rather slow process with an exchange time constant (Ƭex) on the order of several minutes (Figure 7.2).

PPIases can reduce the energy barrier between *cis* and *trans* states (ε^{cat},) and dramatically accelerate isomerization, reducing Ƭex to the millisecond regime, a more meaningful timescale for regulation of the timing of biological processes [6].

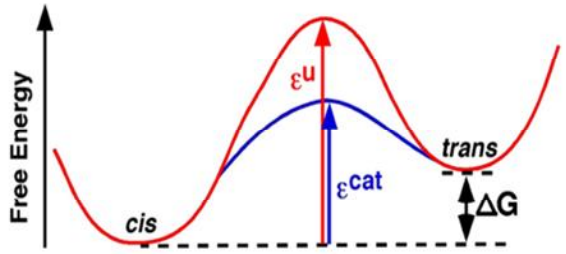

Figure 7.2: Conformational exchange in high-energy transition state. Conformational exchange proceeds through the twisted 90-syn high-energy transition state in the intrinsic (blue curve) or PPIase-catalyzed (red curve) reactions.

The conformational interconversion of the backbones of signaling proteins mediated by peptidyl prolyl *cis-trans* isomerization plays a pivotal role in many aspects of cellular processes, including post-translational modifications like phosphorylation and glycosylation, whose dysregulation does contribute to the development of many human diseases (Figure 7.3) [4, 7-10].

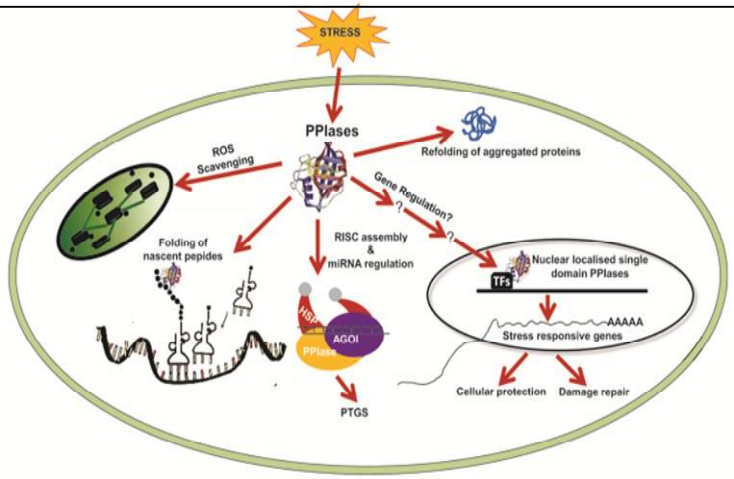

Figure 7.3: Involvement of PPIases function in development of many cellular processes

For this reason, great efforts are spent on the identification of specific PPIase modulators for

therapeutic approaches. However, the discovery of novel inhibitors has been limited by the lack of suitable assays for high-throughput screenings (HTS).
In this study, particular attention is given on the role of Cyclophilin A and its activities as PPIase protein.

7.2 Studies on CypA PPIase activity

CypA is the most important member of the family of human Cyclophilins [11-13]. CypA plays a critical role in a variety of biological processes including protein folding, trafficking, assembly, immunomodulation and cell signaling [14-16].
Moreover, besides its physiological role, the PPIase activity of CypA is also implicated in various pathological conditions and diseases, including viral infection, cancer and neurodegeneration [17].

Conventionally, the enzymatic activity of PPIases has been determined by UV/Vis spectrophotometry with N-succinylated tetrapeptide-4-nitroanilides (pNA) as standard substrates (Succinyl-Ala-Xaa-Pro-Phe-pNA) [18].
This assay is based on the conformational specificity of chymotrypsin, which cleaves the pNA moiety from the substrate only when the Xaa-Pro amide bond is in the *trans* conformation.
In the presence of PPIases, the Xaa-Pro bond is more rapidly converted to the *trans* conformation, and the substrate is then more readily cleaved by chymotrypsin leading to the formation of the colored product pNA [18].
This method, however, suffers from low sensitivity of the chromogenic compound, as well as the fast spontaneous *cis-trans* isomerization which translates in the rapid processing of the substrate (generally in the range of seconds) by Chymotrypsin [18].
Since the spontaneous *cis-trans* isomerization is too fast for reliable calculation of rate constants at room temperature, the assay is usually carried out at or below 10 °C.
However, even under these conditions, a typical half time of the uncatalyzed *cis-trans* isomerization is about 100 s.

In the attempt to develop new more and sensitive assays suitable for HTS programs, several fluorescent new probes and detection methods have been developed for highly sensitive detection of PPIase activity [19-21].
However, to date, no fluorogenic substrates for monitoring PPIase activity in HTS modality have been reported.
The main features of HTS-compatible assays include robustness, sensitivity, automation and

miniaturization. Sensitivity, in this instance, is intended as the capability to generate signals sufficiently higher than the noise but also the ability to detect small inhibition differences. Robustness instead refers to the possibility to have an assay readout stable and reproducible in a time range adequate to the assay timelines [22].

In this framework, we have designed and tested a novel peptide substrate targeting the catalytic site of CypA and useful in HTS-based protease-coupled PPIase assays.

To transfer the assay in a HTS format, we have investigated and optimized parameters like, buffer composition, reaction time, enzyme/substrate ratio, and DMSO content. The conditions for achieving optimal signal-to-noise (S/N) and Z′-factor values have been identified.

Moreover, using the optimized and automated assay, we selected a small molecule inhibitor (< 500 Da) of CypA by the screening of the LOPAC library.

The inhibitor shows an IC_{50} in the low micromolar range, and molecular docking studies suggest how it interacts and occupies the catalytic groove of CypA.

8. AIMS OF THE PROJECT

In this study, we developed a sensitive and robust HTS method for monitoring the peptidyl prolyl *cis-trans* isomerase activity of human Cyclophilin (CypA).

CypA catalyses the slow, rate-limiting cis-trans isomerisation of peptidyl-prolyl bonds.

Great efforts are paid for the development of robust and sensitive assays, useful for selecting specific PPiase modulators for therapeutic approaches.

The catalytic activity of PPIases is normally monitored spectrometrically by using the chymotrypsin-coupled assay.

The discovered HTS method was used to identify prototypical inhibitors from LOPAC, a commercial library of bioactive drugs.

In order to assess its usefulness in High Throughput Screenings, we have optimized the method on 384-well plates and automated the screening process on a HTS platform.

9. MATERIAL AND METHODS

9.1 Substrates and chemicals

Protected amino acids, Coupling agents (HATU) and Fmoc-Rink Amide AM Resin used for peptide synthesis werepurchased from IRIS Biotech GmbH (Marktrewitz, DE). Fmoc-Glu(EDANS)-OH and Fmoc-Lys(Dabcyl)-OH were from PolyPeptide Group (Strabourg, France). Solvents, including acetonitrile (CH_3CN), dimethylformamide (DMF), trifluoroaceticacid (TFA) and methanol (CH_3OH) were purchased from ROMIL (Dublin, Ireland). Other products such as Sym-collidine, DIPEA, Piperidine, CyclosporinA (CsA), α-Chymotrypsin (hereafter only Chymotrypsin) from bovine pancreas (TLCK-treated to inactivate residual trypsin activity) and LOPAC^{1280} small library were from Sigma-Aldrich (Milan, Italy). Analytical HPLC analyses for monitoring the *cis-trans* transition were performed on an AllianceHT WATERS 2795 system, equipped with a PDA WATERS detector 2996. Preparative purifications were carried out on a WATERS 2545 preparative system (Waters, Milan, Italy) fitted out with a WATERS 2489 UV/Visible detector. LC-MS analyses were performed using a ESI Ion Trap HCT ETD IIHCUltraPTM discovery system Bruker mass spectrometer coupled with an HPLC System Alliance e2695 separation module fitted out with a 2998 PDA detector (Waters, Milan, Italy). A automated MICROLAB STAR Liquid Handling Workstation from Hamilton Robotics (Bonaduz, Switzerland) was used to develop the screening assay. The work-station includes a set of eight independent pipetting channels, several positions for sample tubes and plates, the barcode identification for samples, microplates, reagents and carriers. The liquid handler was implemented with the Total Aspiration and Dispense Monitoring (TADM) system, with the Liquid Level Detection system and the Tip Attachment (CO-RE) system. In all procedures, the Monitored Air Displacement (MAD) system was used. All workstation functions and integrated third-party devices were controlled by the Venus software (Hamilton Robotics, Bonaduz, Switzerland). AnEnSpire Multimode Plate Reader (Perkin Elmer) was used to perform fluorescence measurements.

9.2 CypA expression and purification

Recombinant His6tagged-CypA was efficiently expressed in BL21(DE3) *E. Coli* cells and purified and characterized, as previously reported in Materials and Methods section 3.2.1. Protein concentration was determined by reading the absorbance at 280 nm in

combination with the theoretical molar extinction coefficient (8730 $M^{-1}cm^{-1}$) using the NanoDrop200c UV-Vis spectrophotometer (Thermo Scientific). The His6 tag was not removed from the protein.

9.3 Peptide synthesis

Peptides were synthesized on solid phase using Fmoc-protected L-amino acids [23] and RINK AMIDE Resin AM with 0.71 mmol/g loading supplied by IRIS Biotech GmbH.

In particular, the deprotection of Fmoc from the α-amino groups was achieved by a preliminary treatment with 40% piperidine in DMF for 5 min followed by a second treatment with 20% piperidine in DMF for 15 min.

Couplings with amino acids were carried out by pre-activation with 4 equivalent of HATU (2-(1H-7-Azabenzotriazol-1-yl)-1,1,3,3-tetramethyl-uronium-hexafluorphosphate), [24] 4 equivalents of Fmoc-protected amino acids and 8 equivalents of Sym-Collidine (relative to the synthesis scale), for 5 min and adding the mixture to the resin for a reaction time of 45 min under continuous mixing. For HPLC analysis peptides were cleaved from the resin leaving the Fmoc group at N-terminus.

The peptide having the Dabcyl/EDANS FRET pair at the C- and N-terminus (FRET substrate) used in the HTS assay, was generally synthetized as previously reported. However, the introduction of the N-terminal Fmoc-Lys(Dabcyl) and of the C-terminal Fmoc-L-Glu(EDANS)-OH was achieved by a double coupling using 2eq at each coupling round, [25] and a longer reaction time (3 h).

Cleavage of the final peptide from the resin was accomplished by treatment with TFA-TIS-H_2O mixture (90:5:5, v/v/v) and subsequent precipitation in cold diethyl ether.

Lyophilized peptides were purified using an Onyx monolithic semi-PREP C18 column (100x10mm, Phenomenex, Castel Maggiore, Italy) operated at a flow rate of 15 mL/min; H_2O+0.1% TFA and CH_3CN+0.1% TFA were used as eluents, using a linear gradient from 10% to 60% of CH_3CN+0.1% TFA in 20 minutes.

Peptides were characterized by LC-MS, determining purity and MW of final compounds.

9.4 HPLC analysis

Time- and concentration-dependent isomerase activity of CypA were evaluated by HPLC using the new Fmoc substrates. The conditions used were as follows: Onyx monolithic C18 column (50x2 mm) operated at a flow rate of 0.6 mL/min; eluents: H_2O+0.1% TFA and

CH_3CN+0.1% TFA; wavelength 265.8 nm. A linear gradient from 15% to 80% of CH_3CN+0.1% TFA in 4 minutes was applied to elute the products.

The differences between CypA-catalyzed and spontaneous *cis-trans* isomerization rates of the Fmoc-protected substrates were evaluated by following the Fmoc-full length peptide signal reduction and/or the increase of chymotrypsin-hydrolyzed Fmoc-peptide at 265.8 nm (maximum Fmoc absorption).

The assays were carried out at room temperature and in a volume of 200 µL, by using the substrates at 10 ng/µL, commercial Chymotrypsin at 100 ng/µL and CypA at 200 ng/µL. Assays were performed in two different buffers, HEPES 35 mM and LiCl 5 mM or HEPES 35 mM and NaCl 150 mM to evaluate the effect of positive ions on the population of *cis* conformers and on the reaction kinetics.

Signal-to-background ratio (S/B) was defined as the X_P/X_N ratio of peak areas obtained for the PP_{cut} and EPP_{cut} peptides during the CypA-assisted (X_P) and not assisted (X_N) Chymotrypsin cleavage.

9.5 Assay automatization

The chymotrypsin-coupled enzymatic assay was performed in 384-well black solid bottom plates (PerkinElmer) in a total volume of 50 µL in each well using the new FRET substrate. For assays on full 384-well plates, Chymotrypsin, CypA and FRET substrate solutions in Reaction Buffer (PBS 1X, pH 7.4) were prepared at a concentration 4-fold higher than that of the final concentration used in the assay. Solutions of inhibitors were prepared in 96 well plates (mother plates) at 4X concentration in the Reaction Buffer.

The procedure consisted of the following steps:

(1) Dilution of compounds from the stock solution (in DMSO) in the reaction buffer in the mother plate.

(2) Dispensing 12.5 µL of buffer or inhibitor solution into 384-wells of black OptiPlate-384.

(3) Addition of 12.5µL of FRET substrate at concentration of 60 ng/µL.

(4) Addition of 12.5 µL of CypA at concentration of 2.2µg/µL.

(5) 30 min incubation at room temperature, in the dark.

(6) Addition of 12.5 µL of Chymotrypsinsolution at 600 ng/µL.

(7) Reading over time fluorescence, (λex =340 nm and λem=510 nm).

Experiments were run as quadruplicate and reported as averaged values ± standard deviation (±SD).

9.6 Assay Parameter Calculations

The signal-to-noise ratio (S/N) was calculated by using the equation $S/N = \frac{\text{Mean of catalyzed reaction} - \text{Mean of spontaneous reaction}}{\text{Standard Deviation of spontaneous reaction}}$ .The Z'-factor values in all conditions tested were calculated as reported in literature [26].

In the assays, Chymotrypsin at final concentration of 150 ng/µL was added in 384-well plates in which the substrate and CypA were already dispensed following the protocol reported before, and fluorescence was recorded after 30 min.

The assay was performed also in the presence of increasing amounts of DMSO to simulate the experimental conditions where by compounds from stock solutions in this solvent are submitted to screening. The chosen concentrations of DMSO were 1, 2, and 3% to simulate dilutions of 10 mM stock solutions in neat DMSO up to 100, 200, and 300 µM. Most compounds were soluble in this solvent at the indicated concentrations.

The Z'-Factor was determined at 0, 1, 2, and 3% DMSO concentrations on 32 independent data points for each condition.

9.7 IC_{50} Determination

Dose-dependent assays with the known inhibitor CsA and with the hit inhibitors were performed at concentrations ranging between 0.001 and 25 µM for the CsA and between 0.001 and 50 µM for the selected inhibitors.

The FRET substrate, the CypA and the hits were incubated for 30 min at room temperature. After the incubation Chymotrypsin was added and after 30 min fluorescence was detected. For all these assays, each data point was in quadruplicate.

Experimental data were fitted with GraphPad Prism, vers. 5.00, GraphPad Software (San Diego, California).

9.8 Determination of the Steady-State kinetic parameters for EPP substrate

To determine the Km/Kcat values the FRET substrate was serially diluted in PBS 1X pH 7.4 (from 1 to 250 µM). The peptide was then mixed with CypA at final concentration of 600 ng/µL and Chymotrypsin at 150 ng/µL.

After 30 min the fluorescence of EDANS was measured at 510 nm upon excitation at 340 nm.

9.9 NMR spectroscopy

All NMR experiments were carried out at 298.0 K using an Inova 600 MHz spectrometer (Varian Inc., Palo Alto, CA, USA), equipped with a cryogenic probe optimized for ^{1}H detection.

NMR data were collected on samples of EPP substrate without the Fmoc group to improve solubility. We assumed that the presence/absence of this group did not alter the *cis-trans* equilibrium.

Samples were prepared by dissolving the peptide at concentration of 600 μM in 20 mM sodium phosphate buffer pH 7.0 containing 10% $^{2}H_2O$ (500 μL) in presence of 150 mM NaCl or 5 mM LiCl.

For the one-dimensional (1D) ^{1}H spectra, 64 scans were acquired with a spectral width of 6714.8 Hz, relaxation delay 1.5 s, 16.384 data points for acquisition and 32,768 for transformation.

The two-dimensional (2D) [^{1}H, ^{1}H] DQF-COSY [27], TOCSY [28], NOESY [29] and ROESY [30] spectra were acquired using the TPPI method to obtain complex data points in the t_1 dimension.

Typically, 32 or 64 scans per t_1 increment were collected with a spectral width of 6714.8 Hz along both f_1 and f_2, 2048 × 256 data points in t_2 and t_1, respectively, and recycle delay 1.5 s. Water suppression was achieved by means of Double Pulsed Field Gradient Spin Echo (DPFGSE) sequence [31, 32].

The TOCSY experiment was recorded using a DIPSI-2 mixing scheme of 70 ms with 7.7 KHz spin-lock field strength. The NOESY spectra were carried out with a mixing time in the range of 250-450 ms.

The mixing time of the ROESY experiment was 200 ms. The data were typically apodized with a square cosine window function and zero filled to a matrix of size 4096 × 1024 prior to Fourier transformation and baseline correction.

Chemical shifts were referenced to internal water at 4.75ppm.

All NMR data were processed with the software VNMRJ 1.1.D (Varian Inc.). 1D spectra were analyzed using ACD/NMR Processor 12.0 (www.acdlabs.com). 2D spectra were analyzed using CARA (Computer Aided Resonance Assignment) software [33].

9.10 Fluorescence spectroscopy

Fluorescence measurements were performed on an EnSpire Multimode Plate Reader, Perkin Elmer and the assay was adapted to 384 well black plates in a total volume of 50 μL.
The intrinsic tryptophan fluorescence of CypA was determined by excitation at 295 nm and reading the emission at 340 nm.
The equilibrium dissociation constant K_D for the CypA-C3353 interaction was determined by fluorescence titration at 15 μM protein concentration in PBS 1X at pH 7.4.
Aliquots of *the non-fluorescent molecule* in 1% DMSO were added to the protein solution and the resulting fluorescence intensities were measured.
The final and constant DMSO concentration was 1%. A plot of the corrected fluorescence intensity *versus* ligand concentration was fitted with a one-site binding model
The reported K_D values were averages from three independent titrations.

9.11 Molecular Modeling

The coordinates for compounds D138 and C3353 were downloaded from MMsINC database [34], already energy minimized and with the partial charged assigned (MMs03080181 and MMs00455114, respectively).
To identify the more appropriate protocol for molecular docking studies, a self-docking benchmark using DockBench 1.01 software [35] was performed.
This procedure compared the performance of 17 different posing/scoring protocols to reproduce experimental derived complex geometries.
In the benchmark study, four crystal structure available in the protein data bank [36] were submitted to calculations, PDB ID: 3RDD, 4N1N, 4N1Q and 4N1R [37, 38, 39, 40].
Water molecules present in the pdb file were removed and the complexes were subjected to the structure preparation tool of MOE 2015 [41].
Finally the function Protonate3D [42] included in MOE 2015 [41] was used to assign the protomeric state at pH 7.4. The active site was defined using a radius of 12 Å from the centre of mass of the co-crystallized ligand. Each ligand was docked 20 times.
The ligands identified in the HTS were finally docked using the virtual screening tool of DockBench 1.01 on the protein conformation 3RDD, using GOLD [43] and Goldscore [44] as posing algorithm and scoring function respectively, with the same parameters adopted in the benchmark stage. The molecular docking analysis were performed with MOE 2015 [41].

10. RESULTS

10.1 Design and testing of substrates

Two new PPIase substrates, here after named PP and EPP, were designed in order to force their structures, at room temperature and in absence of organic solvents, in a predominantly *cis* conformation and thus to enhance assay sensitivity.

Specifically, besides the consensus sequence Pro-Phe (P-F) present in common PPIase substrates, a second P was inserted before the P-F segment, [46] as suggested by several other studies [47].

Moreover, a lysine (K^6 in PP peptide or K^8 in EPP peptide) was introduced in both sequences to improve the peptide solubility. A glutamic acid was inserted at the N-terminus of the EPP peptide (E^1) to potentially stabilize the *cis* conformation of the X-Pro bond through a salt bridge with the K^8 at the C-terminus [48, 49].

Both peptides bore an Fmoc group on the N-terminus to facilitate identification and detection by HPLC. The sequences of PP and of EPP are reported in Figure 10.1 together with the fragments resulting from Chymotrypsin cleavage.

Peptide	Sequence	MW_{calc}	MW_{exp} ($[M+H)^+$])	R_t(min)[a]
PP	Fmoc-APPFAKA-NH_2	921.33	922.2	3.20
PP_{cut}	Fmoc-APPF-OH	652.60	653.0	3.60
EPP	Fmoc-EAPPFAAKA-NH_2	1121.55	1122.4	3.01
EPP_{cut}	Fmoc-EAPPF-OH	781.60	782.1	3.35

Figure 10.1: Sequences of peptides used for monitoring the CypA isomerase activity through HPLC. Analytical data are reported for both the precursors and the reaction products with Chymotrypsin.

Peptides were easily synthesized using the standard solid-phase-Fmoc method [23]. Yields were on average greater than 60%.

CypA used in the assays was overexpressed in BL21(DE3) *E.Coli* cells with a tag of 6 histidine and purified to homogeneity by a single step of affinity chromatography. Typical yields were 20 mg/L. Time- and concentration-dependent isomerase activity of CypA were evaluated by HPLC using the PP and EPP substrates conjugated with the Fmoc group.

In Figure 10.2 A-D representative HPLC chromatograms of reaction products after 40 minutes incubation time are reported. Substrates were characterized by a single peak with a retention time of 3.20 min and 3.10 min, for PP and EPP respectively (Figure 10.2).

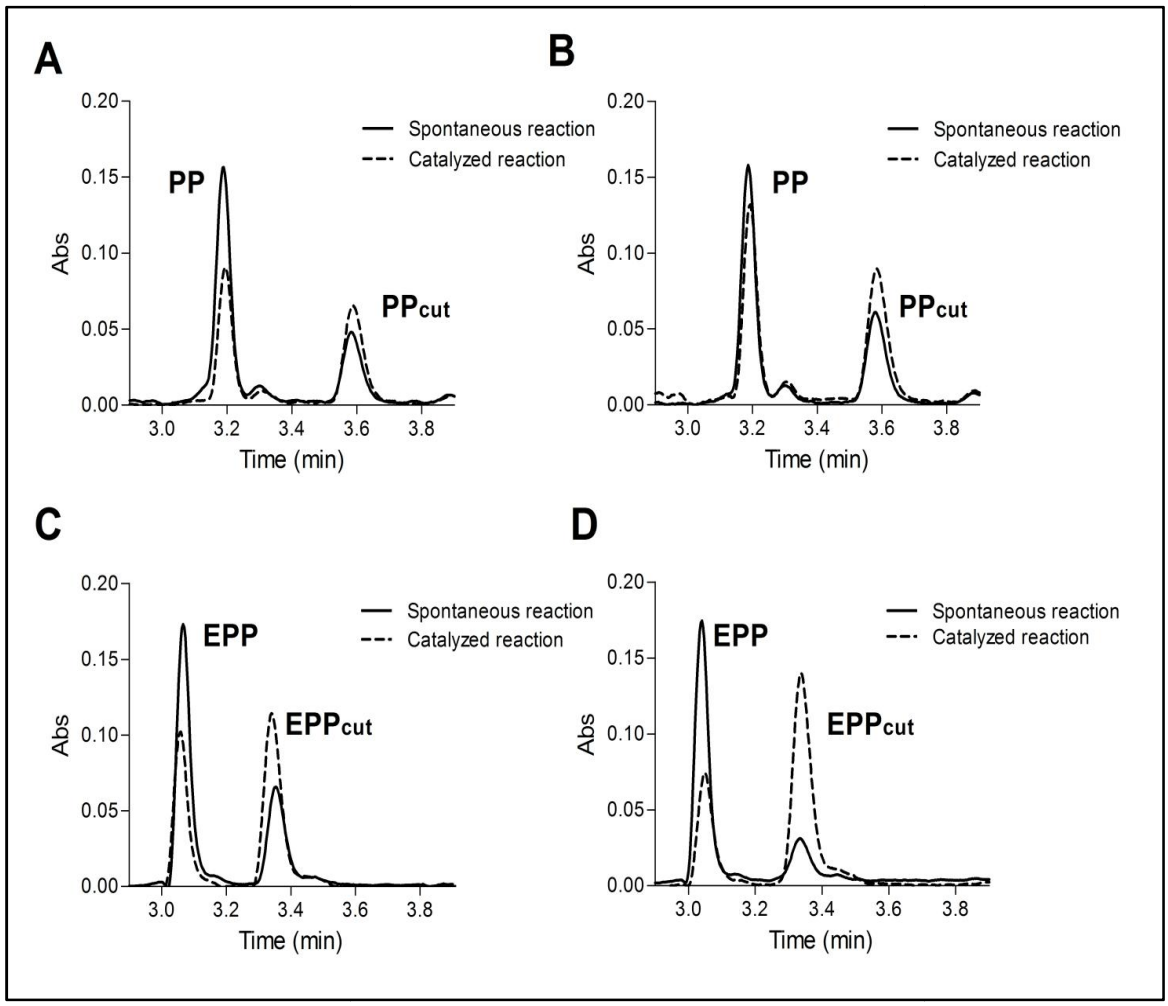

Figure 10.2: Chymotrypsin coupled isomer-specific proteolysis HPLC assay.(**A**-**C**) Representative HPLC chromatograms of spontaneous (solid lines) and CypA-catalyzed *cis-trans* isomerization process (dashed lines), after 40 min incubation at room temperature. In **A** the experiment with the PP substrate in Hepes 5mM, LiCl 5mM, pH 7.4 is shown; in **B** the experiment with PP in Hepes 5mM, NaCl 150 mM, pH 7.4 is shown; in **C** the experiment with the EPP substrate in Hepes 5mM, LiCl 5mM, pH 7.4 is shown; in **D**, the experiment with EPP in Hepes 5 mM, NaCl 150mM, pH 7.4 is shown. The measurement were carried out in the absorbance mode at 265.8 nm.

After treatment with Chymotrypsin alone and/or the Chymotrypsin/CypA mixture, new peaks with retention times of 3.60 min for the cleaved PP (PPcut) and 3.35 min for the cleaved EPP (EPPcut) were detected (Figure 10.2 A-D). Retention times, theoretical and experimental masses of the processed and unprocessed substrates are summarized in Figure 10.1. Results obtained with the PP and EPP indicated that in our experimental conditions, a substantial population of *cis*-conformers was present in both substrates as demonstrated by the presence of large amounts of Chymotrypsin unprocessed peptides in the absence of CypA (see peaks at 3.10 and 3.20 minutes, solid lines in Figure 10.2 A-D).

However, comparative data indicated that Chymotrypsin processing was strongly reduced

with the EPP substrate in the presence of NaCl (Figure 10.2 D), suggesting that, for this substrate, Na^+ ions stabilized more efficiently the *cis* conformers compared to Li^+ ions [50]. The higher population of *cis*-conformers in EPP in the presence of NaCl translated into a the higher efficiency of CypA to convert them into *trans*-conformers, thus prone to Chymotrypsin cleavage (Figure 10.2 D). EPP in NaCl-containing buffer was chosen for subsequent investigations.

10.2 DMSO tolerance, and assessment of CypA inhibitor

Most bioactive compounds are characterized by very low solubility in aqueous solvents, there by compounds used in high throughput screening (HTS) are typically dissolved in DMSO starting stock solutions. For this reason enzymatic assays are mostly developed in presence of this organic solvent.

We therefore carried out time course experiments using the EPP substrate (10 ng/µL), CypA (200ng/µL) and Chymotrypsin (100ng/µL) in Hepes 5 mM, NaCl 150 mM, pH 7.4 at increasing concentrations of DMSO (from 0.5% to 5%) and measuring the enzyme kinetic as described above. Assay performances in these conditions were evaluated in terms of signal-to-background ratios (S/B) calculated as described in the section of Methods.

A detrimental effect of DMSO was observed for concentrations greater than 3% (Figure 10.3 A).

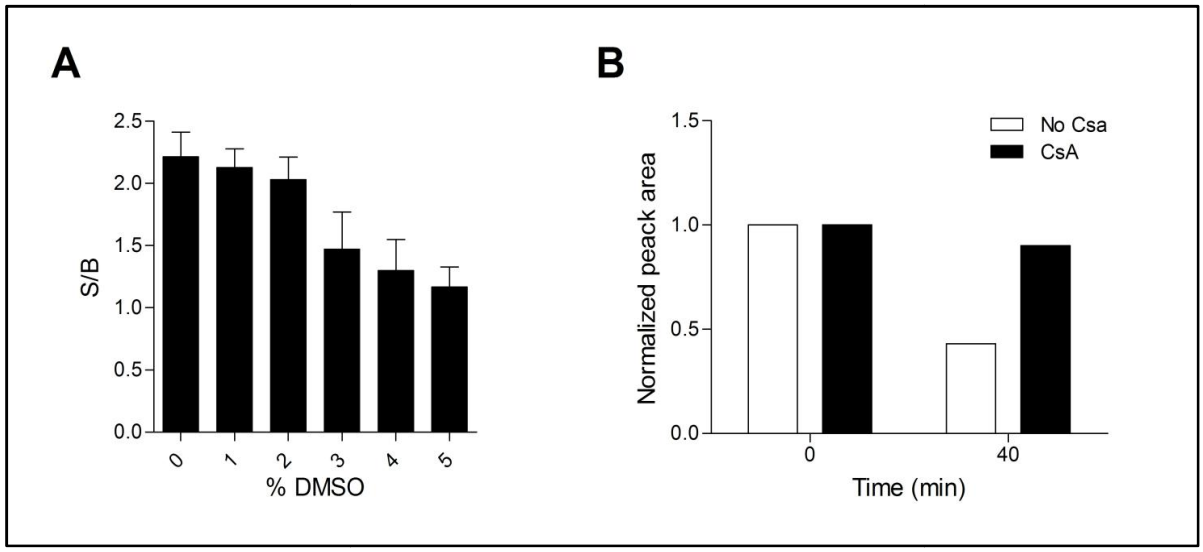

Figure 10.3: DMSO tolerance test and evaluation of the known CypA inhibitor CsA. (**A**) The DMSO tolerance was evaluated calculating the signal-to-background (S/B) at different concentrations of DMSO (from 1% to 5%).Values were calculated as X_P/X_N, as described in the Methods. (**B**) Evaluation of CsA inhibitory effect under the selected conditions. Normalized peak area of HPLC chromatograms of chymotrypsin – processed substrate (EPP) with and without 10 µM CsA, in Hepes 5 mM, NaCl 150 mM, pH 7.4, at zero and 40 min of incubation time. Responses were calculated as ratio between EPP peak area of spontaneous and CypA-catalysed reaction in samples with and without CsA.

However, the value obtained in the presence of 3% DMSO (~1.5) was still sufficiently high to enable optimal performances in the assays.

We also evaluated the effect of the natural inhibitor CsA on CypA isomerase activity in our conditions [2, 3].

Reactions were conducted as described above in the presence of 1% DMSO, because of the low solubility of CsA. In Figure 10.3 B is reported the resulting HPLC chromatogram calculated by subtracting the signal of spontaneous reaction from that of the CypA-catalysed reaction in samples with and without CsA.

Results obtained demonstrated that the presence of CsA interfered with the CypA isomerase activity reaching the total inhibition at 2-fold molar excess over CypA (Figure 10.3 B).

10.3 NMR structural characterization of the new CypA substrate

To provide more useful insights into the conformation of the selected EPP substrate we performed NMR analysis on the Fmoc-free peptide in aqueous buffers containing the different ions. In particular, 1D ^{1}H and 2D [^{1}H, ^{1}H] TOCSY, NOESY and ROESY spectra of the peptide were acquired in phosphate buffer in the presence of either LiCl or NaCl.

According to the presence of two X-Pro peptide bonds (A2-P3 and P3-P4) four conformational states (numbered from 1 to 4) were expected in a slow-exchange equilibrium. Indeed, as can be seen in Figure 10.4, the F5 H^{N}, immediately following the P3-P4 segment exhibited four different chemical shifts in either saline buffer tested (NaCl and LiCl).

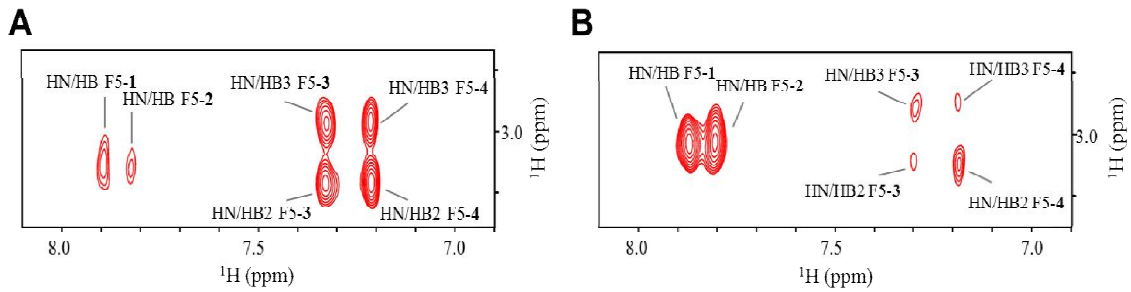

Figure 10.4: NMR structural characterization of the EPP substrate. Expansion of the H^{N}-aliphatic correlation region of the 2D [^{1}H, ^{1}H] TOCSY spectra of the peptide in PBS 1X (**A**) and phosphate buffer containing 5 mM LiCl (**B**). Four correlation H^{N}-H^{β} F5 cross-peaks are observed, one for each of the four (1-4) expected *cis-trans* conformers.

However, different relative peak intensities, correlating with the relative populations of the four conformers, were observed in the two buffer tested. The F5 H^{N}-H^{β} cross-peak volumes

from TOCSY spectra were used to determine the relative conformer populations which are listed in Figure 10.5.

Conformers	AlaPro and ProPro Conformations[b]	% NaCl[a]	% LiCl[a]
1	xt	7	22
2	xt	5	21
3	xc	46	27
4	xc	42	30

Figure 10.5: Relative populations of *cis* and *trans* conformers in H-EPP-NH_2.

Due to the low number of signals in both the NOESY and ROESY spectra, there was ambiguity in assigning the *trans-cis* states of the two X-Pro bonds from the NOE patterns. Nonetheless, considerations on the influence of proximal and distal proline isomerization on the chemical shifts were used to gain insight into the proline isomerization in the peptide [36]. Specifically, since the $F5H^N$ was separated from the P3-P4 peptide bond by one covalent bond, greater chemical shift changes (Δδ) were expected following isomerization of the proximal proline (i.e. P4), while minor changes were expected upon distal proline isomerization (i.e. P3). On this basis, the two $F5H^N$s at 7.88 and 7.82 ppm (conformers 1 and 2, respectively) and those at 7.33 and 7.21 ppm (conformers 3 and 4, respectively), which showed small differences of chemical shift ($\Delta\delta H^{N1-2}$= 0.06 ppm and $\Delta\delta H^{N3-4}$ = 0.12 ppm), can result from the isomerization of the distal A2-P3 bond.

On the other hand, the two sets of peaks (1-2 and 3-4), showing larger differences for the H^N chemical shifts ($\Delta\delta HN^{av1-2/3-4}$= 0.58 ppm), could a rise from the isomerization of the proximal P3-P4 peptide bond (Figure 10.4 A-B; Figure 10.6).

	$\Delta\delta H^N$
1-2	0.06
1-3	0.55
1-4	0.67
2-3	0.49
2-4	0.61
3-4	0.12

Figure 10.6: Chemical shift differences of the Phe^5 H^Ns in the four *cis/trans*.

Taking into account that the P3-P4 peptide bond in *cis* conformation seems to be more favored in NaCl than in LiCl, as indicated by the Chymotrypsin-coupled assay, conformers 1 and 2 should have the P3-P4 peptide bond in *trans* conformation (conformers xt). Conversely, conformers 3 and 4 should correspond to the P3-P4 peptide bond in *cis* conformation (conformers xc).

In this hypothesis, the *cis* P3-P4 population in NaCl is 88%, whereas in LiCl is 57%. Moreover, the A2-P3 bond seems to have the same *cis* and *trans* contents (about 50 % on the basis of the data reported in Figure 10.6) in both buffers.

It is worth to note that in the case of conformers 3 and 4, the F5 H^N chemical shift is up-fielded and the two germinal Hβs appear as distinct signals, exhibiting their magnetic non equivalence and suggesting a more restricted rotation of the F5 ring.

Moreover, the four *cis-trans* states gave also rise to multiple spin systems for the aliphatic protons of the Proline residues. Although the peaks assignment resulted intricate, we could observe a Proline Hα proton highly up-fielded (3.77 ppm), likely due to the close proximity of the P3-F5side-chains, as found in some proteins and peptide containing the segment P-P-F [47], that gives rise to the ring current effect on Hα protons of the first Proline.

Closely interacting P3-F5side-chains are supposed to be at the basis of the observed stability of the Proline-Proline *cis* conformers in the segment P-P-F, when present in a short peptide, devoid of any tertiary interaction.

10.4 Development of a FRET-assay

In order to develop a FRET-assay the selected EPP substrate was endowed with the FRET pair EDANS-Dabcyl [51].

EDANS-Dabcyl is a widely used donor-quencher pair. The optimal absorbance and emission wavelengths of EDANS are λ_{abs} = 336 nm and λ_{em} = 490 nm respectively, and for Dabcyl, the maximum absorbance wavelength is λ_{abs} = 472 nm, which, to a large extent, overlap with the emission spectra of EDANS.

When the two fluorophores are in close proximity (10–100 Å), the energy emitted from EDANS is quenched by Dabcyl. While the intact molecule is internally quenched, EDANS fluorescence is readily restored upon protease cleavage within the peptide chain and the intensity change can be detected continuously and directly [51, 52].

The substrate Ac-EK(Dabcyl)PPFAE(EDANS)KA-NH2 was efficiently synthesized, purified with a high yield (~40%) and characterized by mass spectrometry (Figure 10.7).

Entry	SEQUENCE	MW_{calc}	$M_{exp}[M+H^+]$
1	Ac-EK(Dabcyl)PPFAE(EDANS)KA-NH_2	1556.82	1556.2
2	H-AE(EDANS)KA-NH_2	664.31	665.6

Figure 10.7: Sequences and analytical characterization of the FRET substrate.

In the intact FRET peptide, the fluorescence of EDANS is efficiently internally quenched by the Dabcyl in Hepes 5 mM, NaCl 150 mM and phosphate saline buffered (PBS1X) buffer at pH 7.4, as well. Indeed, the intact substrate showed a very low fluorescence emission at 510 nm upon excitation at 340 nm, in a concentration range between 5 to 100 ng/µL compared to the chemically synthesized cleaved substrate used at same concentrations (Figure 10.8).

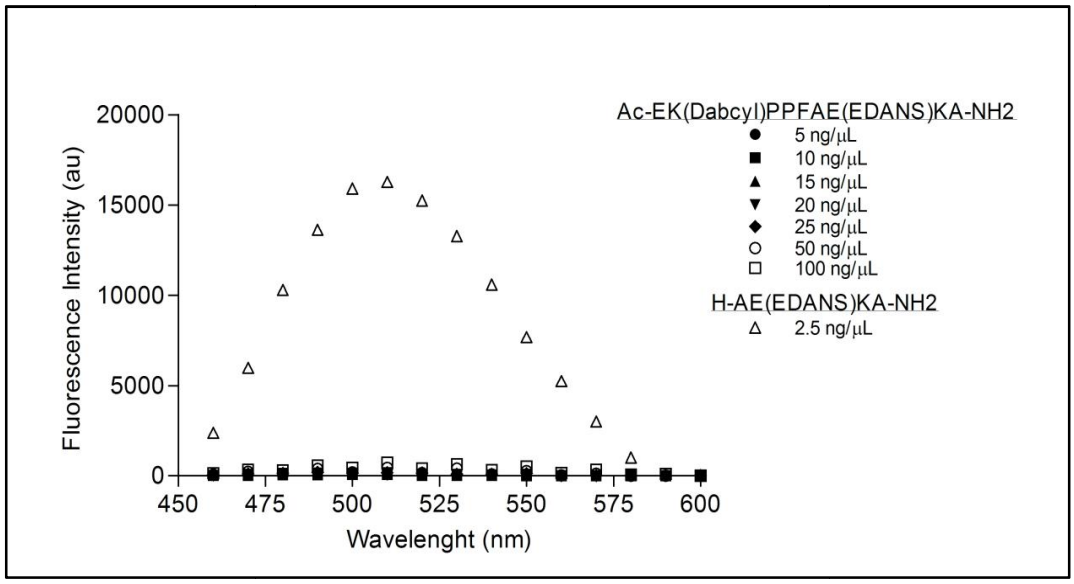

Figure 10.8: Evaluation of concentration –dependent intrinsic fluorescence and quenching effect of Ac-EK(Dabcyl)PPFAE(EDANS)KA-NH_2 substrate. A stock solution of the substrate was diluted in PBS 1X at pH 7.4 to have final concentrations of 100 ng/µL, 50 ng/µL, 25 ng/µL, 20 ng/µL, 15 ng/µL, 10 ng/µL and 5ng/µL. The intrinsic fluorescence and the quenching effects were evaluated recording spectra at wavelengths in the range of 450 – 500 nm. The peptide AE(EDANS)KA-NH2 (2.5 ng/µL) were tested at the lowest concentration as positive control.

The incubation of recombinant CypA at room temperature with the substrate resulted in the specific enzymatic cleavage by Chymotrypsin and a time-dependent increase of fluorescence intensity ($\lambda_{ex}/\lambda_{em}$= 340nm/510 nm) that was linearly-related to the extent of CypA-mediated substrate isomerization.

Assay conditions were standardized manually and subsequently validated in a HTS format using a liquid handler and 384-well black plates.

In particular, firstly we investigated the influence of substrate and chymotrypsin concentration on the kinetic of EDANS release from the substrate in absence of the isomerase. Then, time-course experiments were optimize dusing four substrate concentrations (15, 25, 50 and 100 ng/µL) and four different substrate/chymotrypsin ratios (1:1, 1:5, 1:10 and 1:20 w/w) in a total volume of 50 µL in PBS 1X buffer at pH 7.4.
The choice of the PBS1X as reaction buffer is due to the higher stability of the CypA over time in this compared to the buffer Hepes 5 mM, NaCl 150 mM, pH 7.4.

As expected, a higher fluorescence emission was generated at increasing substrate concentrations and substrate-Chymotrypsin ratios (Figure 10.9).

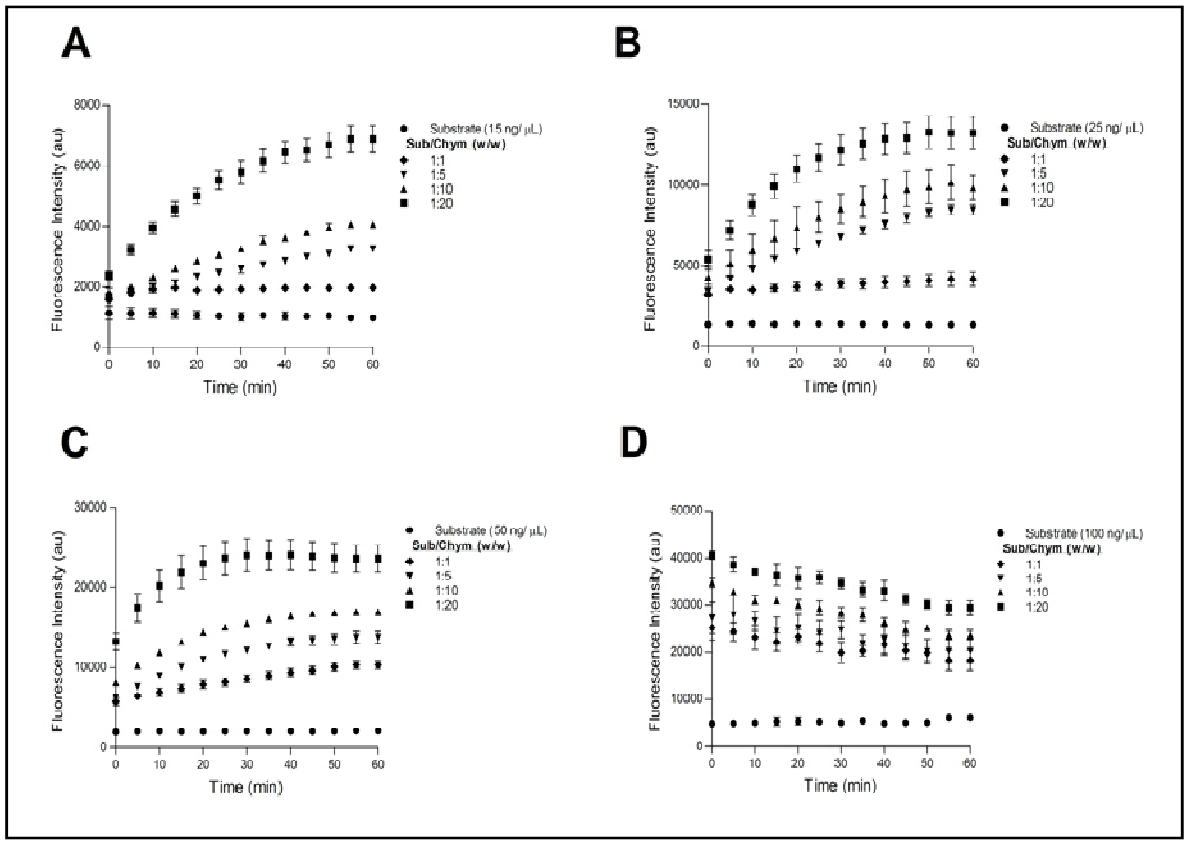

Figure 10.9: Evaluation of the optimal substrate/chymotrypsin ratios for the FRET-protease coupled *cis-trans* assay development. Time and dose – dependent – assays carried out using four different substrate concentrations:15 (**A**), 25 (**B**), 50 (**C**) and 100 (**D**) ng/µL, and four substrate/chymotrypsin ratios (1:1, 1:5, 1:10 and 1:20 w/w) in a total volume of 50 µL. The fluorescence emitted at 510 nm was monitored upon excitation at 40 nm. Experiments were run as quadruplicate and reported as averaged values ± standard deviation (SD).

However, the lowest fluorescence emissions were obtained using the substrate at 15 ng/µL and substrate/Chymotrypsin ratios of 1:1, 1:5 and 1:10, because in these conditions the hydrolysis reaction appare slower (Figure 10.9 A).
We next optimized the concentration of CypA. As shown in Figure 10.10**,** the isomerization activity increased linearly with the increase of CypA concentrations from 25 to 600 ng/µL.

Optimal conditions for the assay, in terms of signal-to-noise (S/N) values, reaction time and amount of substrate were as follows: substrate concentration 15 ng/µL, chymotrypsin 150 ng/µL (1:10 enzyme:substrate ratio), CypA 600 ng/µL.

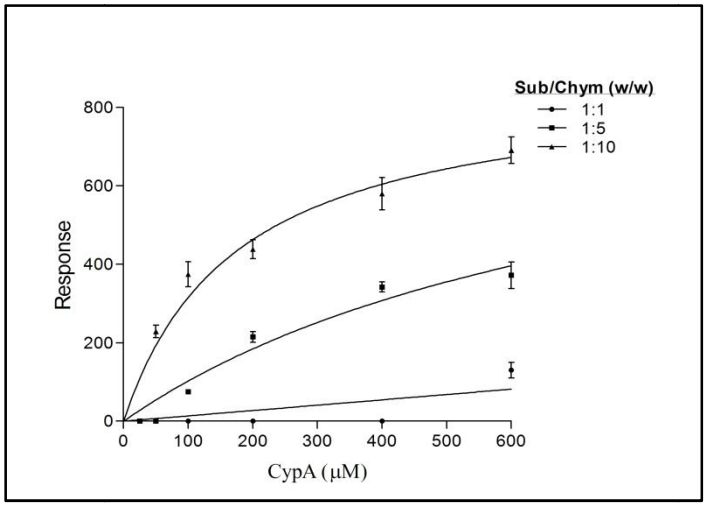

Figure 10.10: Choice of CypA concentration for the FRET-protease coupled *cis-trans* assay development. (**A**) Dose – dependent assays with three different substrate: chymotrypsin ratios (1:1, 1:5 and 1:10 w/w) and using several concentration of CypA (from 25 to 600 ng/µL), in PBS 1X at pH 7.4 after 30 min of reaction time. The responses were calculated by subtracting the signal obtained during the CypA-assisted and not assisted Chymotrypsin cleavage.

An optimal reaction time of 30 min was chosen, because substrate processing was linear for about 30 min and completed after 50 min under our experimental conditions (Figure 10.11 A-B). Under these conditions, an overall signal of around 800 normalized fluorescence units (Figure 10.11 A) was detected.

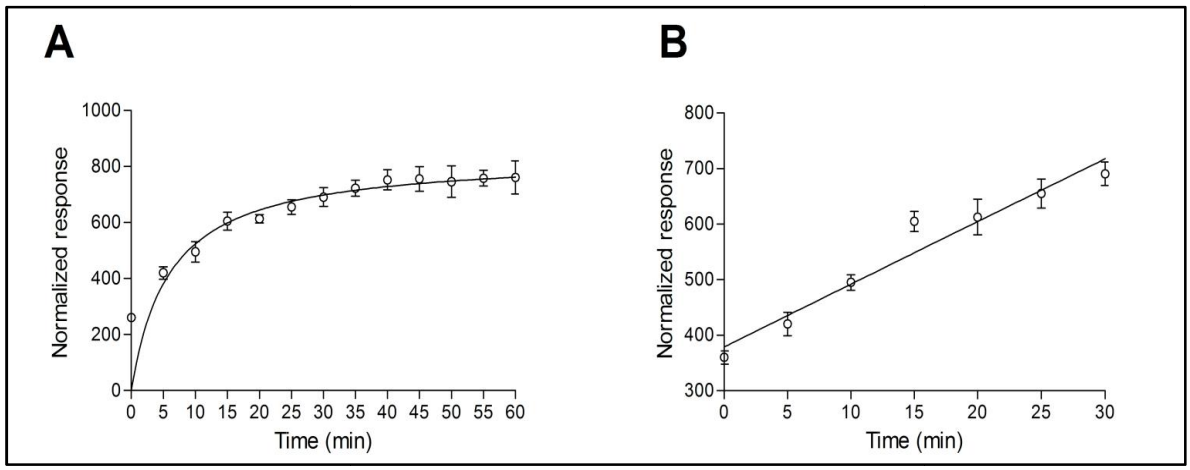

Figure 10.11: **.**Assay set up. (**A**) Time course of FRET-chymotrypsin coupled *cis-trans* isomerization assay using the substrate at concentration of 15 ng/µL, the chymotrypsin at 150 ng/µL and the CypA at 600 ng/µL in PBS1X at pH 7.4.(**B**) Time-dependent assay (in 30 min) using EPP at 15 ng/µL, Chymotrypsin at 150 ng/µL and CypA at 600 ng/µL, in PBS 1X at pH 7.4. Experiments were run as quadruplicate and reported as averaged values ± standard deviation (SD).

The enzyme reaction followed the Michaelis-Menten kinetics with the velocity of the reaction (*v*) increasing with substrate concentration (S) (Figure 10.12).

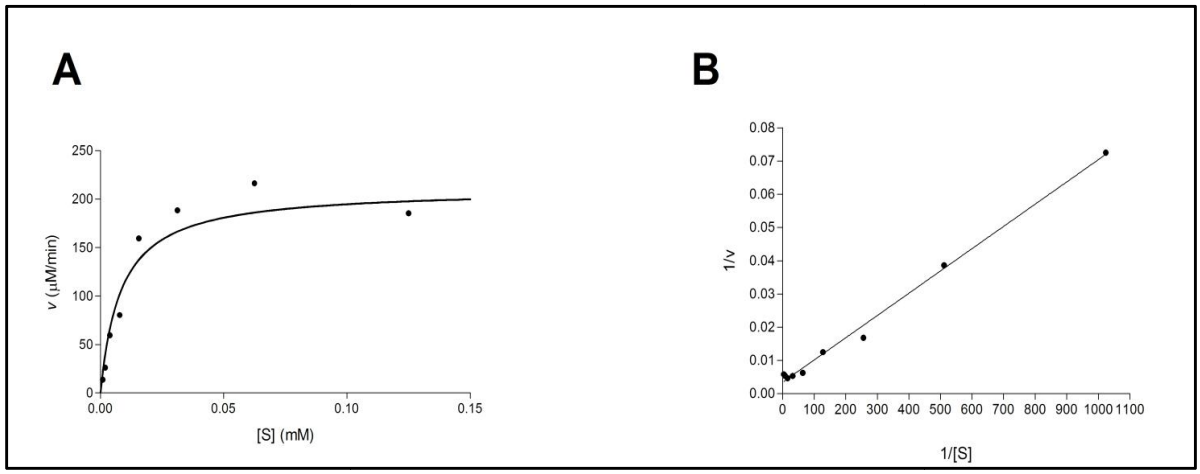

Figure 10.12: Kinetic constants determination of FRET-Chymotrypsin *cis-trans* coupled assay. (**A, B**) Michelis and Menten and Lineweaver-Burk plots, respectively, for the CypA catalyzed *cis-trans* prolyl isomerization of EPP substrate. Increasing concentration of EPP were mixed to CypA at 600 ng/µL and Chymotrypsin at 150 ng/µL in PBS 1X at pH 7.4 and incubated for 30 min.

A first order rate kinetic was observed and a double reciprocal Lineweaver-Burke plot of 1/v against 1/[S] gave values of kcat/Km of 2.5×10^7 M^{-1} s^{-1} at room temperature in physiological condition (PBS 1X , pH 7.4) (Figure 10.12 B). The kinetic constant here determined is in agreement with the value reported in literature (1.4×10^7 M^{-1} s^{-1}), calculated with the chymotrypsin – coupled PPIase assay, using the recombinant wild type CypA and the substrate N-succinyl-AAPF-pNA dissolved in Hepes 35 mM buffer (pH 8.0) and 66% (vol/vol) aqueous dimethyl sulfoxide at 10 C [53].

10.5 Assay Procedure Automation and Validation

The assay procedure described for the manual experiments, was next automated using an integrated platform comprising a 8-channel Starlet station for liquid handling, a robotic arm and a multi-well plate reader (EnSpire Multimode Plate Readers, Perkin Elmer). The assay was performed also in the presence of increasing amounts of DMSO (1%, 2% and 3%) to simulate the experimental conditions whereby compounds from stock solutions in this solvent are submitted to screening. Optimal assay performances were evaluated in terms of signal-to-noise (S/N) and Z'-factor values.

As can be seen in Figure 10.13 excellent S/N values of 11.6, 11.1 and 10.9 were determined for the assays without DMSO and in the presence of 1 and 2 % solvent,

respectively; the S/N value decreased to 9.1 at 3% DMSO.

The Z'-factor values determined in the absence DMSO and at 1 and 2% solvent were 0.80, 0.75 and 0.68, respectively, while in the presence of 3% DMSO the value decreased to 0.56. Altogether, data suggest that Z'-factor and S/N values are still sufficiently high for using the assay in screening campaigns at the highest solvent concentration tested.

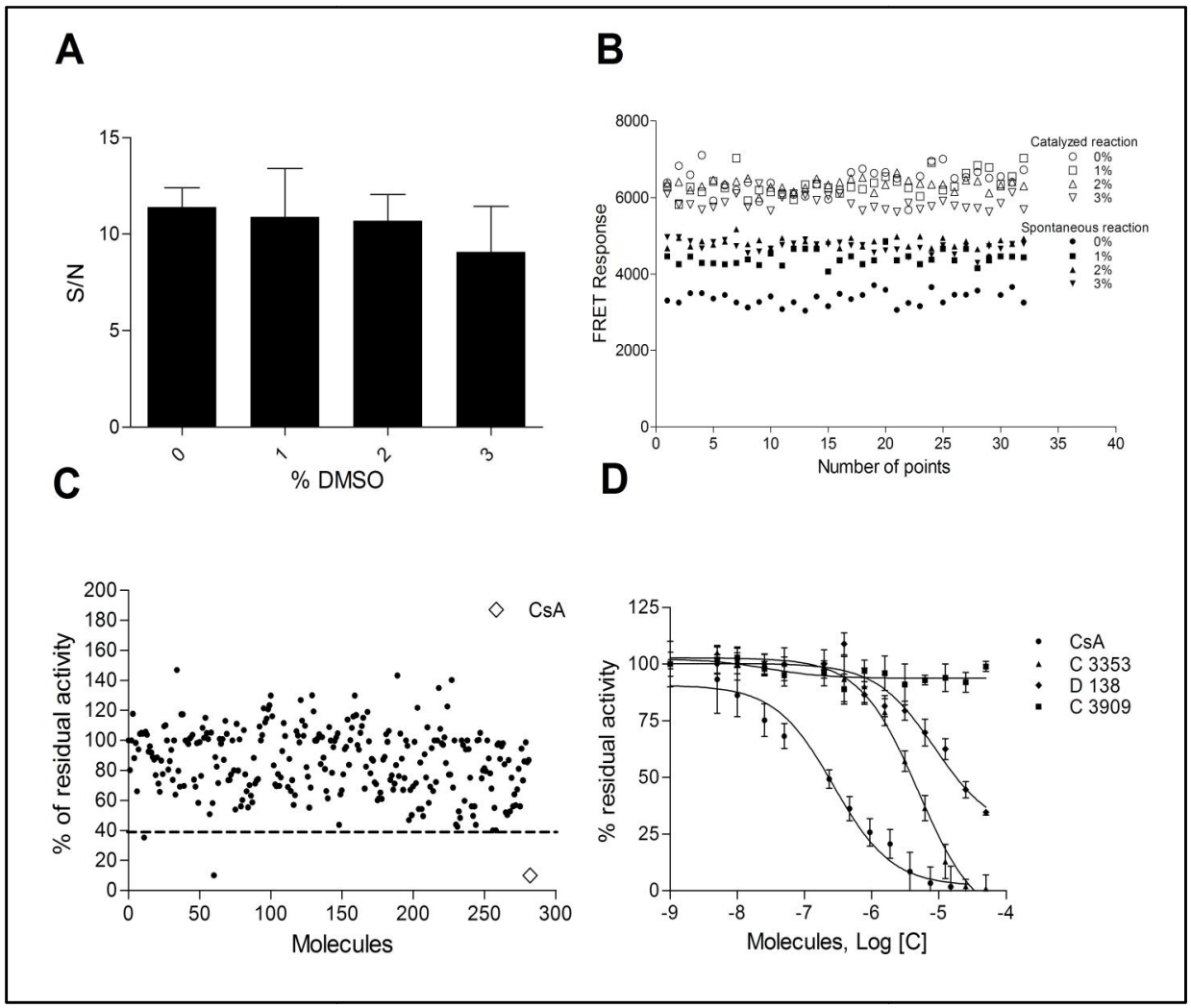

Figure 10.13: Evaluation of FRET - assay performance. Thirty-twowells of a 384-well plates were used to determine the suitability of the assay for high-throughput screening in terms of S/N (**A**) and Z'-factor values (**B**) with and without DMSO. (**C**) Screening of 298 compounds of LOPAC library tested. The plot reported the percentage of residual activity, determined by the FRET-assay, of CypA after an hour incubation with compounds. (**D**) Dose-dependent assays with three selected hits, CsA, C3353, D138 and a negative control (C3909). Data were fitted and the IC50 determined by non-linear regression analysis.

In order to estimate the assay suitability for HTS, a pilot screen against the LOPAC library (n = 1,280 compounds) was performed. Assays were transferred in 384 well plate format using laboratory automation equipment (Microlab star line, Hamilton™) and a final

concentration of LOPAC compounds of 50 μM in quadruplicate in PBS 1X at pH 7.4, supplemented with DMSO 1% (Figure 10.13 B).

In Figure 10.13 C results obtained on the 298 compounds are reported. From this set of compounds, three were selected for further characterization.

They were: N2-(cis-2-Aminocyclohexyl)-N6-(3-chlorophenyl)-9-ethyl-9H-purine-2,6-diamine hydrochlorid (LOPAC code C3353), 5,7-Dichlorokynurenicacid (LOPAC code D138); and as expected also the CsA, present within the set. D-cycloserine (LOPAC code C3909), instead, was used in the next assays as negative control.

The testing was performed in a fourteen-point dose-response format in quadruplicate at a 1:2 serial dilution. As shown in Figure 10.13 D, CsA provided a strong inhibition underlined by an IC_{50} of 100 nM, in agreement with other reports [53].

The compound D138, inhibited the isomerase activity in dose dependent manner without reaching the saturation in the concentration range tested, suggesting a weaker affinity for CypA compared to CsA. On the other hand, compound C3909, used as negative control, as expected, did not provide inhibition of isomerase activity.

Compound C3353 provided a strong dose-dependent inhibition which was nearly complete at 25 μM. The estimated IC_{50} for this compound was 4 μM. Direct binding of compound C3353 with CypA was assessed using fluorescence quenching assays (see Material and Methods section for details). A plot of the corrected fluorescence intensity *versus* ligand concentration was fitted with a one-site binding model (Figure 10.14), providing a K_D of 6 μM, in agreement with the IC_{50} determined in the HTS assay.

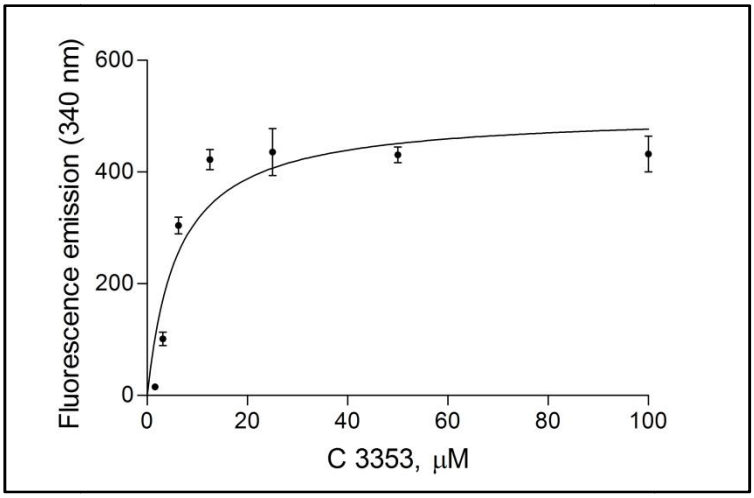

Figure 10.14: CypA Fluorescence titration with the C3353 molecule. The measured fluorescence intensities normalized (dots) are fitted with a nonlinear regression curve (line).

10.6 Molecular Docking studies of C3353 and D138

Molecular docking simulations were carried out to investigate the binding modes of the novel inhibitors identified in the HTS and with the aim to interpret the experimental binding data. First, to identify which docking protocol and which protein conformation were more suitable for our compounds, we performed a self-docking benchmark based on the human CypA complexes available in the protein data bank (PDB).

We selected four complexes in which a unique binding mode was present (PDB code: 3RDD, 4N1N, 4N1Q and 4N1R). In the benchmark performed with Dockbench software, we compared the ability of 17 different protocols in reproducing the four complex conformations (see Methods section for details). Except for 4N1N, all the complex geometries were nicely reproduced by several protocols (Figure 10.15)

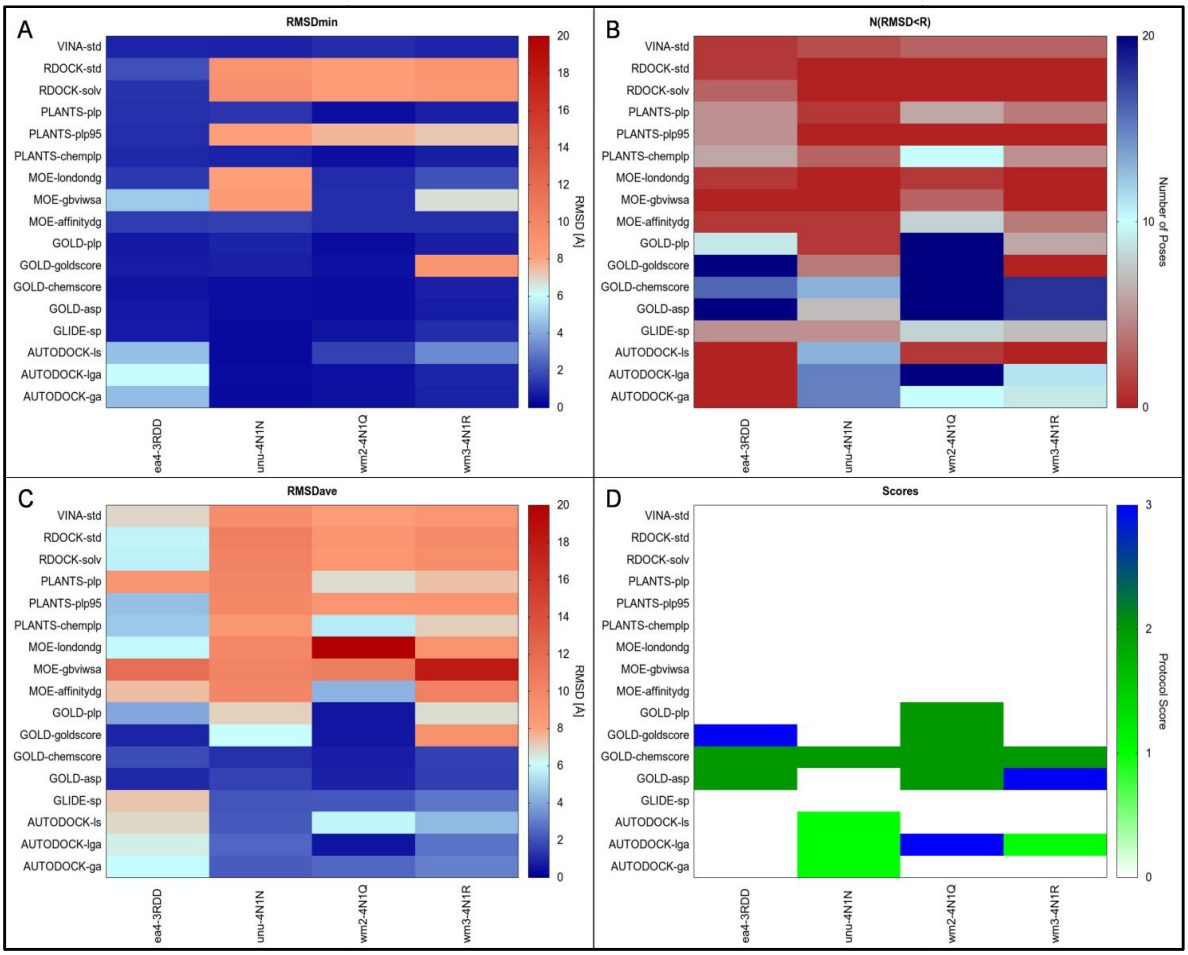

Figure 10.15: Results of the docking benchmark study on human CypA. (**A**) Minimum RMSD values (RMSDmin) performed by the tested docking protocol (y-values) for the considered complex structures (x-values); (**B**) Average RMSD values (RMSDave); (**C**) Total numbers of conformations returned by the docking protocol with a RMSD value lower than the X-ray crystal resolution (N(RSMD < R)); (**D**) The Protocol Score is a resuming score based on the RMSDmin, RMSDave, N-RMSD on a 0–3 points scale. Values are represented by a colour scheme, blue spots identify the best obtained results.

In order to dock D138 and C3353, we selected the protein conformation extracted from the complex with PDB code 3RDD due to the highest similarity in the size of its ligand to C3353. Among the 17 protocols, for the 3RDD complex the GOLD program coupled with Goldscore scoring function was the protocol showing the best performance in the benchmark study. Molecular docking studies of both compounds revealed a clear binding mode, in which a unique cluster of conformations was present for each ligand. In the case of the strongest inhibitor, C3353, the molecule adopts a conformation that is nicely accommodated in the active site of CypA (Figure 10.16, panels A and C).

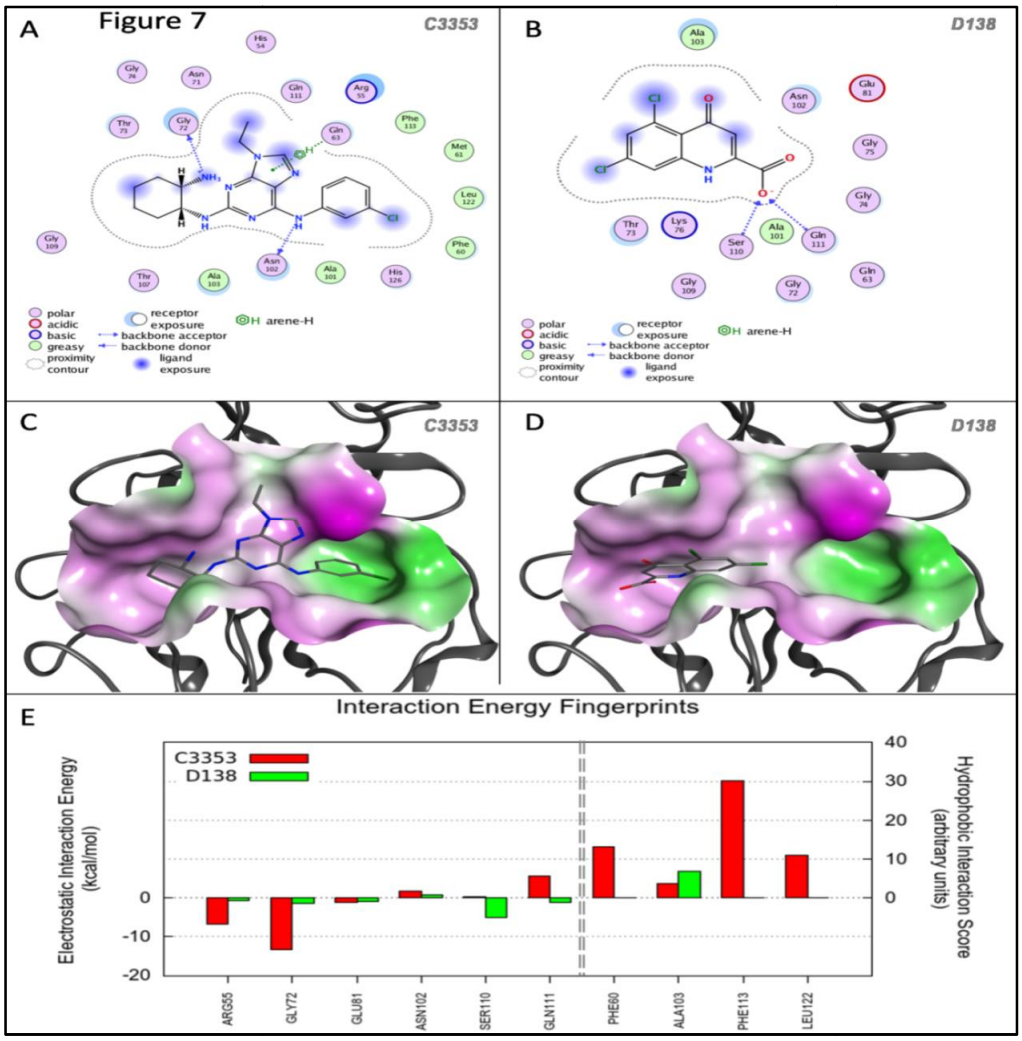

Figure 10.16: Molecular docking studies of D138 and C3353 compounds. In panels A and **C**, the binding mode of C3353 is reported. In **A**, a schematic depiction of the more relevant interactions with the catalytic site of CypA is shown; in **B**, the 3D-conformation with highest score resulted in the docking simulation is reported. The surface of CypA is colored according the hydrophobic propensity of the residues forming the active site (the hydrophobic and hydrophilic features are respectively coded into a green to violet palette color scheme). In Panels B and **D**, the binding mode of D138 is shown. Similarly to C3353, both the 2D depiction of the main interactions (panel B) and the highest score conformation (panel D) are reported using the same color scheme. In Panel E, the per-residue analysis of the protein-ligand interaction for C3353 (red) and D138 ligands(green). In the histogram two component of the interaction energy are computed independently for the residues mostly involved in the binding.

The chorophenyl moiety lies in a hydrophobic pocket formed by F^{60}, F^{113} and L^{122}, while the aminocyclohexyl group occupies a more hydrophilic groove defined by G^{72}, S^{110}, Q^{111}, S^{119}, and T^{107}. In particular, the aminocyclohexyl conformation is stabilized by the presence of a hydrogen bond with the backbone of G^{72}.

The purinic core occupies a third site connecting the two previously mentioned pocket and mainly interacts with R^{55}; the ethyl moiety at N^9 increment the shape complementarity with the protein surface.

The 5,7-dichlorokynurenic acid (D138) showed a clear propensity for the hydrophilic groove of the CypA catalytic site. The carboxylic moiety establishes two hydrogen bonds with S^{110} and Q^{111} while the condensed ring lies in front to the methyl group of A^{103} (Figure 10.16, panels B and D).

The molecular basis explaining the different ability to inhibit the CypA enzymatic activity can be ascribed to the different size of the two compounds and to the number of interactions they are able to establish with the catalytic site.

In particular, C3353 is able to occupy most of the catalytic cleft and the final score returned by Goldscore function was clearly higher than for D^{138}, respectively 76.8 and 48.6.

These observations are more evident when the contribution to the estimated interaction energy of the two compounds are plotted in a per-residue histogram as reported in the panel E of the Figure 10.16.

In this graph, the electrostatic interaction energy and a hydrophobic score are computed for each residue of the binding site and the most relevant ones are reported. While the electrostatic component of the predicted interaction energy is relevant for both ligands, the hydrophobic score is notably weaker in D138 that interact only with A^{103}.

11. DISCUSSION

The peptidyl-prolyl *cis-trans* isomerases represent a large class of biological proteins, such as the cyclophilins, with broad physiological functions, making them valid targets for therapeutic intervention [54].

For example, cyclophlin inhibitors have shown promise as replication inhibitors of several RNA viruses including HIV, HCV, SARS corona virus and influenza virus [54].

Non-immunosuppressive cyclosporin derivatives [54, 55, 56] have reached clinical development for the treatment of hepatitis C infection. Moreover, formulations of cyclosporin itself have also shown some promise in new therapeutic applications, for example in traumatic brain injury [57], muscular dystrophy [58], respiratory disease [59], cardiovascular disease [60] and Alzheimer's disease [61].

In this framework, many efforts are spent on selecting specific PPIase modulators for therapeutic approaches. However, the discovery of novel inhibitors has been limited by the lack of suitable assays for HTS.

The biochemical reaction catalyzed by PPIases interconverts *cis* and *trans* isomers of a proline peptide bond. However, this reaction also occurs spontaneously in the absence of catalysis within a few minutes, especially in short synthetic peptide substrates.

Inhibitor screens therefore have to distinguish between the catalyzed and the spontaneous reactions, which are separated by a time window of a few minutes [62].

Such screens have been developed, but they require low temperatures and elaborated experimental protocols in the presence of organic solvent [19]; they therefore are invariably of low throughput and are unsuitable for large scale screens [53].

Here, we developed and optimized a simple and robust homogenous fluorescent HTS assays for the discovery of Cyclophilin inhibitors in 384-well plates, using a new FRET-based substrate probe useful for Chymotrypsin-coupled isomerase assays. The probe, easily prepared by a straightforward solid phase approach in a highly soluble form, contains the well-known FRET pair Dabcyl-EDANS [50,51].

The donor (EDANS) is separated from the quencher (Dabcyl) by a short peptide linker containing a modified Chymotrypsin cleavage site (Pro-Phe), and residues of Glutamic acids and Lysine at the N- and C- termini, respectively, to potentially increase the *cis* conformation is solution.

Noteworthy, the NMR structural characterization of the probe showed that the *cis* conformation of the substrate was highly favored, as hypothesized in the design.

Treatment of the substrate with recombinant CypA in absence of organic solvents, promoted the rapid proteolytic cleavage by Chymotrypsin and an increase of fluorescence intensity that is linearly related to the extent of CypA-mediated substrate isomerization.

Technical parameters of the HTS assay (Z′-factor, S/N, IC_{50} values of pharmacological control) have been optimized therefore the test appears to be ready for large scale screenings. As an exemplary screening we used here the commercial LOPAC^{1280} library. From such screening some selective CypA inhibitors were identified, including the well-known CsA, present within the library as a positive control.

Among the other compounds showing activity, two were tested in dose response experiments.

The purine-based compound C3353, known as a Cdk inhibitor selective for Cyclin-dependent kinase-1 (Cdk1) (PMID: 21131960), showed a 6 μM IC_{50} inhibition, which is a good starting point for developing new and more selective inhibitors.

To gain insights into the structure-activity relationship of the two compounds, they were subjected to a comparative computational study that confirmed the predilection of the ligands for the CypA active site.

Moreover, the different IC_{50} values detected can be explained by the higher number of interactions established by C3353 with the hydrophobic groove present in the catalytic site.

In conclusion, we have set up a HTS screening assay for the selection of CypA *cis-trans* isomerase activity inhibitors. The assay is based on the use of a new fluorescent peptide substrate we have designed in order to have a high proportion of *cis* conformers and to work by following fluorescence intensity increase or decrease, depending on enzyme activation or inhibition.

The assay is very robust, has been optimized on 384 well plates and can be used in screening campaigns of large compound libraries.

12. REFERENCES

1. Kumari S.; Roy S.; Singh P.; Singla-Pareek S.L.; et al. Cyclophilins. Plant Signal Behav. (2013), 8, e22734.
2. Wang P. and Heitman J. The cyclophilins. Genome Biol. (2005), 6, 226.
3. Galat A. Peptidylprolyl cis/trans isomerases (immunophilins): biological diversity - targets - functions. Curr. Top Med. Chem. (2003), 3, 1315-1347.
4. Fischer G.; Schmid F. X. Peptidyl-prolyl cis/trans isomerases. In: Bukau B., editor. Molecular Chaperones and folding Catalysis: Regulation, Cellular function, and Mechanisms. Amsterdam: Harwood Academic Publishers. (1999), 461-472.
5. Harding M.W.; Galat A.; Uehling D.E.; et al. A receptor for the immunosuppressant FK506 is a cis-trans peptidyl-prolyl isomerase. Nature. (1989), 341, 758-760.
6. Grathwohl C. and Wüthrich K. NMR studies of the rates of proline *cis-trans* isomerization in oligopeptides. Biopolymers (1981); 20, 2623–2633.
7. Lang K.; Schmid F. X.; Fischer G. Catalysis of protein folding by prolyl isomerase. Nature. (1987), 329, 268-270.
8. Lang K.; Schmid F.X.; Fischer, G.; Lu K.P.; Finn G.; Lee T.H.; et al. Prolyl cis-trans isomerization as a molecular timer. Nat. Chem. Biol. (2007), 3, 619–629.
9. Lu K. P.; Finn G.; Lee T. H.; Nicholson L. K; et al. Prolyl isomerase Pin1 in cancer. Cell Research. (2014), 24, 1033-1049.
10. Edlich F. and Fischer G. Pharmacological targeting of catalyzed protein folding: the example of peptide bond cis/trans isomerases. Handb.Exp.Pharmacol. (2006), 172, 359-404.
11. Dornan J.; Page A. P.; Taylor P.; et al. Biochemical and Structural Characterization of a Divergent Loop Cyclophilin from Caenorhabditis elegans. J. Biol. Chemistry. (1999), 274, 34877–34883.
12. Fischer G., Wittmann-Liebold B., Lang K.; et al. Cyclophilin and peptidyl-prolyl cis-trans isomerase are probably identical proteins.Nature. (1989), 337, 476-478.
13. Takahashi N.; Hayano T.; Suzuki M. Peptidyl-prolyl cis-trans isomerase is the cyclosporin A-binding protein cyclophilin. Nature. (1989), 337, 473-475.
14. Song F.; Zhang X.; Ren X-B.; et al., Cyclophilin A (CyPA) Induces Chemotaxis Independent of Its Peptidylprolyl Cis-Trans Isomerase Activity. J. Biol. Chem. (2011), 286, 8197-8203.

15. Handschumacher R. E.; Harding M. W.; Rice J.; et al. Cyclophilin: a specific cytosolic binding protein for cyclosporin A. Science. (1984), 226, 544-547.
16. Galat A. Peptidylproline cis-trans-isomerases: immunophilins. Eur. J. Biochem. (1993), 216, 689-707.
17. Nigro P.; Pompilio G.; Capogrossi M. C. Cyclophilin A: a key player for human disease. Cell Death Dis. (2013), 4, e888.
18. Fischer G.; Bang H.; Mech C. Determination of enzymatic catalysis for the cis-trans-isomerization of peptide binding in proline-containing peptides. Biomed. Biochim. Acta. (1984), 43, 1101-1111.
19. Kofron J. L.; Kuzmic P.; Kishore V; et al. Determination of kinetic constants for peptidyl prolyl cis-trans isomerases by an improved spectrophotometric assay. Biochemistry. (1991), 30, 6127-6134.
20. Kofron J. L.; Kuzmic P.; Kishore V.; et al. Lithium chloride perturbation of cis-trans peptide bond equilibria: Effect on conformational equilibria in cyclosporin-A and on time-dependent inhibition of cyclophilin. J. Am. Chem. Soc. (1992), 114, 2670-2675.
21. Seebach D.; Thaler A.; Beck A. K. Solubilization of Peptides in Non-polar Organic Solvents by the Addition of Inorganic Salts: Facts and Implications. Helv. Chim. Acta. (1989), 72, 857-867.
22. Acker M. G.; Auld D. S. Considerations for the design and reporting of enzyme assays in high-throughput screening applications. Perspectives in Science. (2014), 1, 56-73
23. Fields G. B.; Noble R. L. Solid phase peptide synthesis utilizing 9-fluorenylmethoxycarbonyl amino acids. Int. J. Pept. Protein Res. (1990), 35, 161-214.
24. Knorr R.;Trzeciak A.; Bannwarth W. et al; New coupling reagents in peptide chemistry. Tetrahedron Lett. (1989), 30, 1927.
25. Belvisi L.; Bernardi A.; Checchia A.; et al. Potent integrin antagonists from a small library of RGD including cyclic pseudopeptides. Org. Lett. (2001), 3, 1001.
26. Zhang J. H.; Chung T. D.; Oldenburg K. R. A simple statistical parameter for use in evaluation and validation of high throughput screening assays. Journal of Biomolecular Screening. (1999), 4, 67-73.

27. Rance M.; Sørensen O.W., Bodenhausen G.; et al. Improved spectral resolution in cosy ^{1}H NMR spectra of proteins via double quantum filtering. Biochem. Biophys. Res.Commun. (1983), 117, 479-485.
28. Braunschweiler L.; Ernst R. R. Coherence transfer by isotropic mixing: application to proton correlation spectroscopy. J. Magn. Reson. (1983), 53, 521-528.
29. Kumar A.; Ernst R.R.; Wuthrich K. A two-dimensional nuclear Overhauser enhancement (2D NOE) experiment for the elucidation of complete proton–proton cross-relaxation networks in biological macromolecules. Biochem. Biophys. Res. Commun. (1980), 95, 1-6.
30. Griesinger C.; Ernst R. R. Frequency offset effects and their elimination in NMR rotating-frame cross-relaxation spectroscopy. J. Magn. Reson. (1987), 75, 261-267.
31. Hwang T. L.; Shaka A. J. Water suppression that works: excitation sculpting using arbitrary waveforms and pulsed field gradients. J. Magn. Reson.Ser. A. (1995), 112, 275-279.
32. Dalvit C. Efficient multiple-solvent suppression for the study of the interactions of organic solvents with biomolecules. J. Biomol. NMR. (1998), 11, 437-444.
33. Keller R.L.J. The Computer Aided Resonance Assignment Tutorial. Cantina Verlag. (2004).
34. Masciocchi J.; Frau G.; Fanton M.; et al. A Large-Scale Chemoinformatics Database. Nucl. Acids Res. (2009), 37 (suppl 1), D284-290.
35. Cuzzolin A.; Sturlese M.; Malvacio I.; et al. An Integrated Informatic Platform Bridging the Gap between the Robust Validation of Docking Protocols and Virtual Screening Simulations. Molecules. (2015), 20, 9977-9993.
36. Berman H. M.; Westbrook J.; Feng Z.; et al. The Protein Data Bank. Nucleic Acids Res.2000, 28, 235-242.
37. PDB ID: 3RDD; Colliandre, L.; Ahmed-Belkacem, H.; Bessin, Y.; et al. Human Cyclophilin A Complexed with an Inhibitor.
38. PDB ID: 4N1N; Mcnae I. W.; Dornan D.; Patterson A. F.; et al. Structure of Cyclophilin A in complex with Benzamide.
39. PDB ID: 4N1Q; Mcnae I. W.; Dornan D.; Patterson A. F.; et al. Structure of Cyclophilin A in complex with cyclohexanecarboxamide.
40. PDB ID: 4N1R; Mcnae I. W.; Dornan D.; Patterson A. F.; et al. Structure of Cyclophilin A in complex with benzenesulfonohydrazide.

41. CCG Inc. Molecular Operating Environment (MOE), 2015; http://www.chemcomp.com (accessed October 2015).
42. Labute P. Protonate3D: Assignment of Ionization States and Hydrogen Coordinates to Macromolecular Structures. Proteins. (2009), 75, 187-205.
43. GOLD Suite, Version 5.2; Cambridge Crystallographic Data Centre: 12 Union Road, Cambridge CB2 1EZ, UK.
44. Jones G.; Willett P.; Glen R. C.; et al. Development and Validation of a Genetic Algorithm for Flexible Docking. J. Mol. Biol. (1997), 267, 727-748.
45. Küllertz G.; Lüthe S.; Fischer G. Semiautomated microtiter plate assay for monitoring peptidylprolyl cis/trans isomerase activity in normal and pathological human sera. Clinical Chemistry. (1998), 3, 502-508.
46. Fischer G. Peptidyl-prolyl cis/trans isomerases and their effectors. Angew. Chem. Int. Ed. Engl. (1994), 33, 1415-1436.
47. Dasgupta B.; Chakrabarti P.; Basu G. Enhanced stability of cis Pro-Pro peptide bond in Pro-Pro-Phe sequence motif. FEBS Letters. (2007), 581, 4529-4532.
48. Donald J.E.; Kulp D.W.; DeGrado W.F. Salt Bridges: Geometrically specific, designable interactions. Proteins. (2011), 79, 898-915
49. Berhanu S. M.; Hansmann U. H. E. Structure and Dynamics of Amyloid-b Segmental Polymorphisms. PLOS ONE. (2012), 7, 1-12.
50. Moision R.M.; Armentrout P.B. The Special Five-Membered Ring of Proline: An Experimental and Theoretical Investigation of Alkali Metal Cation Interactions with Proline and Its Four- and Six-Membered Ring Analogues. J. Phys. Chem. A. (2006), 110, 3933-3946.
51. Jiubiao G.; Ci X.; Xuechen Li.; et al., Spectral properties of EDANS-Dabcyl pair and the flowchart of the experimental design. PLOS ONE. (2014), 10.1371/journal.pone.0114124.g001.
52. Doti N.; Raimondo D.; Sabatella M.; et al. Identification of protease inhibitors by a fast fluorimetric assay. Mol. Biotechnol. (2013), 54, 283-291.
53. Liu J.; Albers M. W.; Chen C.-M.; et al. Cloning, expression, and purification of human cyclophilin in Escherichia coli and assessment of the catalytic role of cysteines by site-directed mutagenesis. Proc. Natl. Acad. Sci. USA. (1990), 87, 2304-2308.

54. Austin C.; Davis J. B.; Fliri H. G.; et al. Prolyl Isomerases –Old Proteins as New Therapeutic Targets. Selcia Ltd, Fyfield Business & Research Park, Fyfield Road, Ongar, Essex CM5 0GS, UK. (2015).
55. Paeshuyse J.; Kaul A.; De Clercq, E.; et al. The non-immunosuppressive cyclosporin DEBIO-025 is a potent inhibitor of hepatitis C virus replication in vitro. Hepatology. (2006), 43, 761-770.
56. Hopkins S.; Scorneaux B.; Huang Z.; et al. SCY-635, a novel non immunosuppressive analog of cyclosporine that exhibits potent inhibition of hepatitis C virus RNA replication in vitro. Antimicrob. Agents Chemother. (2010) 54, 660-672.
57. Mazzeo A. T.; Brophy G. M.; Gilman C. B.; et al. Safety and tolerability of cyclosporin a in severe traumatic brain injury patients: results from a prospective randomized trial. J. Neurotrauma. (2009), 26, 2195-2206.
58. Reutenauer J.; Dorchies O. M.; Patthey-Vuadens O.; et al. Investigation of Debio 025, a cyclophilin inhibitor, in the dystrophic mdx mouse, a model for Duchenne muscular dystrophy. Br. J. Pharmacol. (2008), 155, 574-584.
59. Balsley M. A.; Malesevic M.; Stemmy E. J.; et al. A cell-impermeable cyclosporine A derivative reduces pathology in a mouse model of allergic lung inflammation. J. Immunol. (2010), 185, 7663-7670.
60. Nigro, P.; Satoh, K.; O'Dell, M. R.; et al., Cyclophilin A is an inflammatory mediator that promotes atherosclerosis in apolipoprotein E-deficient mice. J. Exp. Med. (2011), 208, 53-66.
61. Bell R. D.; Winkler E. A.; Singh I.; et al. Apolipoprotein E controls cerebrovascular integrity via cyclophilin A. Nature. (2012),485, 512-516
62. Mori T.; Itami S.; Yanagi T.; et al. Use of a Real-Time Fluorescence Monitoring System for High-Throughput Screening for Prolyl Isomerase Inhibitors. Journal of Biomolecular Screening.(2009), 14, 419-424.